

**Synthesis,
Structure and Function of Oligo(1,8-pyrenylenes)**

By

© Joshua C. Walsh

A thesis submitted to the

School of Graduate Studies

in partial fulfillment of the requirements for the degree of

Doctor of Philosophy

Department of Chemistry

Memorial University of Newfoundland

March 2021

St. John's, Newfoundland and Labrador

For my wife, Nicole.

Abstract

This thesis is divided into four chapters. Chapter 1 will show progress towards a review of applications utilizing the pyrene core to show the utility of one of the most studied molecules in chemistry is far from fully realized. Chapter 2 shows a monomer-through-pentamer series of oligo(1,8-pyrenylene)s was synthesized using a two-step iterative synthetic strategy. The trimer, tetramer and pentamer are mixtures of atropisomers that interconvert slowly at room temperature (VTNMR analysis). They are classified as functional molecular liquids (FMLs) well below room temperature, as indicated by POM, DSC and SWAXS analysis. The oligomers are highly fluorescent both in the liquid state and in dilute solution and an investigation of their photophysical properties demonstrated that delocalization plays a larger role in their excited states than it does in related pyrene-based oligomers. Chapters 3 and 4 outline progress in using the oligomers as starting points for different molecular systems will also be covered, attempting to put more 'F' in the FMLs.

Acknowledgements

First, I would like to thank Graham, not only for being an excellent supervisor but for his contagious enthusiasm and curiosity that reaches far beyond organic chemistry. Yuming, for being like a second supervisor to me, always happy to discuss science and full of ideas.

Thank you to my parents, Carl and Joy Walsh, for fostering my love of science at a young age and providing access to my earliest laboratories (kitchen and shed).

Thank you, Nicole, for everything.

Table of Contents

Dedication	II
Abstract	III
Acknowledgements	IV
List of Figures	IX
List of Schemes	XII
List of Abbreviations	XVI
Chapter 1: A Brief Review of the Recent Pyrene Literature (2010-2020) with a Focus on Applications of the Pyrene Core.	1
Chapter 2: Synthesis of Oligo(1,8-pyrenylene)s	32
Chapter 3: From Functional Molecular Liquids to Functional Materials	98
Chapter 4: Oligopyrenylene Extended TTFVs	165

Chapter 1

Foreword	1
Introduction	2
Room Temperature Liquid Pyrenes	7
Pyrene-Based Sensors and Molecules for Information Processing	18
Pyrene as a Nanotube Anchor	21
Conclusion	29
References	29

Chapter 2

Statement of Co-Authorship	32
Introduction	34
Results and Discussion	36
Experimental Section	58
Acknowledgements	72
References	72
Appendix	76

Chapter 3

Synthetic Macrocycles	98
Shape-Persistent Macrocycles	99
Cyclophenylenes	100
[<i>n</i>]Cycloorthophenylenes (COPs)	102
[<i>n</i>]Cyclometaphenylenes (CMPs)	103
[<i>n</i>]Cycloparaphenylenes (CPPs)	112
[<i>n</i>]Cyclopyrenylenes (CPys)	121
[<i>n</i>]Cyclophenyleneacetylenes (CPPAs)	127
[<i>n</i>]Cyclopyrenylene acetylenes (CPyAs)	129
Intermediate CPP/CPPA Hybrids	130
Results	136
Conclusions	153
References	154
Experimental Section	158

Chapter 4

Introduction	165
--------------	-----

Results	172
Conclusions	181
References	182
Experimental Section	183

List of Figures

Figure 1.1 Aromatic compounds 1-4 .	3
Figure 1.2 The family of benzenoid PAHs containing 4 rings and the number of Sci-Finder hits. $k=1000$.	4
Figure 1.3 Energy of stabilization of the static and dynamic excimers of pyrene.	6
Figure 1.4 Absorption and emission spectra of pyrene (10), 11 _(solution) and 11 _(thin film) .	10
Figure 1.5 Pyrene-based RTILs 12-15 .	12
Figure 1.6 Nakanishi's liquid fullerene derivatives 16 showing melting point dependence on alkyl group length.	15
Figure 1.7 Synthesis of bispyrenephosphaviologen 25 .	23
Figure 1.8 Baumgartner's bispyrenephosphaviologen and carbon nanotube composite (26).	24
Figure 1.9 Dai's single-walled CNT appended with protein-binding-pyrene-based-double-anchor.	27
Figure 1.10 AFM imaging of the single-walled CNT without (A) and with functionalized pyrene anchor 27 (B).	27
Figure 2.1 Oligo(pyrenylene)s 1-5 , pyrene-based FMLs 6 and oligo(1,8-pyrenylene)s 7 .	35
Figure 2.2 Aromatic region of the 300 MHz ¹ H NMR spectrum of 19b in CDCl ₃	39

Figure 2.3 TLCs of oligomers, A = CH ₂ Cl ₂ /hexanes and CH ₂ Cl ₂ /toluene/hexanes. B = Purity experiment.	46
Figure 2.4 DSC thermograms for trimer 11a (top pair), tetramer 12a (middle pair) and pentamer 13a (bottom pair) without annealing (black lines) and after annealing at 42 °C for 12 h (red lines).	47
Figure 2.5 Optical microscopy (top) and polarized optical microscopy (bottom) for 11a (left), 12a (middle) and 13a (right).	47
Figure 2.6 Small- (inset) and wide-angle X-ray scattering of trimer 11a .	48
Figure 2.7 TGA trace for trimer 11a .	49
Figure 2.8 Normalized absorption spectra of 11a (green), 12a (purple) and 13a (black) as neat liquid thin films in transmission mode.	50
Figure 2.9 Normalized fluorescence spectra of trimer 11a (green), tetramer 12a (purple) and pentamer 13a (black) as neat liquid thin films measured using front-face emission.	51
Figure 2.10 Absorption spectra of 8a (blue), 10a (red), 11a (green), 12a (purple) and 13a (black) in oxygen-purged cyclohexane solution.	53
Figure 2.11 Emission spectra of cyclohexane solutions of 8a (blue), 10a (red), 11a (green), 12a (purple) and 13a (black) in oxygen-purged cyclohexane solution.	56

Figure 2.12 TGA Thermogram of tetramer 12a .	94
Figure 2.13 TGA thermogram of pentamer 13a .	94
Figure 2.14 Optimized geometry of <i>meso</i> - S1 calculated at the B3LYP/6-31G(d) level of theory.	95
Figure 2.15 Optimized geometry of (\pm)- S1 calculated at the B3LYP/6-31G(d) level of theory.	95
Figure 2.16 Interconversion of 1,1'-bipyrene enantiomers through syn and anti-transition states.	96
Figure 2.17 A plot of the onset energies for transition (centered at 360 nm) vs. $\cos[\pi/(n+1)]$ for 10a-13a .	96
Figure 2.18 A plot of the emission energies vs $\cos[\pi/(n+1)]$ for compounds 10a-13a .	97
Figure 3.1 Pederson's macrocyclic dibenzo-18-crown-6 (1).	98
Figure 3.2 The formal definition of a shape-persistent macrocycle as described by Grosberg and Khoklov (when $d \approx l/\pi$).	99
Figure 3.3 The three substitution patterns of [6]cyclophenylenes 2-4 with internal annulenes highlighted in red.	100
Figure 3.4 Illustration of the electronic communications in <i>para</i> - and <i>ortho</i> -substitutions and the lack of communication in <i>meta</i> substituents.	101

Figure 3.5 The first two members of the $[n]$ COP family: 5 and 6 .	102
Figure 3.6 The current state of affairs in $[n]$ CMP chemistry <i>versus</i> the first synthesis.	111
Figure 3.7 Yamada's cyclotetramer 91 and the end-to-end C_{60} supramolecular complex observed.	124
Figure 3.8 Previous methods to produce biaryl ethers.	125
Figure 3.9 The hybrids that lie between the structures of $[4]$ CPP and $[4]$ CPPA.	131
Figure 3.10 $[3]$ CPP ⁴ A (131) and $[3]$ CPP ⁵ A (132).	133
Figure 3.11 Yamada's CPy 94 to Bodwell's CPyA 144 and the hybrids 142-143 in between.	138
Figure 3.12 Calculated NMR shifts of two cycloalkene isomers 145a and 145b	143
Figure 3.13 Calculated isomers and conformations available to alkene 145 .	144
Figure 3.14 Relative energies of diols 149a – 149d .	145
Figure 3.15 Possible dimerization of trimer dialdehyde (146) under McMurry conditions.	146
Figure 3.16 Calculated relative energies and bond angles of <i>syn</i> - 120 (120a) and <i>anti</i> - 120 (120b).	150

Figure 3.17 Calculated ^1H NMR shifts of <i>syn</i> - 120 (120a) and <i>anti</i> - 120 (120b).	151
Figure 3.18 Comparison of ^{13}C NMR signals in strained alkynes 137 and 142 compared to unstrained models 146 and 144 .	152
Figure 4.1 Stepwise oxidation of parent TTF 16 .	168
Figure 4.2 Redox switching of TTFV.	169
Figure 4.3 Cyclic voltammogram of 37 , Bu_4NBF_4 (0.1 M).	175
Figure 4.4 Oxidative UV-Vis titration of compound 37 .	176
Figure 4.5 Proposed resonance structures accounting for the lack of reactivity.	177
Figure 4.6 Bis(DTF)-pyrene hybrid targets 40 and 41 .	179

List of Schemes

Scheme 1.1 Nakanishi's synthesis of pyrene-based FML 11 .	9
Scheme 1.2 Guerbet reaction of primary alcohols yielding chiral branched alcohols.	12
Scheme 1.3 The Guerbet reaction and application.	17
Scheme 1.4 James' and Jiang's two-step synthesis of glucose sensor 20 .	19
Scheme 1.5 Glucose-selective sensor 20 .	20

Scheme 1.6 Steffanson's pyrene-based SWCNT anchor 31 .	27
Scheme 2.1 Iterative strategy for the synthesis of oligo(1,8-pyrenylene)s	37
Scheme 2.2 Synthesis of 1,8-dipyren-1-ylpyrenes 19a and 19b and a depiction of the two diastereomers of 19b .	37
Scheme 2.3 Synthesis of boronic ester 22 , trimer 11a and pentamer 13a .	40
Scheme 2.4 Synthesis of dimer 10a and tetramer 12a .	44
Scheme 3.1 Rapson and Shuttleworth's synthesis of [4]COP.	101
Scheme 3.2 Wittig's 1957 synthesis of hexabenz[12]annulene ([6]COP)	102
11 .	
Scheme 3.3 Staab's 1964 synthesis of [6]CMP (3).	103
Scheme 3.4 Swager's synthesis of a highly decorated [6]CMP derivative.	103
Scheme 3.5 Isobe's synthesis of [5]-[9]CMP on a gram scale.	104
Scheme 3.6 Isobe's synthesis of 5Me-[5]CMP (22).	105
Scheme 3.7 Isobe's synthesis of phenine-[5]circulene (27).	107
Scheme 3.8 Isobe's synthesis of phenine-[7]circulene.	108
Scheme 3.9 Isobe's synthesis of phenine-nanotube, or the most complex CMP known.	110
Scheme 3.10 Parekh and Guha's attempt at the assuredly impossible target 39 .	112
Scheme 3.11 Vögtle's progress towards [5]CPP.	113
Scheme 3.12 McMurry's synthesis of square planar silver complex 53 .	113
Scheme 3.13 Jasti's synthesis of [9], [12] and [18]CPP.	115

Scheme 3.14 Jasti's synthesis of [5]CPP (67).	116
Scheme 3.15 Itami's selective synthesis of [12]CPP (71).	117
Scheme 3.16 Yamago's synthesis of [8]CPP through platinacycle (73).	118
Scheme 3.17 Tanaka's synthesis of [12]CMP-hexaester 78.	119
Scheme 3.18 Osakada's two-step, high-yielding synthesis of [6]CPP.	119
Scheme 3.19 Yamago's synthesis of the first cyclopyrenylene, [4]-2,7-CPy.	121
Scheme 3.20 Müllen's synthesis of [6]cyclo-1,3-pyrenylene.	122
Scheme 3.21 Yamada's synthesis of cyclic pyrenylene oligomers.	123
Scheme 3.22 Oxygen insertion and biaryl ether formation in 94 under ambient conditions.	125
Scheme 3.23 Sondheimer's extraordinary cyclooctadiyne 103 .	126
Scheme 3.24 Kawase's general synthesis for [6]-[10]CPPAs 109-111 .	127
Scheme 3.25 The limits of Sondheimer's methodology in Kawase's failed synthesis of [4]CPPA 112 .	127
Scheme 3.26 Bodwell's synthesis of [4]- and [3]-1,8-CPy by Sonogashira macrocyclization.	129
Scheme 3.27 Moore's synthesis of CPP/CPPA hybrid 128 .	131
Scheme 3.28 SPAAC reaction of Moore's CPP/CPPA hybrid 128 with Tg-azide 129 .	132
Scheme 3.29 Jasti's application of Cheng's double Sonogashira utilizing calcium carbide as acetylene equivalent.	133
Scheme 3.30 Jasti's synthesis of CPP/CPPA hybrid 137 .	133

Scheme 3.31 Tanaka's synthesis of CPP/CPPA hybrid 141 , which displays both helical and axial chirality.	135
Scheme 3.32 Retrosynthetic analysis of alkyne 142 .	138
Scheme 3.33 Synthesis of cycloalkene 145 .	140
Scheme 3.34 Dialdehyde diastereomers 146a and 146b leading to two cyclic alkene products, 145a and 145b .	141
Scheme 3.35 Possible bromides from the <i>syn</i> -conformers of <i>Z</i> and <i>E</i> geometric isomers of 145 .	146
Scheme 3.36 Application of Sondheimer's methodology on alkene 142 .	147
Scheme 3.37 Possible synthesis of vinyl bromides 151 and 152 .	148
Scheme 3.36 Plausible synthesis of 153 if 150 is present in the 145 mixture.	149
Scheme 3.37 Attempted SPAAC reaction with benzyl azide (154).	152
Scheme 4.1 The high temperature reaction of acetylene with elemental sulfur and the various products.	165
Scheme 4.2 Wudl's synthesis of the parent TTF 16	166
Scheme 4.3 Radical dimerization of a DTF to form a TTFV.	168
Scheme 4.4 Obsolete synthesis of DTFV moieties using the Horner-Wadsworth-Emmons reaction.	169
Scheme 4.5 Large scale synthesis of dithiaalkyl-DTF precursor.	170
Scheme 4.6 Zhao's TTFV containing polymers.	171
Scheme 4.7 Proposed structure for the product of radical polymerization.	172
Scheme 4.8 Synthesis of pyrene-TTFV hybrid 37 .	173

Scheme 4.9 Macrocyclization of 38 in the solid state.	177
Scheme 4.10 Synthesis of pyrene dimer bis(DTF) 40 .	179
Scheme 4.11 Synthesis of pyrene trimer bis(DTF) 41 .	180

List of Abbreviations

1,2,4-TCB	1,2,4-Trichlorobenzene
Å	Angstrom
APPI	Atmospheric pressure photo-ionization
ASE	Aromatic stabilization energy
B2pin2	Bis(pinacolato)diboron
BINAP	Binaphthyl
bipy	Bipyridine

Bpin	Pinacolatoborane
Bu	Butyl
BuLi	Butyl lithium
C	Celsius
cm	Centimeters
CMP	Cyclo <i>meta</i> phenylene
CNT	Carbon nanotube
cod	1,5-Cyclooctadienyl
COP	Cyclo <i>ortho</i> phenylene
CPP	Cyclo <i>para</i> phenylene
CPPA	Cyclo <i>para</i> phenylene acetylene

CPyA	Cyclopyrenylene acetylene
Cy	Cyclohexyl
d	Distance
<i>D</i>	Debye
dba	Dibenzylideneacetone
DDQ	2,3-Dichloro-5,6-dicyano-1,4- benzoquinone
DFT	Density functional theory
DMF	Dimethylformamide
DMSO	Dimethylsulfoxide
dppf	1,1'- Bis(diphenylphosphino)ferrocene

DSC	Differential scanning calorimetry
dtbpy	4,4'-Di-tert-butyl-2,2'-dipyridyl
DTF	Dithiafulvalene
DTFV	Dithiafulvalene vinylogue
EET	Excitation energy transfer
Et	Ethyl
EtOH	Ethanol
FML	Functional molecular liquid
g	Gram
h	Hour
HOMO	Highest occupied molecular orbital

HPLC	High performance liquid chromatography
HRMS	High resolution mass spectrometry
Hz	Hertz
<i>i</i> Pr	Isopropyl
kcal	Kilocalorie
k_{nr}	Rate of non-radiative decay
KOAc	Potassium Acetate
k_r	Rate of radiative decay
l	Length
LCMS	Liquid chromatography mass spectrometry

LUMO	Lowest unoccupied molecular orbital
M	Moles/liter
m/z	Mass to charge ratio
MALDI	Matric-assisted laser desorption/ionization
Me	Methyl
mg	Milligrams
MHz	Megahertz
min	Minutes
mmHg	Millimeters of mercury
mmol	Millimoles
MOM	Methoxymethyl

mp	melting point
MS	Mass spectrometry
NaNp	Sodium Naphthalenide
NBS	<i>N</i> -bromosuccinamide
NICS	Nucleus independent chemical shift
NMR	Nuclear magnetic resonance
ns	Nanosecond
OAc	Acetate
OLED	Organic light emitting diode
OTf	Trifluoromethanesulfonate
PAH	Polycyclic aromatic hydrocarbon

PEPPSI	pyridine enhanced precatalyst preparation, stabilization and initiation
Ph	Phenyl
POM	Polarized optical microscopy
pyr.	Pyridine enhanced precatalyst preparation, stabilization and initiation
R_f	Retardation factor
RTIL	Room temperature isotropic liquid
s	Second
SPM	Shape persistent macrocycle
SWAXS	Small and wide angle xray scattering

SWCNT	Single walled carbon nanotube
TBAB	Tetrabutyl ammonium bromide
<i>t</i> -Bu	<i>tert</i> -Butyl
T_c	Coalescence temperature
TCNQ	Tetracyanoquinodimethane
TEM	Transmission electron microscopy
T_g	Glass transition temperature
TGA	Thermogravimetric analysis
THF	Tetrahydrofuran
TLC	Thin layer chromatography
TMS	Trimethyl silyl
TOF	Time of flight

TTF

Tetrathiafulvalene

TTFV

Tetrathiafulvalene vinylogue

UV-vis

Ultraviolet-visible

W

Watt

δ

Chemical shift

Chapter 1

A Brief Review of the Recent Pyrene Literature (2010-2020) with a Focus on Applications of the Pyrene Core

Foreword

Pyrene is one of the most extensively studied molecules in the chemical literature. It has been named the “gold standard” in the sensing of microenvironments by Vullev^[1] and “the fruit fly of photochemists” by Müllen.^[2] The reasons pyrene has achieved such widespread attention are numerous, its long emission lifetimes for both excited monomer and excimer states, the large separation of fluorescence bands are chief among them. With more than 100 thousand papers published on pyrene, 40 thousand within the last 10 years, a comprehensive review is no longer possible. In 2010, Müllen published a now highly cited review of pyrene-based materials for organic electronics,^[2] separating important publications by the substitution patterns on pyrene. In 2016, Yamato published a review of synthetic methodology for the synthesis of pyrene derivatives,^[3] outlining the current situation in pyrene

substitution chemistry and the order of events required to afford certain patterns of substitution.

This chapter includes a review of recent applications of the pyrene core. Instead of focusing on the substitution pattern like Müllen and Yamato, this review will separate research contributions based on the application of the pyrene core. The aim of this review is to provide a sense of how broadly the pyrene skeleton has been utilized and where recent focus has been concentrated. Coverage begins where Müllen's review left off in 2010 and avoids addressing synthetic methodology that has been dealt with in Yamato's review.

Introduction

In parallel with the homologous series of alkanes that are introduced in the first undergraduate organic chemistry course, an increase in the number of rings in a polycyclic aromatic hydrocarbon (PAH) leads to pseudo-exponential growth in the number of possible isomers. For the sake of simplicity and for comparative purposes, PAHs containing unpaired electrons, sp^3 -hybridized atoms and rings smaller or larger than six will be ignored. Benzene (1) and naphthalene (2) are the only members of their respective one- and two-ring families and two isomers emerge when 3 rings are reached, namely anthracene (3) and phenanthrene (4) (Figure 1.1).

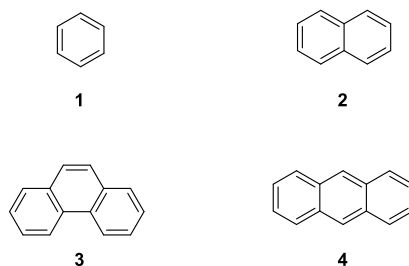


Figure 1.1 Aromatic compounds 1-4.

The family of 4-ring PAHs is significantly larger, containing six members: tetracene (5), benzo[*a*]anthracene (6), benzo[*d*]phenanthrene (7), chrysene (8), triphenylene (9) and pyrene (10) (Figure 1.2). Of this 4-ring series, pyrene is the subject of by far the most publications, with a total of more than 108,000 hits in Sci-Finder including over 40,000 for the decade this review covers. This large number of papers is greater than the sum of the rest of the 4-ring family, both in total (>86,000) and for the time frame covered by this review (>32,000). The disproportionate focus on pyrene in the literature cannot be attributed to natural abundance since every member of the series is commercially available and relatively inexpensive (Figure 1.2).

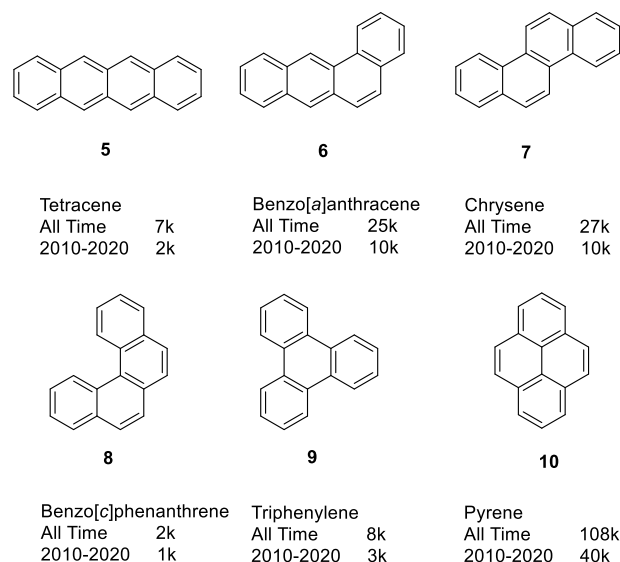


Figure 1.2 The family of benzenoid PAHs containing 4 rings and the number of Sci-Finder hits. k=1000.

Pyrene has such a tremendous body of literature devoted to it owing to its photophysical properties as well as the relative ease with which substituents can be controllably introduced. The sensitivity of pyrene's photophysical properties to its environment is owed to an interesting property that is not unique to pyrene, but is expressed especially strongly in pyrene. As demonstrated by Thomas *et al.*, the relative intensities of the vibronic bands of pyrene's emission spectrum are not equally affected by its environment and this allows for an important parameter to be defined.^[4] The authors found that the third vibronic band (385 nm) of pyrene's emission was strongly perturbed by a change in the dipole of solvent and importantly not the bulk dielectric constant. The ratio of the third (385 nm) and first (375 nm) vibronic bands can be used to assess pyrene's microenvironment and this has been utilized extensively in structural biology and physical biochemistry to determine such parameters as

critical micelle concentrations, water penetration in micelles and in the conformational analysis of biomolecules.^{[5][6]} In addition to pyrene's monomeric emission, it is also the first system in which excimer formation was observed. Excimer formation is also not unique to pyrene, but what is unique is (1) its high propensity to form excimers, having one of the highest known rates of excimer formation ($(3.11 \pm 0.06) \times 10^9 \text{ M}^{-1} \text{ s}^{-1}$),^[1] (2) its lack of photoreactivity^[2] (*cf.* tetracene, which undergoes [4+4] cycloaddition under irradiation)^[7] and (3) the large Stokes shift of its excimer emission, which makes the fluorescence spectral analysis less complicated.

Excimer formation, or the photo-associated dimeric state of pyrene, involves the association of a pyrene molecule in its first singlet excited state with a molecule in the ground state. In order for this dimeric species to form, the singlet excited state must be sufficiently long-lived to diffuse through solution to collide favorably with a ground state molecule (dynamic excimer) and the interaction must be sufficiently long-lived and stable to be observed. Another mechanism for excimer formation involves excitation of a pre-formed van der Waals dimer, typically in polar media (static excimer). For pyrene, the stabilization arises mainly from exciton resonance between the two pi systems. The stabilization of the dynamic excimer with respect to its two components is significant ($\sim 11 \text{ kcal/mol}$) and the inter-pyrene distance in the excimer is approximately 3.28 \AA .^[8] The emission of the dynamic excimer (480 nm) is strongly red-shifted from that of pyrene (405 nm) by $\sim 6100 \text{ cm}^{-1}$. On the other hand, the stabilization of the static excimer is less, as evidenced by its higher energy emission (455 nm). The explanation for the difference is that the pre-formed pyrene dimer is in the conformation to maximize pi-stacking interactions and hydrophobic interactions, which is rarely perfectly face-to-face as seen in the dynamic excimer (Figure 1.3).^{[8][9]} Since the

formation of excimers, like any intermolecular interaction is highly dependent on concentration, two methods have been used to increase the propensity for excimer formation and they have given rise to large bodies of work. The first approach is to tether two pyrene units so as to increase likelihood of interaction^[10] and the second is the use of confining environments (*e.g.* inside cyclodextrins). This bolstering of excimer formation allows routine detection of fluorescence at concentrations as low as $1 \cdot 10^{-7}$ mol/L.^[8]

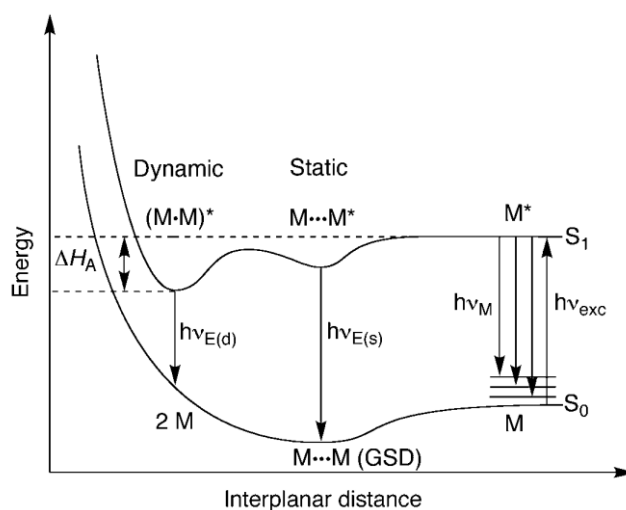


Figure 1.3 Energy of stabilization of the static and dynamic excimers of pyrene. (Reused with permission).^[9]

The use of pyrene as a building block in the construction of functional molecules also comes with a number of advantages, the foremost of which is the well-understood chemical reactivity. Thus, in comparison to other members of the 4-ring PAH family, the elaboration of the pyrene core is relatively easily controlled.^[3] With regard to electrophilic aromatic substitution, the origin of this advantage can be traced back to structure. Triphenylene (**9**) is the most stable of the 4-ring family, being by Clar's definition, fully benzenoid (constructed

solely of sextets and empty rings). It is unreactive towards liquid bromine at room temperature and only undergoes substitution when strong Lewis acid catalysts and elevated temperatures are employed. On the other end of the reactivity spectrum within this PAH family lies tetracene (**5**), which has a single Clar sextet and is destroyed under similar reaction conditions. Indeed, reports of useful chemistry on this 4-ring [*n*]acene are scarce. The remaining four members of the family each have two Clar sextets and exhibit more of a balance between reactivity and stability. Of these four compounds, pyrene (**10**) is the most highly symmetric (D_{2h} point group). This means that it has the smallest number of unique positions (three) that are available for monosubstitution. As previously reviewed by Yamato,^[3] each of the positions can be addressed rationally. Thus, pyrene's overwhelming presence in the literature can be attributed to a combination of its large natural abundance, the extreme sensitivity of its monomer fluorescence to its environment, its ability to serve as a probe of other systems by watching excimer formation and its well fleshed out substitution chemistry. The unabated trend of increasing use suggests that it still has much to offer.

Room Temperature Liquid Pyrenes

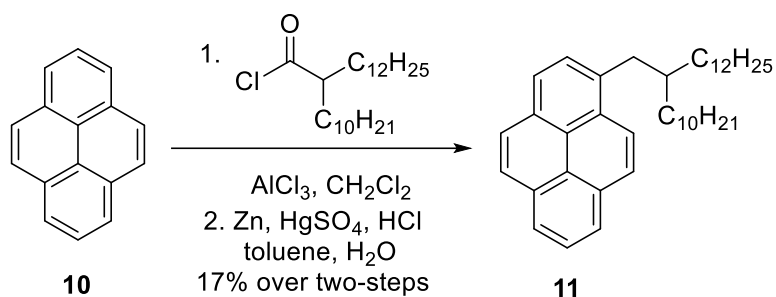
Pyrene (**10**) is an easily crystalized solid that melts at 145-148 °C (418-421 K). It has been utilized in its liquid form as both a chromophore^[12] and a solvent.^[13] The focus of this Section will be on pyrene derivatives that are room temperature isotropic liquids (RTILs), which are distinct from molten solids, supercooled liquids, liquid crystals and elastic solids (the differences between them are outlined in detail in Chapter 2). Nevertheless, some insight can be gained first by comparing the photochemistry and electrochemistry of pyrene in solution

state *vs* its molten state and then looking towards pyrene-based room temperature liquids. Unadorned pyrene (**10**) in its molten state at 425 K shows two main absorption bands that differ significantly from pyrene in solution. Molten pyrene shows a strong, long-lived absorption at ~ 570 nm that has been assigned to the triplet state of the monomer.^[12] This is presumably formed by initial excimer formation between a ground and singlet state pyrene to give a singlet excimer. Decay of this excimer then affords a triplet excimer, dissociation of which leads to the formation of a ground state pyrene molecule and a triplet excited state monomer. Since the concentration of pyrene in its molten state is at its highest possible level, a high concentration of excimer is produced upon irradiation. In stark contrast to sodium chloride, which becomes dramatically more conducting when it goes from the solid state to the liquid state, pyrene is a much better electrical conductor in the solid state than in the melt.^[1] Indeed, as shown by LeBlanc in 1962,^[13] the electrical mobility and conductivity of pyrene decreases subtly as temperature increases and falls by a factor of 3 at its melting point. The interpretation of this phenomenon is complex, but significant.

Based on the marked differences in behavior between dissolved pyrene (**10**) and neat molten pyrene (**10**), one might expect that suitably derivatized pyrenes that exist as RTILs would have drastically different properties in dilute solution than in the neat liquid state. Interestingly, this is not always the case.

^[1] This point is illustrated in a common first year chemistry demonstration, where a circuit with a power source and light-emitting diode (LED) is connected through a vessel containing solid sodium chloride. The sodium chloride is slowly heated and, dramatically, the light comes on when the sodium chloride becomes molten.

Although functional molecular liquids have been reviewed recently,^[14] this section will continue the focus on the pyrene core. The first pyrene-based functional molecular liquid (FML) **11** came from the Nakanishi lab in 2016.^[15] It features a Guerbet^{[16]#} alcohol-derived side chain on the 1 position of pyrene system. It was installed via a straightforward, two-step synthetic sequence consisting of a Friedel-Crafts acylation of pyrene (**10**) using the acid chloride obtained from the corresponding Guerbet alcohol and a subsequent Clemmensen-type reduction of the resulting aryl ketone to give (**11**).



Scheme 1.1 Nakanishi's synthesis of pyrene-based FML **11**.

Comparing **11** to unadorned pyrene (**10**) yields some interesting differences. The absorption spectra taken in dichloromethane show that the longest wavelength absorption maximum of the alkylated derivative is slightly red-shifted (by 9 nm), indicating a slight narrowing of the HOMO-LUMO gap. This is consistent with alkyl substitution of a chromophore. Upon moving from dilute solution to the neat liquid phase, further red shifting is observed and broadening of the absorption spectrum, both of which are characteristic of aggregation, and the authors attributed this small shift to solvatochromism, since in the neat liquid phase the solvent is other molecules of **11**. With regard to the emission spectra,

alkylpyrene **11** shows a dramatic red shift and an increase in fluorescence intensity in going from dilute solution ($\varphi_{em}=0.13$) to the neat liquid state ($\varphi_{em}=0.65$). This observation sharply contrasts the behaviour of previously reported room temperature liquid luminescent materials based on anthracene^[15] and oligo(*p*-phenylenevinylene),^[16] which exhibit decreases in quantum yield when moving from the solution to neat liquid phase.

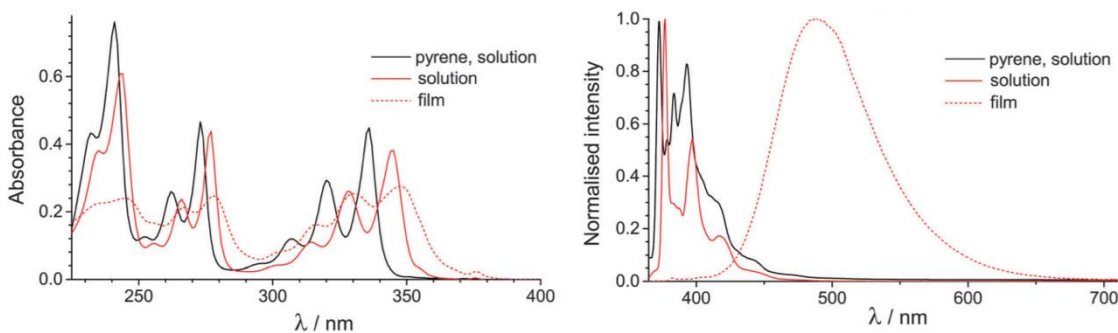


Figure 1.4 Absorption and emission spectra of pyrene (**10**), **11**_(solution) and **11**_(thin film). Reused with permission.^[15]

In dichloromethane, the quantum yields of pyrene (**10**) and **11** were found to be 0.06 and 0.13, respectively. The moderate increase in quantum yield upon alkylation was attributed to *p-s* conjugation.^[17] Like the absorption spectra, the emission of **11** is similar to and red shifted in comparison to pyrene. The emission of the thin film, however, is dramatically different in that intense excimer emission dominates the spectrum. The authors hypothesized that the film's density is perhaps in a Goldilocks zone, in which the pyrene-pyrene contacts are close enough to favor excimer emission, but with enough space and disorder to discourage self-quenching. This subtle interplay of sterics and electronics causes a large leap in the quantum yield ($\varphi_{em}=0.13$ to $\varphi_{em}=0.65$) in the thin film. In an attempt to take advantage of the

unique high fluorescence quantum yield in sensing applications, Nakanishi found the compound could be used to prepare oil in water droplets, stabilized by hexaethyleneglycol monomethyl ether.^[18] The oil droplets were found to be stable in water and the size could be controlled by a number of factors. Importantly the emission spectra were characteristic of the droplet size indicating potential applications in *in vivo* and *ex vivo* sensing.

Having observed that alkylpyrene **11** displayed very different properties in the liquid state versus dilute solution, the Nakanishi group turned their attention to investigating the possibility of synthesizing pyrene-based RTILs that displayed identical (or nearly identical) emission and absorption spectra in the solution phase and as neat liquids. Molecules that behave this way would have various applications as functional molecular liquids (FML, see Chapter 2). This led to a 2017 report of a new set of seven pyrene-containing RTILs **12-15**.

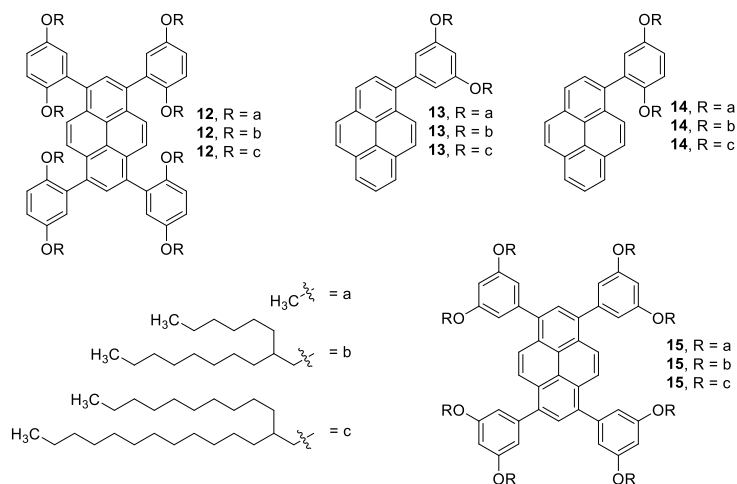
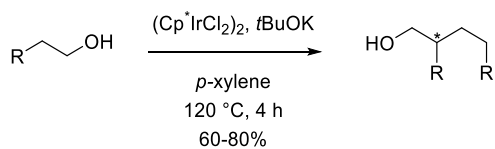


Figure 1.5 Pyrene-based RTILs **12-15**.

It bears repeating that pyrene is a privileged core for such a study because, unlike most other PAHs, its monomer-excimer fluorescence is extraordinarily sensitive to its microenvironment. A key design feature of **12-15** is the use of dialkoxyphenyl substituents rather than alkyl groups. By varying three parameters, namely the number of aryl groups (one or four), the length of the alkoxy groups (a, b, c, Figure 1.5) and the substitution pattern of dialkoxyphenyl groups (2,5- or 3,5-), the authors looked for trends in the extent of pyrene-pyrene interactions with the goal of correlating the degree of intermolecular pyrene-pyrene interactions with molecular structure. The utilization of racemic branched Guerbet alcohol derived (Scheme 1.2) alkoxy groups had a stereochemical consequence that was not acknowledged, *i.e.* that **12** and **13** are mixtures of two diastereomers and **14** and **15** are mixtures of numerous diastereomers. The straightforward syntheses of **12-15** relied upon the use of Suzuki-Miyaura cross-coupling reactions of dialkoxyphenylboronic acids with either 1-bromopyrene or 1,3,6,8-tetrabromopyrene.



Scheme 1.2 Guerbet reaction of primary alcohols yielding chiral branched alcohols (asymmetric center denoted with asterisk).

The choice of 2,5- and 3,5-dialkoxyphenyl substituents deserves comment. The key differences between the two are their local symmetry and the directions in which the

substituents point. In the 3,5-disubstituted rings, the two substituents exchange positions by rotation about the biaryl bond, but the same is not true for the 2,5-disubstituted rings. As a consequence of the local symmetry, the two alkoxy groups point away from the pyrene core in the 3,5-disubstituted rings. In contrast, one of the alkoxy groups in the 2,5-disubstituted is oriented toward one face of the pyrene core while the other point away. In this case, rotation about the biaryl bond would be expected to have a higher energy barrier than in the systems bearing 3,5-disubstituted rings, but not so much that atropisomerism would arise.

A number of interesting trends emerge when looking at the thermograms obtained by DSC and the melting points of the various pyrene-based compounds. Unsurprisingly, the two derivatives having only methoxy groups **13a** and **15a** are solids that melt at 113-116 °C and 316-318 °C, respectively. On the other hand, the rest of the series were found to be liquids at room temperature. Careful analysis of the thermograms show that while the 5 compounds are liquid, not all liquids are created equal. Compounds **15c**, **13b**, **14b** and to a lesser extent **15b**, all show melting curves during DSC scans (mp = -51.9 °C, T_g = -45.5 °C, -43.0 °C and -53.5 °C, respectively), while **12b** uniquely goes through a glassy transition to liquid phase (at -57.6 °C) without melting. Compounds **15b** and **15c** only differ by 8 carbons and, on first inspection, one might assume that if **15b** was a liquid then **15c** should perhaps be, for lack of a better descriptor, more “liquidy”, in fact, this is not the case. It turns out that for efficient liquefaction, the alkyl chains must be long enough (*i.e.* significantly longer than methyl in this system) to inhibit pyrene-pyrene interactions, but not so long that van der Waals forces between alkyl chains work against with liquefaction. The three alkyl groups chosen by Nakanishi do not represent a systematic change in structure very well, so this point is better

illustrated by the series of compounds **16** (Figure 1.6), which demonstrate the striking effect the alkyl chain length has on bulk properties.^[19] In this study, the Bingel reaction was used to attach a 2,4,6-trialkoxyphenyl unit to C_{60} . The loss of icosahedral symmetry and the introduction of the three alkoxy groups through the Bingel reaction have an immediate and pronounced effect on the melting point. With three octyl chains, the observed melting point of 150 °C is dramatically lower than that of unadorned C_{60} , which does not melt under normal conditions, but rather undergoes sublimation at ~600 °C.^[20] Increasing the chain length to dodecyl renders the molecule a RTIL (mp = 13.7 °C), and elongating to hexadecyl chains affords a system that remains liquid well below 0 °C (mp = -36.5 °C). Upon further elongation of the alkyl chains, the melting point begins to rise, presumably as a result of increasing van der Waals interactions. Viewed in this light, the observation of a sharp melting peak (-51.9 °C) in the thermogram for **15c** (longer alkyl chains) and the absence of one in **15b** (shorter alkyl chains) makes corroborates Nakanishi's theory.

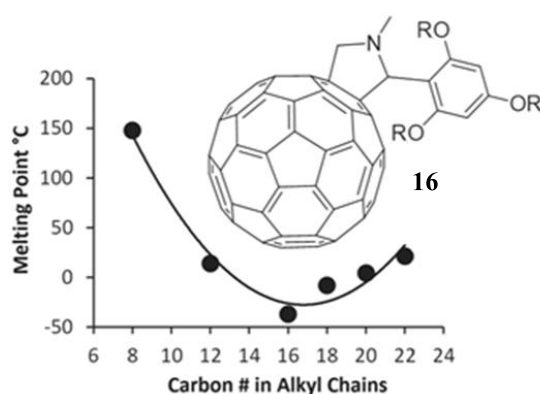


Figure 1.6 Nakanishi's liquid fullerene derivatives **16** showing melting point dependence on alkyl group length.

Returning to Nakanishi's pyrene-based RTILs, rheological analysis of **12-15** showed that the viscosity is primarily dependent on alkyl chain length. The authors coined the term "alkyl friction" for this effect. In addition to the strong correlation between viscosity with alkyl chain length, the substitution pattern of the phenyl groups also has a predictable and explainable effect on viscosity. Compound **15b** displays higher viscosity than compound **12b**, presumably because the substitution pattern inherently orients the alkyl groups away from the pyrene core. Consequently, the alkyl groups of neighboring molecules tend to point toward one another and possibly interdigitate, which is a favorable environment for alkyl friction. On the other hand, the more inward orientation of one of the alkyl groups on each phenyl group in **15b** provides a less favorable environment for alkyl friction. The alkyl friction hypothesis nicely explains the experimental rheological data. The complex viscosities are in the following order: $\eta^*_{15b} > \eta^*_{15c} > \eta^*_{12b} \geq \eta^*_{13b} > \eta^*_{14b}$.

The photophysical properties of the pyrene derivatives **12-15** were measured and the dilute solution phase emission and absorption analyses of all members of the series showed simple monomeric spectra reminiscent of the parent pyrene (**10**). The absorption maxima of **14b** and **12b** (341 and 377 nm) were observed to be slightly blue-shifted with respect to those of **13b** and **15b** (345 and 382 nm). This was explained by the difference in dihedral angles about the biaryl bonds, which could be traced back to the difference in substitution pattern of the alkoxy groups. The calculated structures of 3,5-disubstituted model compounds **13a** and

15a (with methyl groups for computational ease) had dihedral angles of 57.8° and 58.7°, whereas those of the corresponding the 2,5-disubstituted compounds **14a** and **12a** were found to be slightly larger (62.2° and 61.6°). It was argued that the larger dihedral angle leads to a decrease in the conjugation between the two pi systems and thus leads to the observed blue shift.

Monosubstituted pyrene **13b** shows a broadening of absorption peaks when moving from the dilute solution phase to the neat liquid. The broadening was attributed to pyrene-pyrene interactions and the large red-shifting (by 90 nm) and broadness of the emission is characteristic of excimer emission. Clearly compound **13b** like **14b** (*vide supra*) has strong pyrene-pyrene interactions and is not a candidate for the desired type of FML (*i.e.* one that displays identical neat liquid and solution photophysical properties). Compound **15b** with four times the alkyl groups of **13b** still shows a broad absorption spectrum but not broad to the degree of **13b** indicating weaker but significant pyrene-pyrene interactions. The absorption peaks of **15b**, very similar to **15c**, are broadened. In the context of material design, this is an interesting finding as it indicates that with a poor substitution pattern (3,5- in this case) for liquefaction increasing the length of the alkyl chains is unlikely to bring liquefaction. Comparing **15b** and **12b**, the power of the 2,5-pattern (atropisomerism + directionality) is apparent. **12b**'s absorption spectrum is essentially identical in both the dilute solution and neat liquid phases, indicating there are almost no pyrene-pyrene interactions. In addition, the fluorescence spectrum is still sharp, excimer free and only red shifted 12 nm. The authors explained that a small red shift going from dilute solution to neat liquid in the true liquids (*cf.* 22 nm in **15b**) as simple solvatochromism is brought upon by a change in vibronic structure,

and essentially the compound is solvated by other molecules of **15b**, not typical solvent molecules.

The series of liquids **12** through **15** are all highly fluorescent with fluorescent quantum yields between 0.57 and 0.85 and all give a blue luminescent color. It was discovered that excimer formation in the neat liquids that do allow pyrene-pyrene interactions, especially **13b** can do so on very fast time scales. Compound **13b** formed excimers much faster in the neat liquid phase than it or pyrene does in solution (0.65 ns neat, *cf.* < 5 ns in solution), and this result has implications in the theory of excimer formation which assumes the predominant mechanism of excimer formation in the condensed phase was through excitation of preformed van der Waals dimers. SWAXS analysis reveals in **13b** an absence of stacked pyrene structures however the excimer yield is very high. Diffusion of molecules through the high viscosity medium is too slow to allow such fast excimer formation. The theory of EET (exciton energy transfer) was invoked to explain this. Through dipole-dipole coupling the exciton can hop to a neighbor that is well stacked, rationalizing the seemingly, impossibly high excimer yield given the apparent scarcity of well stacked structures in liquid **13b**.

Taking a closer look at the emission spectra of **12** through **15** reveals another interesting feature of two members of the series. While **13b** shows pure excimer emission, **14b** a mix of monomer and excimer and **12b** pure monomer emission, **15b** and **15c** display a spectrum that is intermediate between monomer and excimer emission. The small changes observed in the intermediate spectrum were assigned to monomer exciton decaying by interacting strongly with neighboring pyrenes but not through face-to-face excimer formation from the high viscosity of the bulk liquid. The authors noted that this intermediate type of

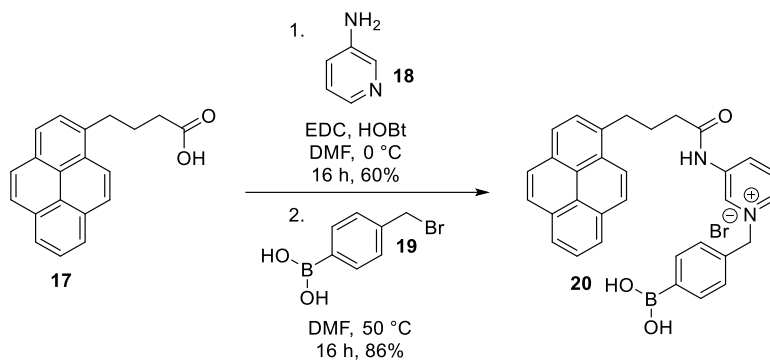
emission found in **15b** and **15c**, is difficult to engineer and rarely seen except in the solid state. The pyrene-based FMLs have a serious advantage over solid materials in that the color of emission is essentially independent of external influence and thus devices utilizing the liquids would be stable to deformation unlike its solid counterparts.

Pyrene-Based Sensors and Molecules for Information Processing

As outlined earlier, pyrene has a long and ever-developing history of being used as a fluorescent probe in the development of chemical sensors. In this regard, one area of intense current research interest is the sensing of glucose in human blood.^[20] Ratiometric sensors based on boronic acids are the industry standard, but the development of highly effective sensors is hampered by the unfortunate fact that fructose binds to boronic acids with a binding constant nearly two orders of magnitude larger than glucose. This serious issue of selectivity has been somewhat mitigated by the artful design of complex molecules, either bearing multiple boronic acid docking sites or by the careful design of a molecular cavity to promote selectivity.^[20] The downside of such systems is the need for extensive and complicated synthesis, which has a serious impact on the cost and time associated with production. The current value of the glucose sensing market is \$1.7 billion and this is expected to rise to \$10 billion by 2027.^[20] In this arena, competition is high and easily scalable chemistry is therefore highly desirable.

In this context, the synthesis of a new pyrene-based glucose sensor was recently reported by the groups of James and Jiang.^[20] The synthesis of **20** had a number of significant

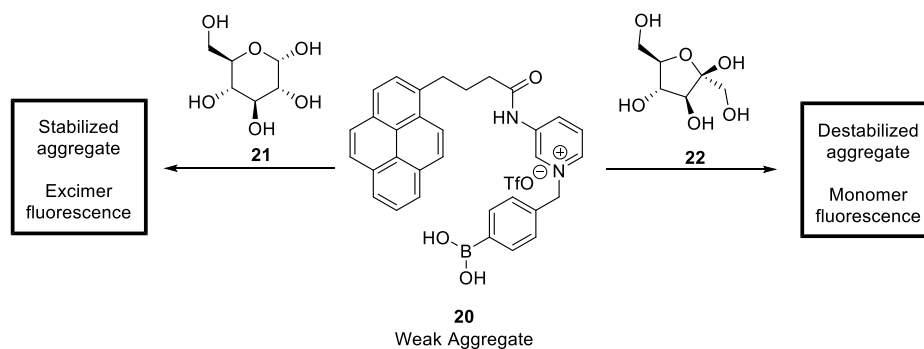
advantages. It required just two steps, used only commercially available materials (**17**, **18** and **19**) and proceeded using reactions that are known to be robust and reliable (amide formation and S_N2 reaction). The function of the sensor **20** took advantage of pyrene's hydrophobicity, electron donating ability and strong fluorescence.



Scheme 1.4 James' and Jiang's two-step synthesis of glucose sensor **20**.

Cationic pyrene-containing sensor **20** forms “weak aggregates” in aqueous solution and consequently displays weak excimer emission. This rather simple molecule shares a complex relationship with saccharides in aqueous solution and overcomes the problem of fructose binding affinity in an elegant way. With glucose, a 2:1 complex is formed, the exact structure of which was not determined. Whatever it may be, the two-pyrene complex forms stronger aggregates in aqueous solution, which strongly enhances excimer emission. Interestingly, glucose is the only saccharide (of those tested) that exhibits this property. Fructose (and to lesser extent mannose and galactose) still has the same problematic higher binding affinity to the boronic acid moiety of **20** as previous sensors, but it does so with a 1:1 stoichiometry. Fructose binding now destabilizes the aggregates and thus causes a modest boost in monomer emission (Scheme 1.5). Remarkably, for a molecule of such structural and

synthetic simplicity, the unique binding ratio of **20** with glucose in comparison to other saccharides and the resulting destabilization/stabilization of the pyrene aggregates render **20** the most sensitive and selective boronic acid-based glucose sensor published to date.



Scheme 1.5 Glucose-selective sensor **20**.

Pyrene as a Nanotube Anchor

Among pyrene's most interesting properties is its propensity to irreversibly bind to graphene and carbon nanotubes (CNT).^[20] This being the case, appropriately functionalized pyrene systems have been used for some time in attempts to solubilize single-walled CNTs. One of the main objectives of this work is to achieve selectivity in the type of nanotube that is solubilized. Success in this endeavor would allow for separation using top-down methods to solve bottom-up problems. In the same vein, the strong pyrene-nanotube interaction is being exploited by various groups for other purposes, such as to drive the self-assembly of redox-active composite materials, or as an anchor chain in the immobilization of biomolecules.

Within the realm of redox-active composite materials, one important area of application is in batteries. Lithium-based batteries are currently the industry standard and enjoy a \$US 37 billion market share, which is expected to rise by \$100 billion in the next seven years. There are several drawbacks to lithium-based batteries and organic chemistry potentially has much to offer in this field.

As pointed out by Baumgartner,^[21] lithium is not highly toxic, but conventional lithium-based battery systems still use heavy metals (including cadmium and lead) in the electrodes and are therefore a significant contributor to worldwide pollution. Carbon nanotubes are an attractive electrode material. They are abundant, conductive/semiconductive and (as far as we know) environmentally less harmful, though not benign.^[22] Furthermore, they have tremendous advantages over traditional inorganic crystalline materials. The process of charging a battery generates a significant amount of heat, which results in thermal expansion. The repeated expansion and contraction cycles that accompany charging and discharging are the most important contributor to degradation. Mechanically robust carbon nanotubes heat less during charging and are therefore less prone to degradation than their inorganic counterparts. CNT-based batteries can also be charged and discharged more quickly than conventional inorganic material-based batteries.

Thinking of CNTs as molecular wires, methods to connect, intercalate, promote or deny interactions between wires is highly valuable. Baumgartner *et al.*^[21] have devised a phosphaviologen-based system **25** that utilizes pyrene's strong interaction with nanotubes (Figure 1.7). While the intimate details of the electrochemical properties of the phosphaviologen core are outside of the scope of this introduction (and elegantly detailed in

Baumgartner's paper), the use of peripheral pyrenes is not. In fact, the electronic disconnection of the pyrene from the phosphaviologen using a methylene spacer is enough to allow the phosphaviologen system to act on its own. What the pyrene units bring to the table is the formation of a junction point between two nanotubes. This is an intriguing concept, which has been addressed through other methods, although certainly not with the experimental simplicity of Baumgartner's achievement. The bispyrenephosphaviologen **25** is simply dissolved in acetonitrile with a suspension of single-walled CNTs and the mixture is sonicated (Figure 1.8). Amazingly, this is the only step required to achieve the preparation of an electrode material with significantly different electronic properties from the original CNT. In this regard, another aspect to thinking of a carbon nanotube as a molecular wire is that the strong binding of pyrene to its surface results in modification of the intrinsic electrical and photophysical properties of the tubes themselves.

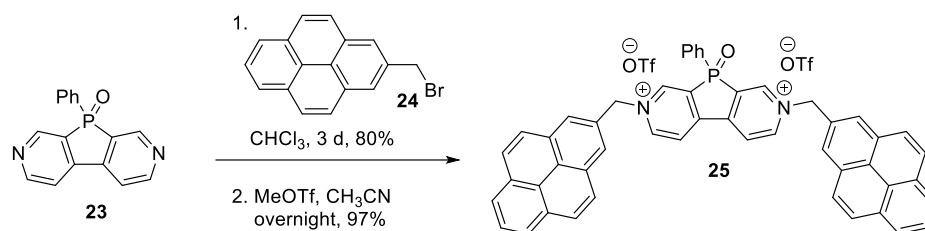


Figure 1.7 Synthesis of bispyrenephosphaviologen **25**.

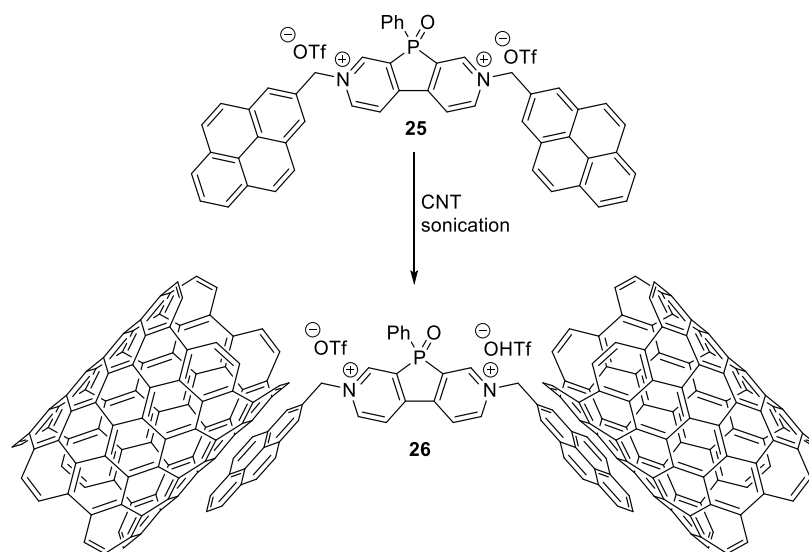


Figure 1.8 Baumgartner’s bispyrenephosphaviologen and carbon nanotube composite (**26**).

Pyrene may also be used as an anchor from biomolecules such as proteins, which are distinct from what the chemist would call a molecule. In asymmetric organic synthesis, the use of proteins (enzymes) is very attractive because they are known to achieve a broad range of reactions with diastereo- and enantioselectivities that are unachievable chemically, at least at this time. A striking example is cytochrome p450 oxidase, which brings about the smooth conversion of hexadecenoic acid to (*R*)-13-hydroxyhexadecanoic acid with total selectivity for both the site of oxidation and the absolute configuration of the newly-formed stereogenic centre.^[23] While research in the field of C–H activation has furnished many successes in recent history,^[24] any chemist would agree that the complete selectivity in this reaction is unachievable at this time using “normal” chemical methods. Slightly detracting from the tremendous power of enzyme catalysis is the difficulty associated with running these reactions under ordinary conditions. Indeed, a major obstacle to the advancement of this field is that many enzymes

are relatively unstable and are easily denatured. Once denatured, they cannot always be re-natured. The ultimate dream of enzymatic catalysis is that of made-to-order synthetic enzymes, which are tailored for specific transformations. While synthetic enzymes have been achieved in the laboratory thanks to native chemical ligation,^[26] the brain child of Stephen B. H. Kent, we are still very far away from switching from using natural enzymes in a limited way to using designer enzymes to make whatever we require.

Immobilized enzymes may be the answer to some of these problems. One attractive method for protein immobilization comes from the binding of useful proteins to carbon nanotubes, which act as an insoluble scaffold and several groups have begun laying the groundwork for such systems. There are (at least) two motifs available to furnish the desired systems (Figure 1.9). First, a pyrene system could be incorporated into the non-essential amino acids of an enzyme to enable anchoring to the carbon nanotubes. Alternatively, one could make a double-ended anchor consisting of a pyrene, an appropriate spacer and an end that binds proteins.

Along the same lines, applications in sensing are also possible. The immobilization of proteins can bring together the tremendous selectivity of substrate binding allowed by enzymes coupled to the signature absorption and emission of CNTs provides access to interesting hybrid materials. Utilizing a commercially available pyrene-based compound, 1-pyrenebutanoic acid, succinimidyl ester, **27**, Dai *et al.*^[27] have achieved the functionalization of carbon nanotubes with an appropriate handle to bind enzymes in solution. By prefunctionalization of the tubes with a pyrene double anchor, two biologically relevant molecules, ferritin and streptavidin have been immobilized near the tubes surface. The

complexity of systems that can be made in this manner is mind boggling. CNTs can be patterned on gold surfaces to allow TEM imaging, electrochemistry and surface-enhanced Raman spectroscopy (SERS). Using an appropriately functionalized pyrene, one can imagine now binding nearly any biomolecule with an affinity for polar groups to the SWCNT-gold surface composite, thereby allowing the synthesis of highly complex systems through only in-solution mixing. This was illustrated by Dai *et al.*, who grew SWCNTs by laser ablation of graphite could and then deposited them on gold or SiO₂ surfaces. The functionalized surfaces were then bathed in a solution of **27** and the ternary composite material was finally exposed to a dilute solution of ferritin to afford a four-component assembly (surface, CNT, double-anchor, biomolecule). To ensure the ferritin was binding to the pyrene-appended anchors and not the gross substrate, AFM was used to locate the SWCNT and ferritin molecules. In comparison to a control experiment where the addition of **27** was omitted, it was clear that the binding was indeed selective, and a single-walled CNT tagged with pyrene had ferritin molecules anchored along its length (Figure 1.10). The availability of appropriate pyrene anchors both commercially and of higher complexity though synthesis coupled with the ease of preparation shown by Dai *et al.* testifies to the power and great potential of this approach. Coupling the ease of synthesis with the plethora of biomolecules or even small molecule sensors presents the exciting possibility of turning any sensor (be it enzyme, supramolecular assembly, small molecule or biomolecule) into a nanotube-sensor composite. Certainly, coupling of any system to a nanotube is not always advantageous, but the possibility of combining two sensor molecules through a decoupling spacer has possible applications in electrochemistry and molecular logic gates.

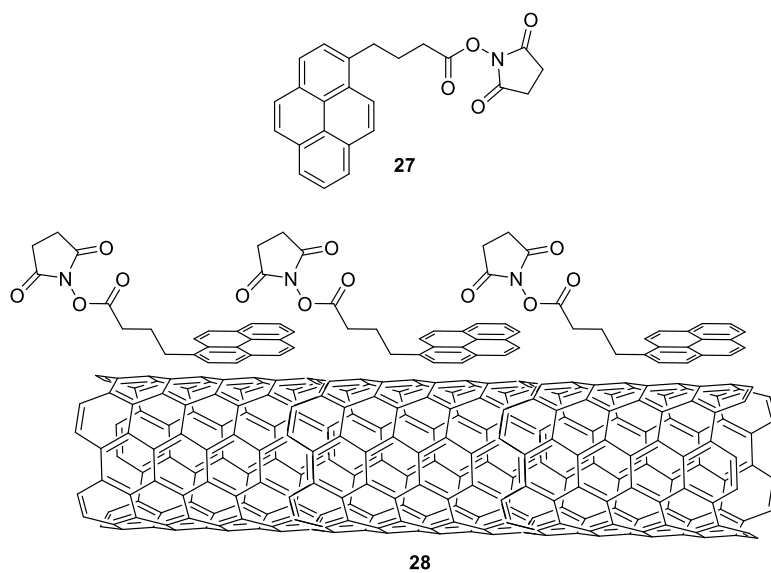


Figure 1.9 Dai's single-walled CNT appended with protein-binding-pyrene-based-double-anchor.

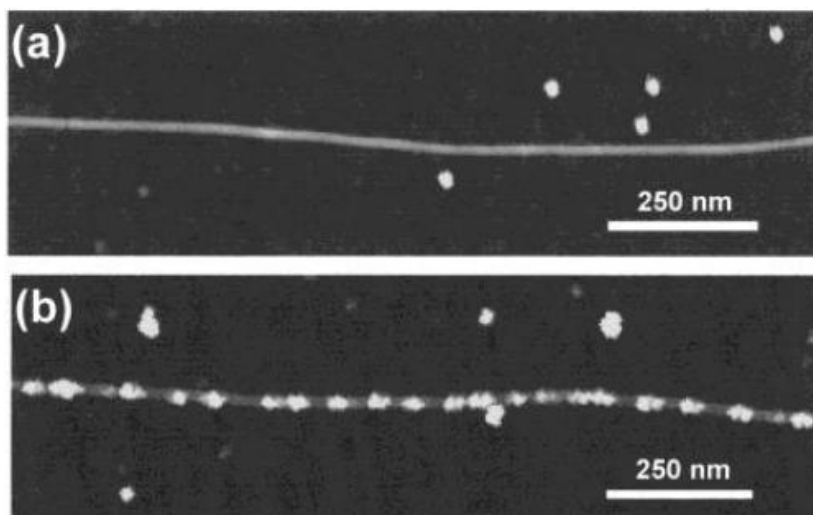
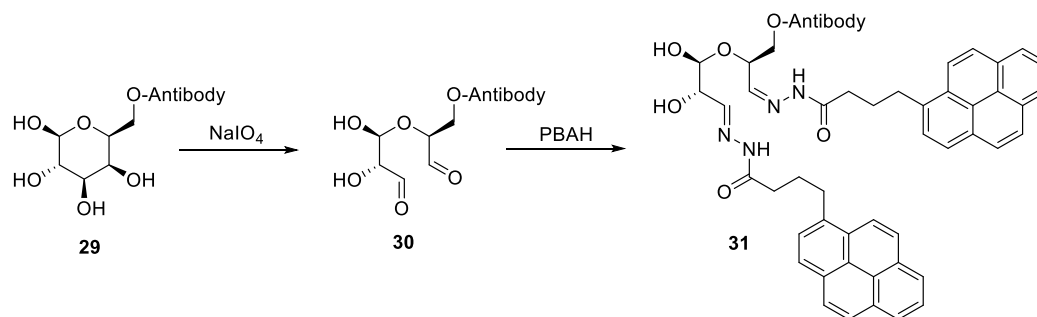


Figure 1.10 AFM imaging of the single-walled CNT without (A) and with functionalized pyrene anchor 27 (B).

An obvious advantage of the aforementioned type of protein immobilization is that the synthetic chemistry comes in at the double anchor point. The proteins themselves need not be modified, which obviates the need for a feat in either synthetic biology or synthetic organic chemistry. A major drawback comes from the size of biomolecules. If substrate binding occurs outside the Debye sphere² (Debye cylinder in this case) of the single-walled CNT, then no electronic or magnetic interactions will take place due to charge screening.

In contrast to Dai's strategy, Stefansson and coworkers have taken advantage of the highly selective modification of specific carbohydrates appended to antibodies, which allowed for the direct functionalization of the antibody with pyrene (Scheme 1.6).^[30] This structural motif has at least two advantages over immobilization. The antibody binding to living cells was found to be more uniform and the dual anchoring to the nanotubes brought the binding pocket of the antibody within the Debye length of the carbon nanotube, which resulted in much higher sensitivity. This, unlike Dai's sensors, allowed antibody binding to be seen in the emission spectra of the nanotubes themselves.



Scheme 1.6 Steffansson's pyrene-based SWCNT anchor **31**.

²¹ The Debye sphere is a measure of how far a charge's electrostatic effect extends in solution.

The number of systems and composite materials that could potentially be produced by utilizing pyrene's binding to nanotubes is staggering. The sheer number of possibilities coupled with the synthetic ease in docking pyrene anchors to tubes promises many more applications in the near future.

Conclusion

Even a brief review of the recent literature reveals that pyrene's elite status as a multi-purpose molecular gadget, whether at the business end of a particular assembly or in a supporting role, is in no danger of being lost. To the contrary, it appears to be picking up steam. The future for pyrene is very bright, as there are many exciting prospects for the development of new applications.

References

1. V. I. Vullev, H. Jiang, G. Jones, (2005) Excimer Sensing. In: C. D. Geddes, J. R. Lakowicz (eds) *Advanced Concepts in Fluorescence Sensing. Topics in Fluorescence Spectroscopy*, vol 10. Springer, Boston, MA.
2. T. M. Figueira-Duarte, K. Müllen, *Chem. Rev.* **2011**, *111*, 7260–7314.
3. X. Feng, J.-Y. Hu, C. Redshaw and T. Yamato, *Chem. – Eur. J.*, **2016**, *22*, 11898–11916.
4. M. Graetzel, J. K. Thomas, *J. Am. Chem. Soc.*, **1973**, *95*, 6885–6889.
5. P. Conlon, C. J. Yang, Y. Wu, Y. Chen, K. Martinez, Y. Kim, N. Stevens, A. A. Marti, S. Jockusch, N. J. Turro, W. Tan, *J. Am. Chem. Soc.* **2008**, *130*, 1, 336–342.

6. A. Mohr, P. Talbiersky, H.-G. Korth, R. Sustmann, R. Boese, D. Blaser, H. Rehage, *J. Phys. Chem. B* **2007**, *111*, 12985–12992.
7. J. Fritzsche. *Comptes Rendus Acad. Sci.*, **1867**, *69*, 333–343.
8. J. Hoche, H.-C. Schmitt, A. Humeniuk, I. Fischer, R. Mitric, M. I. S. Rohr, *Phys. Chem. Chem. Phys.* **2017**, *19*, 25002–25015.
9. S. Karuppannan, J.-C. Chambron, *Chem. Asian J.* **2011**, *6*, 964 – 984.
10. S. Grimme, *Angew. Chem. Int. Ed.* **2008**, *47*, 3430–3434.
11. M. K. Smalley, S. K. Silverman, *Nucleic Acids Res.* **2006**, *34*, 152–166
12. K. A. Hodgkinson, I. H. Munro, *Chem. Phys. Lett.* **1972**, *19*, 260–262.
13. R. Goddard, M. W. Haenel, W. C. Herndon, C. Kruger, M. Zander, *J. Am. Chem. Soc.*, **1995**, *117*, 30–41.
14. O. H. LeBlanc, *J. Chem. Phys.* **1962**, *37*, 916–917.
15. F. Lu, T. Nakanishi, *Adv. Opt. Mater.*, **2019**, *16*, 1900176 (1–29).
16. M. Guerbet, *C. R. Acad. Sci.* **1909**, *149*, 129–132.
17. F. Lu, T. Takaya, K. Iwata, I. Kawamura, A. Sacki, M. Ishii, K. Nagura, T. Nakanishi, *Sci. Rep.* **2017**, *7*, 3416.
18. S. S. Babu, T. Nakanishi, *Chem. Commun.* **2013**, *49*, 9373–9382.
19. A. Ghosh, T. Nakanishi, *Chem. Commun.* **2017**, *53*, 10344–10357.
20. F. Lu, K. Jang, I. Osica, K. Hagiwara, M. Yoshizawa, M. Ishii, Y. Chino, K. Ohta, K. Ludwichowska, K. J. Kurzydowski, S. Ishihara, T. Nakanishi, *Chem. Sci.* **2018**, *9*, 6774–6778.
21. J.-C. Li, T. Yu, M.-S. Ye, X.-J. Fan, *Thin Solid Films* **1999**, *345*, 236–239.
22. N. Kobayashi, H. Izumi, Y. Morimoto, *J. Occup. Health* **2017**, 394–407.

23. S. S. Babu, J. Aimi, H. Ozawa, N. Shirahata, A. Saeki, S. Seki, A. Ajayaghosh, H. Möhwald, T. Nakanishi, *Angew. Chem. Int. Ed.* **2012**, *51*, 3391–3395.
24. Y. Huang, W. Ouyang, Z. Li, J. S. Fossey, T. D. James, Y. Jiang, *J. Am. Chem. Soc.*, **2013**, *135*, 1700–1703.
25. C. R. Bridges, M. Stolar, T. Baumgartner, *Batter. Supercaps.* **2020**, *3*, 1–8.
26. Y.-S. Chen, W.-I. Luo, C.-L. Yang, Y.-J. Tu, C.-W. Chang, C.-H. Chiang, C.-Y. Chang, S. I. Chan, S. S.-F. Yu, *J. Inorg. Biochem.* **2014**, *134*, 118–133.
27. X. Tang, X. Jia, Z. Huang, *Chem. Sci.* **2018**, *9*, 288–299.
28. P. E. Dawson, T. W. Muir, I. Clark-Lewis, S. B. H. Kent, *Science* **1994**, *266*, 776–779.
29. R. J. Chen, Y. Zhang, D. Wang, H. Dai, *J. Am. Chem. Soc.* **2001**, *16*, 3838–3839.
30. S. Stefansson, H. H. Kwon, S. N. Ahn, *J. Nanotechnol.* **2012**, 1–8.

Chapter 2

Synthesis of Oligo(1,8-pyrenylene)s: A Series of Functional Molecular Liquids

Statement of Co-Authorship

This chapter has been published under the above title in *ChemPlusChem* **2019**, *84*, 754–765.

Authors: Joshua C. Walsh, David T. Hogan, Kerry-Lynn M. Williams, Simon D. Brake, Dr. Gandikota Venkataramana, Tara A. Misener, Brandon J. Wallace, Prof. Richard P. Johnson, Prof. David W. Thompson, Prof. Yuming Zhao, Prof. Brian D. Wagner, Prof. Graham J. Bodwell

This article was a group effort combining the work of several graduate and undergraduate student co-authors from the research groups of Brian D. Wagner and Graham J. Bodwell

Joshua C. Walsh (listed in the paper as 1st author): Performed the large majority of the synthetic work, physical data collection (aside from photophysical data) and contributed significantly to the preparation of the manuscript.

David T. Hogan, Kerry-Lynn M. Williams, Simon D. Brake and Gandikota Venkataramana: Contributed to the early development of the iterative synthetic strategy.

Tara A. Misener and Brandon J. Wallace: Contributed to collection of the photophysical data.

Richard P. Johnson: Calculated the rotational energy barrier for the 1,1'-bipyrenyl system.

David W. Thompson: Contributed to the analysis of photophysical data and the writing of the corresponding section of the manuscript.

Yuming Zhao: Calculated optimized structures, dipole moments and energy differences in the diastereomers of the pyrene trimer.

Brian D. Wagner: Supervised Tara A. Misener and Brandon J. Wallace, contributed to the collection and interpretation of the photophysical data and the writing of the corresponding section of the manuscript.

Graham J. Bodwell: Is the principal investigator of this work, who led the project and contributed to the interpretation/analysis of data and the writing of the manuscript.

The article has been reproduced in this chapter in a modified form that includes the contributions of all the co-authors for the purpose of a complete discussion.

Introduction

Pyrene is an increasingly useful building block for the synthesis of designed π systems, due mainly to its intense fluorescence and the sensitivity of its fluorescence to its microenvironment. Although pyrene has featured prominently in a large number of designed π systems,^[1] only a few oligoarylenes composed exclusively of pyrene units have been reported. This includes, but is not limited to, dendrimers **1** and **2**,^[2] cyclic oligo(1,3-pyrenylene) **3**,^[3] poly(2,7-pyrenylene) **4**^[4] and oligo(1,6-pyrenylene)s **5** (Figure 2.1).^[5] Some poly(pyrene)s with varying degrees of polydispersity and integrity of the substitution pattern, as well as oligomers with mixed substitution patterns have also been reported.^[6] Oligopyrenes **1-5** all exhibit strong fluorescence, which makes them candidates for use as luminescent materials in organic optoelectronic devices.

Unlike oligo(pyrenylene)s **1-5**, which are all solids, some recently reported pyrene-containing oligoarylenes, e.g. **6**, were found to be liquids at room temperature.^[7] This property is very unusual for an aromatic molecule of its size. Combined with their luminescence, this property renders them functional molecular liquids (FML).^[8] Organic FMLs have been described as “the third generation of liquid chemicals after the first and second generations of solvent liquids and ionic liquids, respectively”^[8b] and are a rapidly-emerging class of compounds owing to their ease of processability in device fabrication (e.g. using painting and printing techniques), ease of deformation within devices, high thermal stability and their ability to act as solvents for dopants.^[8] FMLs have also been used as the basis for the formation of white-light emitting luminescent inks.^[8e]

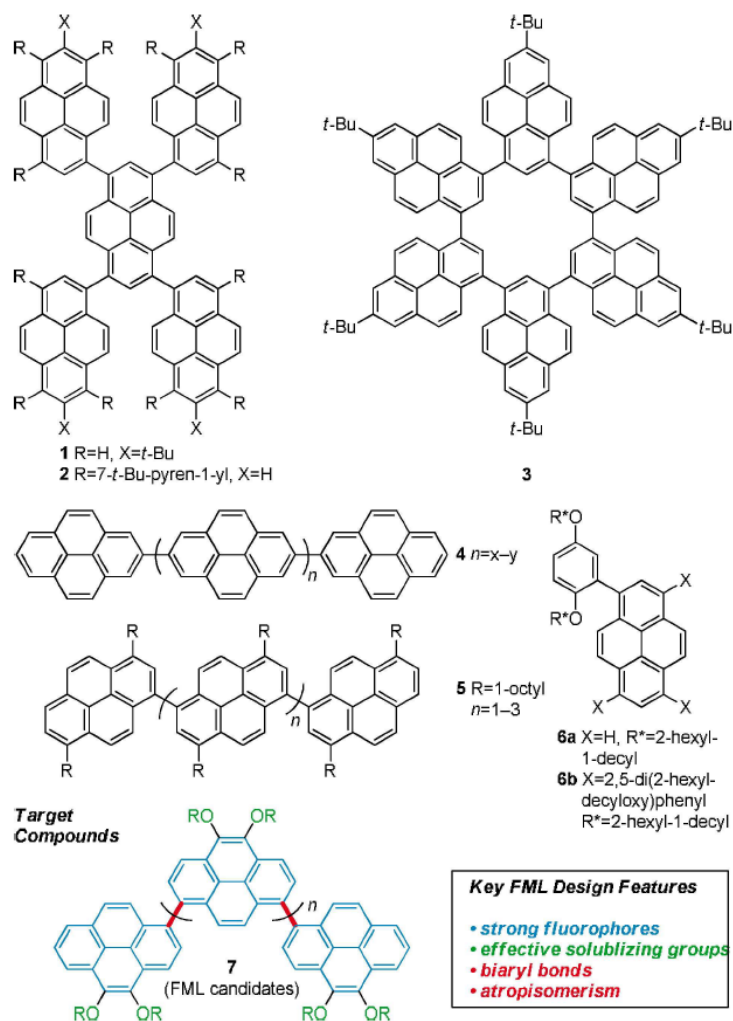


Figure 2.1 Oligo(pyrenylene)s **1–5**, pyrene-based FMLs **6** and oligo(1,8-pyrenylene)s **7**.

Nakanishi's guidelines for the design of FMLs address certain key structural features that disfavor $\pi-\pi$ interactions and thus suppress solidification.^[7] These include biaryl bonds, alkoxy substituents with branching and low symmetry in the pi skeleton. The notion that some combination of these structural features underpins the room temperature liquid

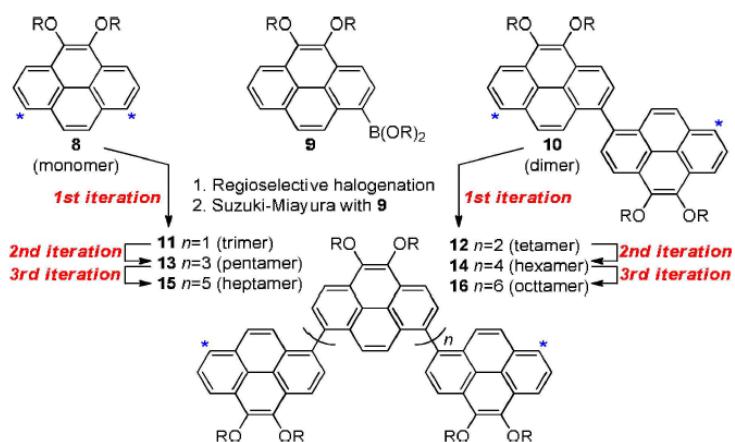
behavior and our recent interest in the synthesis of designed π systems featuring 1,8-pyrenylene units^[9] fueled work in our group aimed at the synthesis of oligo(1,8-pyrenylene)s **7**. Like **6**, these purely pyrene-based oligoarylenes have biaryl bonds and are adorned with alkoxy substituents. Furthermore, the high barrier to rotation about the 1,1'-bipyrenyl bond (25.8 kcal/mol)^[10] means that atropisomerism comes into play and mixtures of diastereomers will be expected starting with the trimer (**7**, n=1). These (or any) diastereomers will have different shapes, which would be expected to disfavor long-range ordering and thus inhibit solidification. In fact, Nakanishi's FMLs are also mixtures of diastereomers due to the presence of a stereorandom stereogenic center in each of the eight Guerbet-alcohol-derived side chains. For example, there are eight side chains in **6b**, which gives rise to 44 diastereomers. Thus, diastereoisomerism is a separate issue from branching alone, which may or may not bring with it stereochemical consequences. Finally, with multiple pyrene units in the oligo(1,8-pyrenylene)s **7**, strong fluorescence would be expected, so they appear to be promising candidates for new FMLs. We report here the synthesis and characterization of the monomer through the pentamer.

Results and Discussion

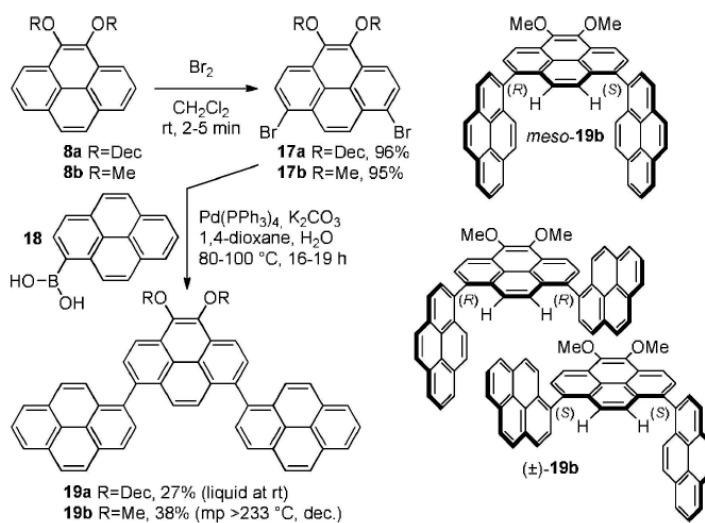
Akin to Rathore's synthesis of the oligo(1,6-pyrenylene)s **5**,^[5] an iterative strategy was envisioned for the synthesis of the oligo(1,8-pyrenylene)s **7** (Scheme 2.1). Each iteration consists of a regioselective bromination (at the starred positions) followed by a Suzuki-Miyaura cross-coupling with an appropriate boronic ester **9**. Application of this strategy to the

monomer **8**^[11] would successively give rise to the odd-numbered oligomers (**11**, **13**, **15**, etc.) and dimer **10** would serve as a starting point for the synthesis of the even-numbered oligomers (**12**, **14**, **16**, etc.). The success of this strategy hinges on the maintenance of the complete regioselectivity of the bromination step for the starred positions of each oligomer and the development of a way to gain access reliably to synthetically usefully quantities of a boronic acid/ester **9**, which comes into play during every iteration.

Synthetic work aimed at realizing the iterative strategy commenced with 4,5-dialkoxypyrenes **8a** and **8b**, which were synthesized from pyrene by *K*-region oxidation^[12] and reductive alkylation as previously described (Scheme 2.2).^[11] Reaction with Br₂ afforded the corresponding dibromides **17a** and **17b** in high yield. The Suzuki-Miyaura step was first tested using commercial pyrene-1-boronic acid (**18**) and this afforded 1,8-dipyren-1-ylpyrenes **19a** and **19b**. The yields were modest, but the observation that **19b** is a high-melting solid (mp >233 °C, dec) and **19a** is a room-temperature liquid was striking. For these compounds, side chain length is clearly an important contributor to the suppression of solidification. It was therefore decided to employ decoxy groups for the synthesis of the targeted oligo(1,8-pyrenylene)s.



Scheme 2.1 Iterative strategy for the synthesis of oligo(1,8-pyrenylene)s.



Scheme 2.2 Synthesis of 1,8-dipyren-1-ylpyrenes **19a** and **19b** and a depiction of the two diastereomers of **19b**.

The branched (chiral) alkyl groups employed by Nakanishi, which rendered his FMLs mixtures of diastereomers, were not considered here because the atropisomerism of the 1,1'-

bipyrenyl system was expected to result in the formation of mixtures of diastereomers. Indeed, the ^1H NMR spectra of **19a** and **19b** (Figure 2.2) exhibit two sets of signals, which is consistent with the presence of two slowly interconverting atropisomeric diastereomers, i.e. *meso*-**19a** and (\pm)-**19a**. For both compounds (**19a** and **19b**), the highest-field aromatic signals are a pair of singlets (no COSY cross-peaks, see Supporting Information) attributable to the *K*-region protons of the central pyrene unit (δ 7.53 and 7.49 ppm for **19a**; δ 7.50 and 7.47 ppm for **19b**). In both cases, the higher-field signal is slightly more intense and integration points to a 53:47 ratio of the two diastereomers. Some broadening was observed upon heating to 110 $^\circ\text{C}$, but the system was clearly not close to coalescence. This is in line with the calculated barrier of 25.8 kcal/mol.^[10] For **19b**, where $\Delta\nu = 14.7$ Hz for the two *K*-region singlets, this barrier would correspond to a coalescence temperature (T_c) of 217 $^\circ\text{C}$.

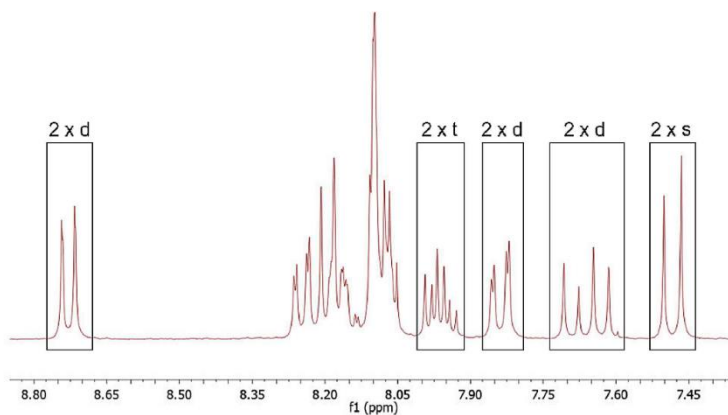


Figure 2.2 Aromatic region of the 300 MHz ^1H NMR spectrum of **19b** in CDCl_3 .

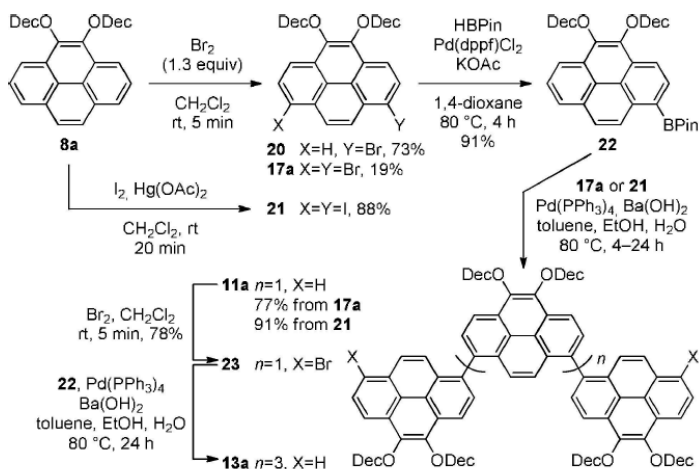
Progress with the iterative strategy could not be made with **19a** and **19b** because each of the terminal pyrene units has three sites available for electrophilic aromatic substitution.

Accordingly, attention was turned to the synthesis of a boronic acid or ester of the general structure **9**. The main challenge in accomplishing this was the selective monofunctionalization of 4,5-didecoxy pyrene (**8a**).

Monobromination of **8b** with Br₂ at -78 °C has been reported,^[13] but the compound was used without purification and no indication of the distribution between unbrominated, monobrominated and dibrominated products was given. Nevertheless, this result suggested that selective monobromination of **8a** was achievable. Preliminary attempts to monobrominate **8a** using Br₂, CuBr₂ and NBS all gave mixtures of unbrominated, monobrominated and dibrominated products under a variety of conditions. To better understand the progress of the reaction, an experiment was performed in which Br₂ was added to a CH₂Cl₂ solution of **8a** (500 mg) in 0.1 equivalent portions at room temperature. TLC analysis following each addition showed that the expected new spot for monobromide **20** (R_f=0.10, 20% CH₂Cl₂/hexanes) appeared after the first addition, a little ahead of the one for **8a** (R_f=0.15). A second, new faster-moving spot corresponding to dibromide **17a** (R_f=0.20) appeared after the addition of just 0.3 equivalents of Br₂. The starting material **8a** was fully consumed only after the addition of 1.3 equivalents of Br₂ and the last vestiges of monobromide **20** disappeared after the addition of 2.2 equivalents. The addition of 10 equivalents of Br₂ or the use of neat Br₂ as the solvent does not result in further bromination.

In an attempt to delay the onset of dibromination, the reaction was performed at lower temperatures. At 0 °C and -20 °C, dibromide **17a** again appeared after the addition of just 0.3 equivalents of Br₂. At -40 °C and -78 °C, **8a** precipitated from the reaction. Based on these results, it was decided to move forward with the addition of 1.3 equivalents of Br₂ at room

temperature, which would require the separation of just two compounds and not three. For practical purposes, slow addition of a solution of 1.3 equivalents Br₂ in CH₂Cl₂ was also found to result in the complete consumption of **8a** and the reaction could be scaled up to 5 g of **8a**. At this scale, a 73% yield of **20** was obtained along with 19% of **17a** (Scheme 2.3). It is worth noting that the chromatographic separation of **20** from **17a** was found to be easier than the separation of **20** from **8a**, even though the differences in R_f values did not suggest this.



Scheme 2.3 Synthesis of boronic ester **22**, trimer **11a** and pentamer **13a**.

With access to multigram quantities of **20**, its conversion to boronic ester **22** was investigated. Lithiation-borylation protocols were found to be unsatisfactory and, after screening various sets of conditions, it was found that Miyaura borylation using HBpin, Pd(dppf)Cl₂ and KOAc in 1,4-dioxane enabled the synthesis of **22** in 91% yield on a 1.5 g scale. The synthesis of the odd-numbered oligomers then commenced with the Suzuki-Miyaura cross-coupling between dibromide **17a** and boronic ester **22**, which afforded trimer

11a (77%) (Scheme 2.3). The use of Ba(OH)₂ instead of K₂CO₃ was found to give much better yields. No dimeric species arising from incomplete Suzuki-Miyaura reaction or protodebromination were observed (TLC, NMR analysis). As in the case of **19a** and **19b**, the ¹H NMR spectrum of **11a** showed the presence of two diastereomers. Singlets for the central *K*-region protons were observed at δ 7.50 and 7.48 ppm, but this time the lower-field signal was slightly more intense (51:49). Again, broadening of the signals was observed at 110 °C, but nothing approaching coalescence. No TLC conditions could be found that resulted in even the slightest separation of the two diastereomers of **11a**, so the determination of which isomer is dominant presented a stiff challenge. Structures of the *meso* and (\pm) diastereomers (using MeO substituents instead of DecO for computational ease) were calculated at the B3LYP/6-31G(d) level of theory using a chloroform solvent model. The *meso* isomer ($\mu_{\text{calc}}=0.57$ D) was calculated to be 0.12 kcal/mol lower in energy than the (\pm) isomer ($\mu_{\text{calc}}=0.22$ D), which corresponds to a 55:45 ratio.

The bromination of **11a** was not as straightforward as that of **8a**. As with **8a**, TLC monitoring of the addition of successive 0.1 equivalent portions of Br₂ revealed the appearance of first one faster-moving spot and then another corresponding to the formation of a monobromide and then dibromide **23**. The differences in the *R_f* values, however, were smaller than before, which did not bode well for chromatographic separation, and the starting material spot persisted until the addition of 1.9 equivalents of Br₂ (*cf.* 1.2 equivalents for **8a**). Additionally, while **8a** was found to be resistant to over-bromination, exceeding 2 equivalents of Br₂ resulted in overbromination of **11a**, as indicated by TLC (appearance of a new spot ahead of dibromide **23**). The best result was obtained when **11a** was reacted with 2.03

equivalents of Br₂. This afforded dibromide **23** in 78% yield after repeated chromatography. Suzuki-Miyaura reaction of **23** with boronic ester **22** then afforded pentamer **13a** (84%), which has six possible diastereomers (statistical ratio = 1:2:2:1:1:1), arising from the four axes of asymmetry.

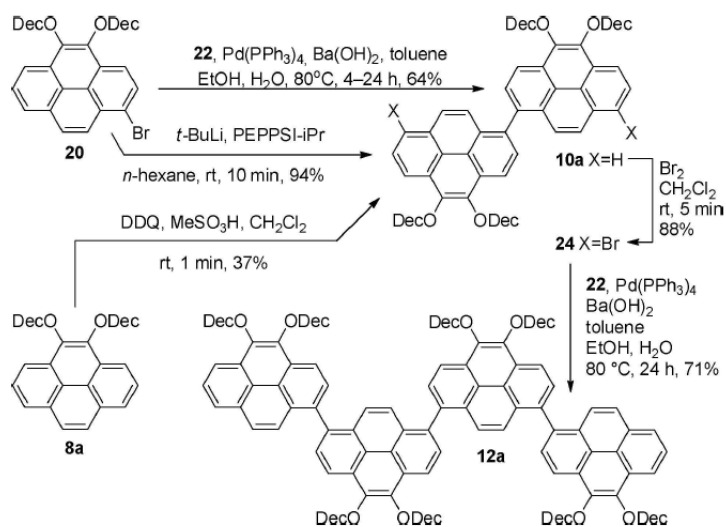
For the even-numbered oligomers, dimer **10a** was required. This compound was synthesized using three methods (Scheme 2.4). First, Suzuki-Miyaura coupling of bromide **20** with boronic ester **22** gave **10a** in 64% yield. Second, Feringa's PEPPSI-iPr catalyzed homocoupling^[14] of bromide **20** delivered **10a** in 94% yield. Finally, intermolecular Scholl reaction of monomer **8a** using Rathore's DDQ/MeSO₃H method^[15] proceeded in 37% yield. Although the yield of the latter reaction is substantially lower than those of the first two, it is attractive from a practical perspective. It uses a less precious starting material, is trivially easy to perform and is finished within seconds. Higher oligomers (up to hexamer) could also be observed by MALDI-MS and trimer **11a** could be reliably isolated from this reaction in up to 17% yield.

Dimer **10a** underwent bromination smoothly using 2.0 equivalents of Br₂ to afford dibromide **24** in 88% yield. When a small excess (up to 3 eq.) of Br₂ was employed, overbromination did not occur. Instead, a new bright yellow compound with a much lower R_f value began to form. It was never formed in sufficient quantities to enable the acquisition of an NMR spectrum, but MS analysis ($m/z = 902$; most abundant signal for C₅₂H₅₄Br₂O₄) was consistent with one of the 4,5-dideoxypyrene units having been converted to a pyrene-4,5-dione unit. Tetramer **12a** was obtained in 71% yield upon Suzuki-Miyaura reaction of dibromide **24** with boronate **22**. This oligomer has four possible diastereomers (statistical ratio

= 1:1:1:1) arising from the three axes of asymmetry. The use of aryl iodides instead of bromides was investigated as a possible way of improving the yields of the Suzuki-Miyaura cross-coupling reactions. Monomer **8a** was found to undergo rapid (20 min) and fully regioselective diiodination upon reaction with I₂, Hg(OAc)₂ to afford diiodide **21** (88%). Upon increasing the reaction time to 2 h, the yield plummeted to 50%. The drop in yield is clearly due to a dealkylation/oxidation reaction as pyrene-4,5-dione was isolated. In fact, this diketone is also present at the end of the 20-minute reaction (TLC analysis). The use of the diiodide **21** in the Suzuki-Miyaura reaction with boronic ester **22** led to a significant improvement of the yield of trimer **11a** (91%) (Scheme 2.3). The same improvement could not be achieved for higher oligomers because attempted iodination of dimer **10a** and trimer **11a** resulted in rapid and complete consumption of the starting materials to give mainly TLC immobile compounds. Clearly, the ease of the dealkylation/oxidation process increases with the size of the oligomer.

A key concern with tetramer **12a** and pentamer **13a** was the ability to assess purity. The presence of four and six diastereomers, respectively, complicates the NMR spectra to the point that it is impossible to tell whether they are contaminated with lower oligomers (with or without bromine atoms), which might arise from incomplete Suzuki-Miyaura reaction and/or protodebromination. Using a number of standard TLC solvent systems, e.g. 10:90 dichloromethane / hexanes, dimer **10a** through pentamer **13a** were barely distinguishable (Figure 2.3A, left). After extensive experimentation, it was found that the use of 5:5:90 toluene / dichloromethane / hexanes gave far better separation (Figure 2.3A, right). This allowed for more effective chromatography and, coupled with the intense fluorescence of the oligomers

(see below), enabled visual assessment of purity. To demonstrate this point, a 1:100 mixture of **11a:12a** was prepared and the minor component was clearly visible to the naked eye (Figure 2.3B). MS analysis using various techniques was initially very problematic due to extensive fragmentation, but it was ultimately discovered that LC-MS with APPI(+) ionization gave very reliable spectra, but only when the standard solvent system (90% acetonitrile / toluene) was changed to 90% isopropanol / toluene and the injection temperature was maximized. Under these conditions, no signals attributable to dealkylated compounds or lower oligomers arising from biaryl cleavage were observed.



Scheme 2.4 Synthesis of dimer **10a** and tetramer **12a**.

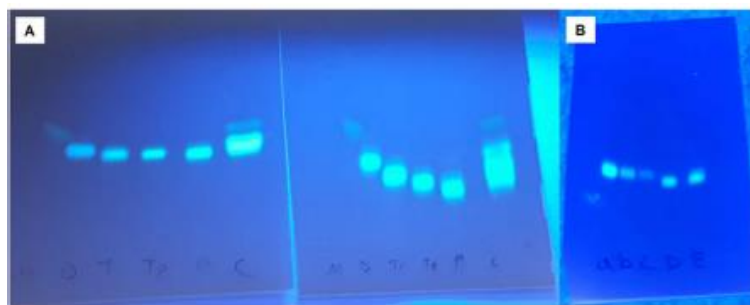


Figure 2.3 TLCs of oligomers, A = CH₂Cl₂/hexanes and CH₂Cl₂/toluene/hexanes. B = Purity experiment.

It is interesting to note that Rathore's monomer through pentamer series of oligo(1,6-pyrenylene)s **5**,^[5] which may also appear to be candidates for FMLs, are all solids with melting points that increase steadily from monomer (92–93 °C) to pentamer (198–200 °C). The oligo(1,8-pyrenylene)s **8a**, **10a–13a** behave very differently. The monomer **8a** is a low-melting solid (mp=38.4–39.5 °C) and the dimer remains a supercooled liquid for as long as six months after purification before eventually crystallizing (mp=30–34 °C). The trimer **11a**, tetramer **12a** and pentamer **13a** are all liquids that have never solidified. One sample of trimer **11a** has remained a liquid after ambient aging for over 7 years. No crystallization peaks were observed in DSC traces for **11a–13a** even after annealing at –42 °C for 12 hours (Figure 2.4),^[8c] which further supports the notion that these compounds are in fact room temperature liquids and not supercooled liquids.

The total absence of birefringence in samples of **11a–13a**, as observed by polarized optical microscopy (POM) (Figure 2.5), provided further evidence that these compounds are isotropic liquids at room temperature.

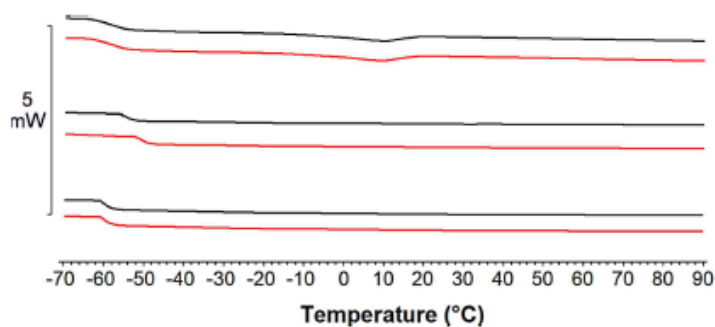


Figure 2.4 DSC thermograms for trimer **11a** (top pair), tetramer **12a** (middle pair) and pentamer **13a** (bottom pair) without annealing (black lines) and after annealing at -42°C for 12 h (red lines). Scale bar=2.1 W/g for **11a**, 2.4 W/g for **12a** and 2.3 W/g for **13a**.

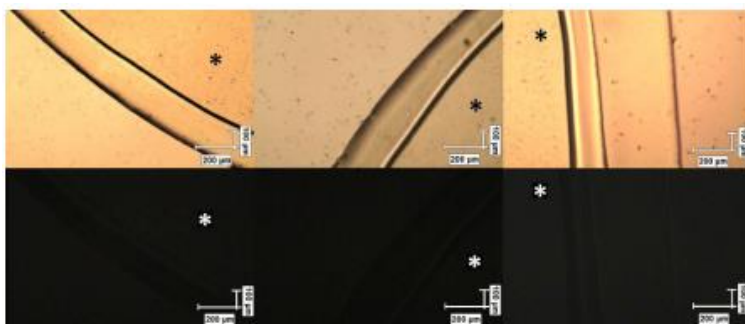


Figure 2.5 Optical microscopy (top) and polarized optical microscopy (bottom) for **11a** (left), **12a** (middle) and **13a** (right).

Small- and wide-angle X-ray scattering (SWAXS) measurements of trimer **11a** showed no features at all in the small-angle range and just very broad peaks at 21.0° and 42.5° in the wide-angle region (Figure 2.6). The former corresponds to a distance of 4.23 \AA , which is typical of an alkyl halo,^[8d] and the peak at 42.5° is likely the corresponding second order peak (corresponds to a distance of 4.25 \AA). The absence of any sharp peaks is indicative of the absence of long-range molecular ordering, which speaks to **11a** being a liquid. SWAXS was

not measured for **12a** and **13a** due to insufficient sample sizes, but the consistency of their DSC and POM suggest that they are also liquids.

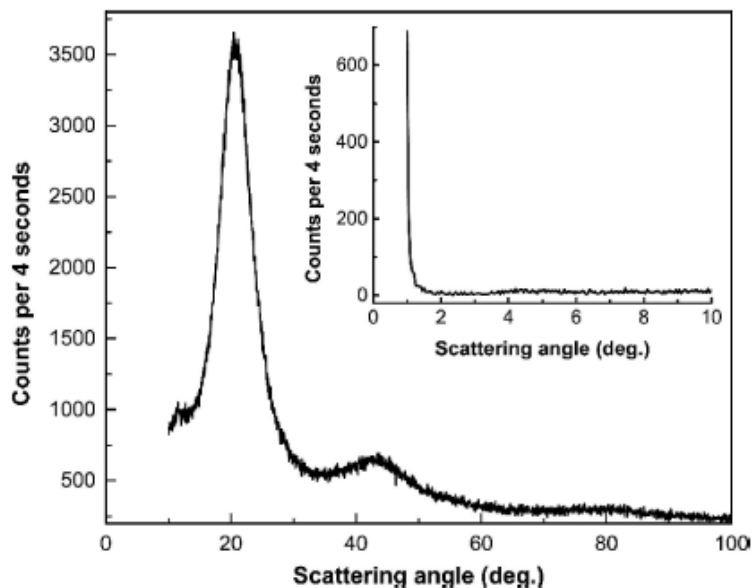


Figure 2.6 Small- (inset) and wide-angle X-ray scattering of trimer **11a**.

An aspect of Nakanishi's FMLs, e.g. **6**, that does not appear to have been addressed is that they are mixtures of diastereomers by virtue of the presence of a stereorandom stereogenic center in each of the side chains. Oligo(1,8pyrenylene)s **11a–13a** are also mixtures of diastereomers, but this arises due to axial chirality (atropisomerism in the π skeleton). Atropisomerism in the oligo(1,6-pyrenylene)s **5** was also not addressed, but based on the appearance of their NMR spectra, the trimer, tetramer and pentamer are clearly mixtures of diastereomers. The fact that they are increasingly high-melting solids may be attributable to the presence of alkyl instead of alkoxy side chains and the more linear (1,6) substitution pattern

of the pyrene units *vs.* the more bent pattern (1,8) for **11a-13a**. Based on the existing evidence, it is difficult to assess the relative importance of the various factors that contribute to keeping **11a-13a** in the liquid state. High thermal stability and low volatility of **11a** was revealed by thermogravimetric analysis (TGA), where no loss of mass was observed until *ca.* 325 °C (Figure 2.7). A 35% loss of mass was observed starting at 325 °C, followed by an 18% loss of mass starting at 560 °C. The first event is consistent with the loss of four of the six decyl side chains (36.7% of the initial mass) and the second loss of mass agrees very well with the cleavage of the remaining two decyl groups (18.3% of the initial mass). TGA of the tetramer **12a** and pentamer **13a** were similar to that of **11a**, showing the ultimate loss of *ca.* 55% of the original mass (all of the alkyl groups). For these compounds, only a slight (3-6%) loss of mass was observed prior to 325 °C.

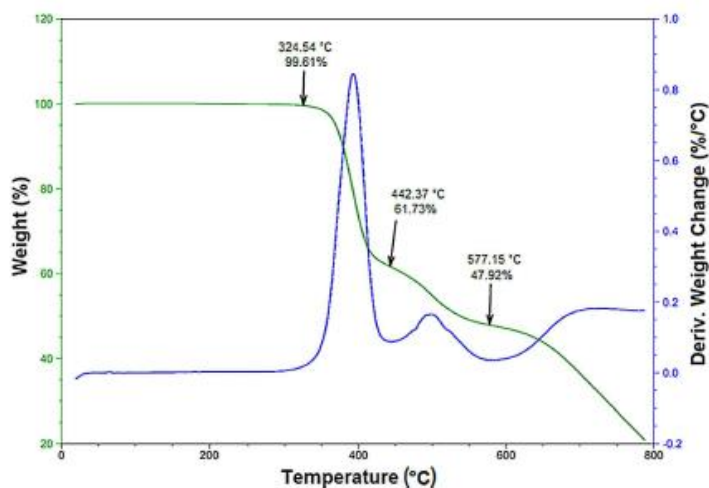


Figure 2.7 TGA trace for trimer **11a**.

The UV-vis and emission spectra for pure liquid samples are shown in Figures 2.8 and 9. The neat liquid oligomers **11a-13a** appear highly fluorescent to the naked eye under a UV lamp (254 nm) and also fluoresce visibly in ambient light. These optically opaque liquids present experimental challenges in the acquisition of spectroscopic data to characterize their ground and excited state properties. The absorption spectra (Figure 2.8, Table 1) were obtained using a thin film on the surface of a cuvette and the emission spectra (Figure 2.9, Table 2.2) were acquired using a front-face geometry as described in the experimental section. The determination of quantum yields in this manner can have large errors and often there are issues with the reproducibility of the quantum yield data. Thus, initial characterization of the excited states using dilute solutions in cyclohexane and conventional protocols was undertaken. As discussed below, the absorption and emission spectra closely resemble those obtained using dilute solutions in terms of band shapes and energetics. More detailed studies of the photophysics of the neat liquids **11a-13a** will be undertaken in the near future.

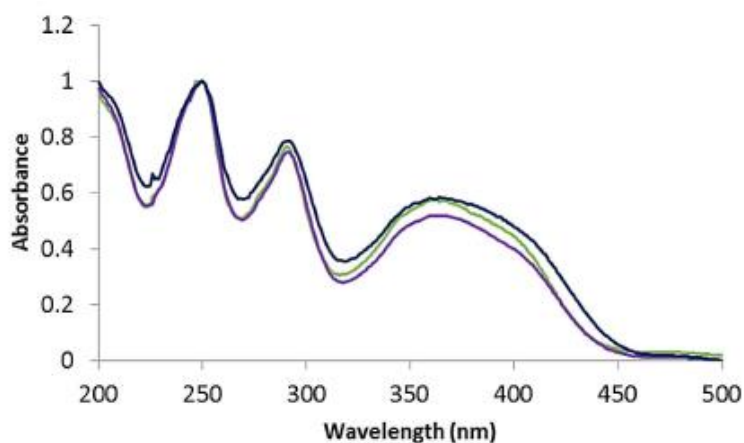


Figure 2.8 Normalized absorption spectra of **11a** (green), **12a** (purple) and **13a** (black) as neat liquid thin films in transmission mode.

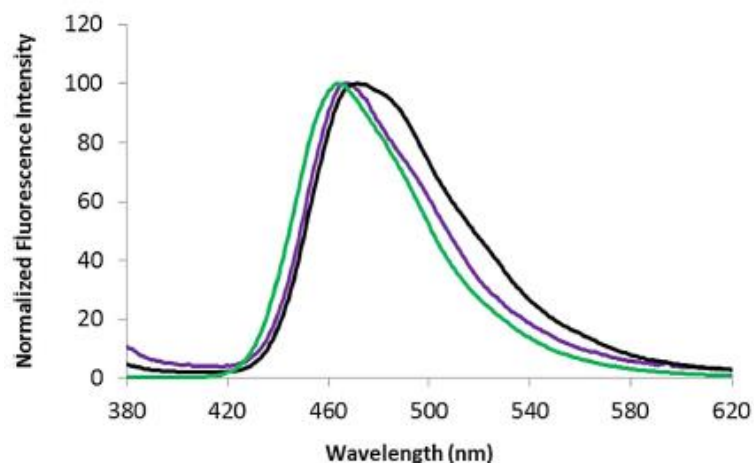


Figure 2.9 Normalized fluorescence spectra of trimer **11a** (green), tetramer **12a** (purple) and pentamer **13a** (black) as neat liquid thin films measured using front-face emission. $\lambda_{exc}=350$ nm.

UV-vis and emission spectra obtained from dilute solutions of **8a** and **10a-13a** in cyclohexane are shown in Figures 2.10 and 2.11, and spectroscopic data are summarized in Tables 1 and 2. The UV-vis spectrum of **8a** is dominated by three intense overlapping $\pi-\pi^*$ transitions (Bands 1–3) and their associated vibronic progressions. The most intense transitions for the structured band envelopes are observed at 243 nm (41152 cm^{-1}), 281 nm (35587 cm^{-1}), and 347 nm (28820 cm^{-1}) along with weak transitions at 357 nm (28011 cm^{-1}) and 376 nm (26595 cm^{-1}). The emission spectrum for **8a** (Figure 2.10) is complex and highly structured, comparable to the emission spectrum of pyrene. Taken together, the photophysical properties of **8a** are analogous to those found for pyrene.^[16]

The following observations are discernable from the UV-vis spectral data: (a) the vibronic resolution observed in **8a** diminishes in successive oligomers and is essentially all gone once the trimer **11a** has been reached, (b) the band maxima at 357 ± 1 nm, 288 ± 1 nm and 247 ± 1

nm for **10a-13a** are all redshifted from the analogous bands in **8a** by $834\pm34\text{ cm}^{-1}$, $865\pm121\text{ cm}^{-1}$ and $707\pm82\text{ cm}^{-1}$, respectively; (c) the spectral band envelope at 355 nm gains intensity on going from **10a** to **12a** and then levels off; (d) the energetics of the $\pi-\pi^*$ transitions at 247 nm (40485 cm^{-1}), 288 nm (34722 cm^{-1}), and 357 (28010 cm^{-1}) for **10a-13a** do not change significantly (Table 1). The absorption spectra of **11a-13a** as neat liquids closely resemble those obtained from dilute solutions, exhibiting three broad and intense bands at $365\pm1\text{ nm}$, $291\pm1\text{ nm}$ and $249\pm1\text{ nm}$. These bands are only slightly redshifted from the corresponding bands in the solution spectra, i.e. by $613\pm38\text{ cm}^{-1}$, $357\pm59\text{ cm}^{-1}$ and $324\pm162\text{ cm}^{-1}$, respectively. The small magnitude of these changes indicates a very low degree of pyrene-pyrene interactions.

Table 2.1 Wavelength maxima for **8a** and **10a-13a** in solution and as neat liquids (in brackets).

Compound	Band 1 (nm)	Band 2 (nm)	Band 3 (nm)
Monomer 8a	347	281	243
Dimer 10a	357	287	247
Trimer 11a	357 (365)	288 (291)	247 (248)
Tetramer 12a	357 (365)	299 (291)	247 (250)
Pentamer 13a	358 (366)	289 (292)	248 (250)

The emission spectral profiles for **10a-13a** are distinctly different from the highly structured emission spectrum of **8a**. The emission spectra for **10a-13a** have similar emission band shapes, which shift to longer wavelength as the oligomer grows in size: **10** ($\lambda_{\text{em}} = 429\text{ nm}$ (23310 cm^{-1}))

¹): **11** ($\lambda_{\text{em}} = 444 \text{ nm}$ (22520 cm^{-1}); **12** ($\lambda_{\text{em}} = 453 \text{ nm}$ (22075 cm^{-1}); and **13** ($\lambda_{\text{em}} = 457 \text{ nm}$ (21880 cm^{-1})). For **10a-13a**, the following trends are evident from the data given in Table 2: (a) φ_{F} increases from 0.74 to 0.80 and levels off at trimer **11a**; (b) τ_{F} decreases from 2.8 ns to 2.2 ns and levels off at tetramer **12a**; (c) the radiative rate constant (k_{r}) increases from $2.6 \times 10^8 \text{ s}^{-1}$ to $3.6 \times 10^8 \text{ s}^{-1}$ and levels off at tetramer **12a**; and (d) the rate constant for non-radiative decay, ($k_{\text{nr}} \sim 9 \times 10^7 \text{ s}^{-1}$) is more or less constant even though the energy gap changes from 23310 cm^{-1} for **10a** to 21880 cm^{-1} for **13a**. A quantitative analysis of the spectroscopic data to delineate the microscopic origin that underlies the photophysical properties is accommodated by the proposed mechanism described below. In going from the monomer **8a** to the oligomers **10a-13a**, a broad absorption feature at *ca.* 360 nm emerges, which is absent in **8a**. The oligomers contain pyrene units that are linked by C–C bonds, thereby providing a structural basis for π interchromophoric coupling that mediates electron delocalization.

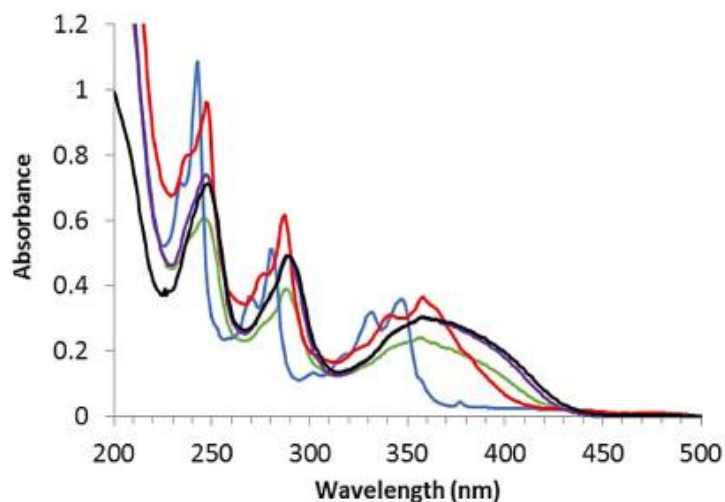


Figure 2.10 Absorption spectra of **8a** (blue), **10a** (red), **11a** (green), **12a** (purple) and **13a** (black) in oxygen-purged cyclohexane solution.

Table 2.2 Fluorescence and photophysical data for **8a** and **10a–13a** in solution and neat liquid state (in brackets).

Compound	λ_{Fmax} (nm)	Φ_F	τ_F (ns)	k_r (s ⁻¹)	k_{nr} (s ⁻¹)
Monomer 8a	379, 401, 424	0.20±0.01	39±3	5.1×10 ⁶	2.0×10 ⁷
Dimer 10a	429	0.74±0.08	2.80±0.03	2.6×10 ⁸	9.3×10 ⁷
Trimer 11a	444 (463)	0.80±0.04	2.71±0.01	3.0×10 ⁸	7.4×10 ⁷
Tetramer 12a	453 (467)	0.80±0.04	2.2±0.1	3.6×10 ⁸	9.5×10 ⁷
Pentamer 13a	457 (471)	0.80±0.01	2.2±0.1	3.6×10 ⁸	9.5×10 ⁷

In the ground state, each 1,1'-bipyrenyl unit of the oligomers **10a–13a** adopts a non-coplanar orientation characterized by a dihedral angle (θ) between pyrenyl planes, which represents a compromise between steric repulsion and π -electron delocalization.^[17] Absorption of a photon occurs on an ultrafast time scale ($\sim 10^{-15}$ s) to form the Franck-Condon excited state, which possesses the electronic coordinates appropriate for the excited state with the

nuclear and solvent coordinates still in their ground state coordinates. The absorption energy is given by:

$$E_{abs} = \Delta G_{es} + \lambda_t + E(\theta)$$

Equation 2.1

where ΔG_{es} is the free energy of the excited state and λ_t is the total reorganization energy, which includes the vibrational (λ_{vib}) and solvent reorganization (λ_o) energies. The parameter $E(\theta)$ is the energy component that depends on the dihedral angle. $E(\theta)$ contains contributions for the extent of π delocalization between the ring systems and reflects the distribution of rotational conformers that exist in the ground state.^[18] With time, the atomic nuclei that make up the chromophore and the solvent orientations in the Franck-Condon excited states will adjust their orientations to minimize the potential energy of the thermalized excited state. The lowest lying excited states of **10a-13a** decay primarily through radiative decay (Table 2). The emission energies move to longer wavelength as the number of monomer units of the oligomer increases. The kinetics are mono-exponential, which is consistent with emission coming from a very narrow conformational distribution. Taken together, it can be inferred that there is a substantial structural change on going from the Franck-Condon state to the emitting state, presumably due to a reduction of the dihedral angle. A decrease of the dihedral angle in the excited state would allow the system to more effectively delocalize the excited electron. Delocalization reduces bond length changes in the excited state and thus lowers the excited state energy on going from **10a** to **13a**. If true, one would anticipate that the transition moment (M) should correlate with the number of monomer units in the

oligomers. The rate constant for radiative decay is given by equation 2 and $\langle \nu^{-3} \rangle^{-1}$ is proportional to the energy of emission ($\langle \nu^{-3} \rangle^{-1} \cong (E_{em})^3$) and the transition moment M is given by Equation 3.

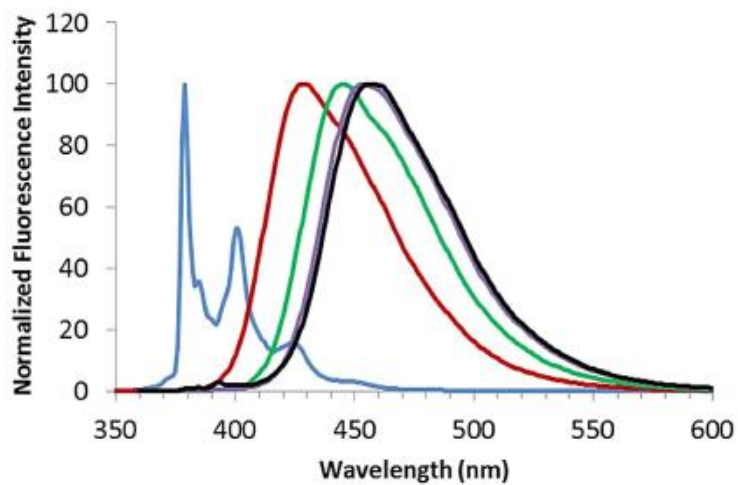


Figure 2.11 Emission spectra of cyclohexane solutions of **8a** (blue), **10a** (red), **11a** (green), **12a** (purple) and **13a** (black) in oxygen-purged cyclohexane solution. λ_{exc} =340 nm (**8a**, **10a**, **11a**) or 350 nm (**12a**, **13a**).

$$k_r = \left(\frac{64\pi^4 n^2}{3h} \right) |\vec{M}|^2 \langle \nu^{-3} \rangle^{-1}$$

Equation 2.2

$$\vec{M} = \vec{\mu} \langle \psi * | \psi \rangle$$

Equation 2.3

The transition moments were calculated for **10a** (1.31 D), **11a** (1.48 D), **12a** (1.60 D) and **13a** (1.74 D) using the experimental spectral data and Eq. 2, and they do indeed correlate with the number of monomer units in the oligomers. The spectroscopic properties of π -conjugated oligomers are often used to predict the properties at the polymeric limit.^[19] The basis of the analysis is the linear evolution of the spectroscopic energies with $\cos[\pi/(n+1)]$ where n is the number of monomer units that make up the oligomer. Plots of the onset energies for the 360 nm absorbance *vs.* $\cos[\pi/(n+1)]$ for **10a-13a** were found to exhibit a linear trend with a slope of $-0.60 (\pm 0.05)$, which is very close to the slope reported by Rathore for oligo(1,6-pyrenylene)s **5** (-0.56).^[5] Additionally, plots of the emission energies *vs.* $\cos[\pi/(n+1)]$ for **10a-13a** were also found to be linear with a slope of -0.50 , but this is a factor of 2 larger than the corresponding slope for oligo(1,6pyrenylene)s **5** (-0.26). These observations indicate that delocalization plays a larger role in the excited states of **10a-13a** than it does in **5**. The more extensive delocalization in the excited states of **10a-13a** may ultimately prove to be important when these compounds are used as materials in organic electronic devices.

Conclusions

Oligo(1,8-pyrenylene)s **8a**, **10a-13a** were synthesized using a two-step iterative synthetic strategy. The trimer **11a**, tetramer **12a** and pentamer **13a** are room temperature liquids, which are intensely fluorescent in dilute solution ($\phi_F = 0.80$) and also in the liquid state. Like other FMLs, several factors likely contribute to the suppression of solidification in **11a-13a**. The 1,8-substitution pattern of pyrene units and the presence of mixtures of 2, 4 and 6

diastereomers (atropisomers), respectively, may well be among them. With regard to the issue of diastereoisomerism, it is distinct from side chain branching (an existing guideline for the design of FMLs) and a prominent feature of other FMLs. As such, it deserves to be considered in the context of future FML design. Photophysical studies of **11a-13a** in dilute solution indicate that interchromphoric coupling manifests itself in radiative decay and that delocalization plays a larger role in the excited states than for Rathore's oligo(1,6-pyrenylene)s

5. Work aimed at the use of **11a-13a** as solvents for chemical reactions and as functional materials is underway.

Experimental Section

Commercial reagents and solvents were used without purification. Pd(PPh₃)₄ was prepared^[20] and used before discoloration occurred (within 7 d; storage under Ar in a freezer). ¹H and ¹³C NMR spectra were recorded on a Bruker 300 MHz AVANCE III or Bruker AVANCE 500 MHz spectrometers. High-resolution APPI-TOF-MS were recorded on a GCT Premier Micromass Technologies instrument. Thermogravimetric analysis was performed on a Waters TGA-Q-500 instrument. Differential scanning calorimetry was measured using a Mettler Toledo DSC 1 STAR system. Absorption spectra were measured in cyclohexane solutions using a Cary Bio UV-vis spectrophotometer manufactured by Varian. Fluorescence spectra were measured in oxygen-free cyclohexane solution, using a Photon Technologies International (PTI) RF-M2004 fluorescence spectrometer, with excitation wavelengths of 340 nm (**8a**, **10a** and **11a**) or 350 nm (**12a** and **13a**). Oxygen was removed

from these solutions by sparging with Ar. Solutions for the fluorescence measurements were prepared to obtain an absorbance of 0.25 to 0.35 at the excitation wavelength. Fluorescence quantum yields were determined using the relative method,^[21] using 9,10-diphenylanthracene in cyclohexane as the quantum yield standard ($\phi_F = 0.90$).^[21] Fluorescence lifetimes were measured on the same samples used for fluorescence spectra measurements, using a Photon Technologies International instrument, which is based on the stroboscopic optical boxcar technique.^[22] Absorption spectra of the neat liquids of **11a-13a** were measured on samples prepared by depositing highly concentrated solutions of the liquids in cyclohexane on the front surface of thin 1 mm path length quartz cuvettes laid flat, with the solvent allowed to evaporate to leave a thin, transparent film of the liquid, which allowed for the measurement of the absorption spectrum in transmission mode. Fluorescence spectra of the neat liquids of the **11a-13a** were measured as thin films manually spread directly on the front surface of the thin 1 mm path length quartz cuvettes, which were placed in the fluorimeter sample holder at 45° to both the excitation light and emission collection path, in a front-face emission configuration with 350 nm excitation. Density functional theory (DFT) calculations were performed with the Gaussian 16 software package,^[23] using the B3LYP functional in conjunction with the 6-31G(d) basis set. SWAXS data were collected on a 2 mm thick sample held horizontally using a Siemens D5000 θ - θ diffractometer equipped with a copper target X-ray tube and a diffracted beam monochromator. The divergence and anti-scatter slits were set to 1° and the receiving slit was set to 0.6 mm. Data was collected every 0.05° in scattering angle with a 4 s count time.

1,8-Dibromo-4,5-didecoxyrene (17a): To a solution of 4,5-didecoxyrene (**8a**)^[11] (5.00 g, 9.71 mmol) in CH₂Cl₂ (250 mL) was added bromine (3.41 g, 21.4 mmol). The reaction was

stirred at room temperature for 5 min. Excess bromine was quenched by the addition of saturated sodium thiosulfate solution (150 mL). The layers were separated and the aqueous phase was extracted with CH₂Cl₂ (3×100 mL). The combined organic layers were dried over anhydrous Na₂SO₄ and the solvent was removed under reduced pressure. The resulting brown solid was subjected to column chromatography (10% CH₂Cl₂/hexanes) to afford 1,8-dibromo-4,5-didecoxy pyrene (**17a**) (6.27 g, 96%) as a pale-yellow solid. *R_f* (20% CH₂Cl₂/hexanes) = 0.90; mp = 79.3–80.5 °C (recrystallized from ethanol); ¹H NMR (CDCl₃, 300 MHz) δ = 8.52 (s, 2H), 8.36 (d, *J*=8.5 Hz, 2H), 8.27 (d, *J*=8.5 Hz, 2H), 4.31 (t, *J*=6.7 Hz, 4H), 2.00–1.90 (m, 4H), 1.64–1.56 (m, 4H), 1.45–1.23 (m, 24H), 0.89 (t, *J*=6.7 Hz, 6H); ¹³C NMR (CDCl₃, 75 MHz) δ = 143.78, 130.72, 129.43, 128.70, 127.47, 123.48, 120.85, 119.91, 73.90, 31.92, 30.53, 29.67, 29.61, 29.55, 29.36, 26.27, 22.70, 14.13 ppm; HRMS [APPI(+)], calcd for C₃₆H₄₈⁸¹Br⁷⁹BrO₂ ([M]⁺): 674.2034, found: 673.2004.

1,8-Dibromo-4,5-dimethoxy pyrene (17b): To a solution of 4,5-dimethoxy pyrene (**8b**)^[11] (1.00 g, 3.81 mmol) in CH₂Cl₂ (30 mL) was added bromine (1.34 g, 8.37 mmol). The reaction was stirred at room temperature for 5 min. Excess bromine was quenched by the addition of saturated sodium thiosulfate solution (25 mL). The layers were separated and the aqueous phase was extracted with CH₂Cl₂ (3×100 mL). The combined organic layers were washed with water (30 mL), washed with brine (30 mL), dried over anhydrous Na₂SO₄ and the solvent was removed under reduced pressure. The resulting brown solid was subjected to column chromatography (10% CH₂Cl₂/hexanes) to afford 1,8-dibromo-4,5-dimethoxy pyrene (**17b**) (1.52 g, 95%) as a white solid. *R_f* (40% CH₂Cl₂/hexanes) = 0.60; mp = 212–214 °C; ¹H NMR (CDCl₃, 300 MHz) δ = 8.51 (s, 2H), 8.35 (d, *J*=8.4 Hz, 2H), 8.27 (d, *J*=8.4 Hz, 2H), 4.19 (s,

6H); ^{13}C NMR (CDCl_3 , 75 MHz) δ = 144.45, 130.79, 129.45, 128.14, 127.46, 123.46, 120.70, 120.09, 61.18 ppm; HRMS [APPI(+)], calcd for $\text{C}_{18}\text{H}_{12}^{81}\text{Br}^{79}\text{BrO}_2$ ($[\text{M}]^+$): 419.9185, found: 419.9184.

1,8-Dipyren-1-yl-4,5-didecoxy pyrene (19a): A 50 mL round-bottomed flask equipped with a side arm and capped with a rubber septum was charged with pyrene-1-boronic acid (**18**) (0.091 g, 0.037 mmol), 1,8-dibromo-4,5-didecoxy pyrene (**17a**) (0.101 g, 0.150 mmol), K_2CO_3 (0.414 g 3.00 mmol), 1,4-dioxane (4 mL) and water (1 mL). The resulting slurry was subjected to four freeze-pump-thaw cycles before $\text{Pd}(\text{PPh}_3)_4$ (0.0036 g, 0.031 mmol) was added under a positive pressure of N_2 . The flask was then resealed with a rubber septum and heated at 80 °C in an oil bath for 16 h. After cooling to room temperature, the solvent was removed under reduced pressure and the residue was subjected to column chromatography (2% CH_2Cl_2 /hexanes) to yield 1,8-dipyren-1-yl-4,5-didecoxy pyrene (**19a**) (0.037 g, 27%) as a pale yellow-green viscous liquid. R_f (20% CH_2Cl_2 /hexanes) = 0.60; ^1H NMR (CDCl_3 , 500 MHz) δ = 8.760 and 8.757 (2×d, J =8.0 Hz, 2H), 8.283 and 8.278 (2×d, J =7.8 Hz, 2H) or 8.28 (dd, J =7.8, 12.8 Hz, 2H), 8.22–8.18 (m, 2H), 8.21 (d, J =7.9 Hz, 2H), 8.14–8.08 (m, 8H), 8.00 and 7.99 (2×t, J =7.6 Hz, 2H), 7.872 and 7.866 (2×d, J =9.3 Hz, 2H), 7.73 and 7.67 (2×d, J =9.3 Hz, 2H), 7.53 and 7.49 (2×s, 2H), 4.54 (t, J =6.7 Hz, 4H), 2.17–2.10 (m, 4H), 1.78–1.72 (m, 4H), 1.56–1.50 (m, 4H), 1.48–1.25 (m, 20H), 0.95–0.85 (m, 6H); ^{13}C NMR (CDCl_3 , 125 MHz) δ = 144.32, 136.22, 136.19, 135.78, 131.45, 130.98, 130.88, 130.07, 129.96, 129.30, 129.24, 129.05, 129.03, 128.94, 128.87, 127.57, 127.45, 126.03, 125.78, 125.21, 125.02, 124.79, 124.48, 123.31, 123.25, 119.36, 119.28, 74.12, 32.02, 30.83, 29.84, 29.76, 29.48, 26.51, 22.80, 14.22 ppm (only

27 of the 48 expected aromatic signals and only 9 of the 20 expected aliphatic signals observed); HRMS [APPI(+)], calcd for C₆₈H₆₆O₂ ([M]⁺): 914.5063, found: 914.5070.

1,8-Dipyren-1-yl-4,5-dimethoxyppyrene (19b): A 50 mL round-bottomed flask equipped with a side arm and capped with a rubber septum was charged with pyrene-1-boronic acid (**18**) (0.469 g, 1.91 mmol), 1,8-dibromo-4,5-dimethoxyppyrene (**17b**) (0.200 g, 0.476 mmol), K₂CO₃ (2.11 g 15.3 mmol), 1,4-dioxane (10 mL) and water (2 mL). The resulting slurry was subjected to three freeze-pump-thaw cycles before Pd(PPh₃)₄ (0.0176 g, 0.152 mmol) was added under a positive pressure of N₂. The flask was then resealed with a rubber septum and heated at 100 °C in an oil bath for 19 h. After cooling to room temperature, the mixture was diluted with CH₂Cl₂ (100 mL). The resulting solution was washed with H₂O (3×100 mL), washed with brine (200 mL), dried over anhydrous MgSO₄ and the solvent was removed under reduced pressure. The residue was pre-adsorbed on silica gel and subjected to column chromatography (40% CH₂Cl₂/hexanes) to yield 1,8-dipyren-1-yl-4,5-dimethoxyppyrene (**19b**) (0.194 g, 38%) as a pale yellow solid. *R_f* (40% CH₂Cl₂/hexanes) = 0.31; ¹H NMR (CDCl₃, 300 MHz) δ = 8.729 and 8.727 (2×d, *J*=8.0 Hz, 2H), 8.251 and 8.245 (2×d, *J*=7.8 Hz, 2H) or 8.25 (dd, *J*=7.8, 1.7 Hz, 2H), 8.20–8.13 (m, 2H), 8.19 (d, *J*=8.0 Hz, 2H), 8.12–8.04 (m, 8H), 7.97 and 7.96 (2×t, *J*=7.6 Hz, 2H), 7.84 and 7.83 (2×d, *J*=9.3 Hz, 2H), 7.69 and 7.63 (2×d, *J*=9.2 Hz, 2H), 7.50 and 7.47 (2×s, 2H), 4.38 (s, 6H); ¹³C NMR (CDCl₃, 75 MHz) δ = 144.95, 136.07, 136.04, 135.98, 135.91, 131.42, 130.92, 130.86, 130.01, 129.95, 129.94, 129.29, 129.23, 128.86, 128.80, 128.43, 128.41, 127.54, 127.41, 127.40, 126.01, 125.96, 125.92, 125.68, 125.19, 125.00, 124.78, 124.73, 124.43, 124.35, 123.24, 123.18, 119.13, 119.06, 61.38 ppm (only 34 of the 48 expected

aromatic signals observed); HRMS [APPI(+)], calcd for $C_{50}H_{30}O_2$ ($[M]^+$): 662.2246, found: 662.2299.

1-Bromo-4,5-didecoxyppyrene (20): To a solution of 4,5-didecoxyppyrene (**8a**)^[11] (5.00 g, 9.77 mmol) in CH_2Cl_2 (100 mL) in a 500 mL round-bottomed flask was added dropwise a solution of bromine (2.03 g, 12.7 mmol) in CH_2Cl_2 (127 mL, 0.1 M) over 35 min. The resulting solution was transferred to a separatory funnel, washed with water (100 mL), washed with brine (100 mL), dried over anhydrous $MgSO_4$ and concentrated under reduced pressure. The resulting pale pink-orange solid was adsorbed on silica gel and subjected to column chromatography (1% CH_2Cl_2 /hexanes) to afford 1,8-dibromo-4,5-didecoxyppyrene (**17a**) (1.26 g, 19%) and 1-bromo-4,5-didecoxyppyrene (**20**) (4.20 g, 73%) as a waxy white solid. R_f (1% CH_2Cl_2 /hexanes) = 0.10; mp=45.4–46.8 °C (recrystallized from ethanol); 1H NMR ($CDCl_3$, 300 MHz) δ = 8.52 (dd, $J=7.8$, 1.0 Hz, 1H), 8.42 (d, $J=9.2$ Hz, 1H), 8.33 (d, $J=8.5$ Hz, 1H), 8.24 (d, $J=8.5$ Hz, 1H), 8.17 (dd, $J=7.8$, 0.7 Hz, 1H), 8.15 (d, $J=9.0$ Hz, 1H), 8.05 (t, $J=7.7$ Hz, 1H), 4.34 (t, $J=6.7$ Hz, 4H), 2.01–1.88 (m, 4H), 1.64–1.58 (m, 4H), 1.41–1.22 (m, 24H), 0.87 (t, $J=6.7$ Hz, 6H); ^{13}C NMR ($CDCl_3$, 75 MHz) δ = 144.15, 143.76, 130.94, 130.11, 129.51, 129.11, 128.93, 128.54, 126.55, 125.88, 124.85, 124.07, 122.26, 120.18, 120.18, 119.34, 73.88, 73.85, 31.95, 30.61, 30.59, 29.71, 29.64, 29.60, 29.59, 29.38, 26.33, 22.72, 14.15 ppm (only 13 of the 20 expected aliphatic signals observed); HRMS [APPI(+)], calcd for $C_{36}H_{49}^{81}BrO_2$ ($[M]^+$): 592.2916, found: 592.2893.

2-(4,5-Didecyloxyppyren-1-yl)-4,4,5,5-tetramethyl-1,3,2-dioxaborolane (22): A 250 mL round-bottomed flask equipped with a side arm and capped with a rubber septum was charged with 1-bromo-4,5-didecoxyppyrene (**20**) (1.50 g, 2.53 mmol), 1,4-dioxane (50 mL), KOAc

(0.744 g, 7.58 mmol) and HBPIn (0.970 g, 7.58 mmol). The mixture was subjected to three freeze-pump-thaw cycles before Pd(dppf)₂Cl₂ (0.092 g, 0.13 mmol) was added under a positive pressure of nitrogen. The mixture was heated at 80 °C in an oil bath for 4 h. The rubber septum was then replaced with a distillation head and the majority of the solvent was removed by distillation. After cooling, the resulting brown sludge was dissolved in CH₂Cl₂ (200 mL) and the resulting solution was washed with water (100 mL), washed with brine (100 mL), dried over anhydrous MgSO₄. The solvent was removed under reduced pressure and the crude mixture was subjected to column chromatography (20% CH₂Cl₂/hexanes) to afford 2-(4,5-didecoxyphen-1-yl)-4,4,5,5-tetramethyl-1,3,2-dioxaborolane (**22**) as a pale brown oil (1.47 g, 91%). *R_f* (50% CH₂Cl₂/hexanes) = 0.60; ¹H NMR (CDCl₃, 300 MHz) δ = 9.05 (d, *J*=9.1 Hz, 1H), 8.55 (d, *J*=7.9 Hz, 1H), 8.51 (d, *J*=7.9 Hz, 1H), 8.46 (d, *J*=7.9 Hz, 1H), 8.16 (d, *J*=7.7 Hz, 1H), 8.11 (d, *J*=9.3 Hz, 1H), 8.02 (t, *J*=7.7 Hz, 1H), 4.37 (t, *J*=6.7 Hz, 2H), 4.30 (t, *J*=6.7 Hz, 2H), 2.01–1.94 (m, 4H), 1.62–1.57 (m, 4H), 1.49 (s, 12H), 1.40–1.28 (m, 24H), 0.91–0.87 (m, 6H); ¹³C NMR (CDCl₃, 75 MHz) δ = 145.05, 143.79, 136.33, 134.03, 131.37, 130.71, 128.66, 127.93, 127.70, 125.73, 124.70, 122.88, 122.59, 119.61, 118.36, 83.85, 73.85, 73.81, 31.93, 30.63, 30.57, 29.70, 29.63, 29.59, 29.37, 26.34, 26.31, 25.06, 22.71, 14.13 ppm (only 15 of the 16 expected aromatic signals and only 15 of the 22 expected aliphatic signals observed); HRMS [APPI(+)], calcd for C₄₂H₆₁BO₄ ([M]⁺): 640.4669, found: 640.4716.

1,8-Diiodo-4,5-didecoxyphenylene (21): To a solution of 4,5-didecoxyphenylene (**8a**) (2.00 g, 3.88 mmol) in CH₂Cl₂ (100 mL) was added iodine (2.96 g, 11.7 mmol) and Hg(OAc)₂ (3.71 g, 11.7 mmol). The reaction was stirred for 20 min at room temperature. The slurry was passed through short plug of silica gel and Celite® (*ca.* 1:1). Water (150 mL) was added and the layers

were separated. The organic phase was dried over anhydrous Na_2SO_4 and the solvent was removed under reduced pressure. The solid pink residue was subjected to column chromatography (10% CH_2Cl_2 /hexanes) to yield 1,8-diiodo-4,5-didecoxyppyrene (**21**) (2.62 g, 88%) as a white solid. R_f (20% CH_2Cl_2 /hexanes) = 0.90; mp >95 °C dec.; ^1H NMR (CDCl_3 , 300 MHz) δ = 8.53 (d, $J=8.4$ Hz, 2H), 8.35 (s, 2H), 8.21 (d, $J=8.4$ Hz, 2H), 4.30 (t, $J=6.7$ Hz, 4H), 2.02–1.86 (m, 4H), 1.65–1.50 (m, 4H), 1.42–1.23 (m, 24H), 0.95–0.81 (m, 6H); ^{13}C NMR (75 MHz, CDCl_3): δ = 143.91, 137.47, 132.94, 132.40, 129.38, 123.13, 121.31, 96.17, 73.90, 31.93, 30.52, 29.67, 29.61, 29.54, 29.36, 27.26, 22.70, 14.13; HRMS [APPI(+)], calcd for $\text{C}_{36}\text{H}_{48}\text{I}_2\text{O}_2$ ($[\text{M}]^+$): 766.1744, found: 766.1757.

4,5-Didecoxy-1,8-bis(4,5-didecoxyppyren-1-yl)pyrene (11a): Method A (using dibromide **17a**) – A 250 mL round-bottomed flask equipped with a side arm and capped with a rubber septum was charged with 2-(4,5-didecoxyppyren-1-yl)-4,4,5,5-tetramethyl-1,3,2-dioxaborolane (**22**) (2.84 g, 4.46 mmol), 1,8-dibromo-4,5-didecoxyppyrene (**17a**) (1.00 g, 1.49 mmol), anhydrous $\text{Ba}(\text{OH})_2$ (5.09 g, 29.7 mmol), toluene (80 mL), ethanol (20 mL) and water (10 mL). The resulting slurry was subjected to three freeze-pump-thaw cycles before $\text{Pd}(\text{PPh}_3)_4$ (0.017 g, 0.015 mmol) was added under a positive pressure of N_2 . The flask was then resealed with a rubber septum and heated at 80 °C in an oil bath for 24 h. After cooling to room temperature, the solvent was removed under reduced pressure and the resulting brown oil was dissolved in CH_2Cl_2 (2×100 mL). The resulting solution was washed with H_2O (200 mL), dried over anhydrous MgSO_4 and the solvent was removed under reduced pressure to afford a yellow oil. The residue was subjected to column chromatography (1:1:10 toluene/ CH_2Cl_2 /hexanes) to yield 4,5-didecoxy-1,8-bis(4,5-didecoxyppyren-1-yl)pyrene (**11a**)

(1.77 g, 77%) as a bright yellow viscous oil. R_f (7.5:7.5:85, toluene/ CH_2Cl_2 /hexanes) = 0.60; ^1H NMR (CDCl_3 , 300 MHz) δ = 8.720 and 8.718 (2×d, J =8.1 Hz, 2H), 8.56 and 8.55 (2×d, J =8.1 Hz, 2H), 8.49 and 8.48 (2×dd, J =7.6, 1.5 Hz, 2H), 8.17 (d, J =8.1, 2H), 8.09 and 8.08 (2×d, J =8.1 Hz, 2H), 8.04 and 8.02 (2×dd, J =7.7, 1.3 Hz, 2H), 7.98 and 7.97 (2×t, J =7.6 Hz, 2H), 7.82 (d, J =9.3 Hz, 2H), 7.68 and 7.62 (2×d, J =9.2 Hz, 2H), 7.50 and 7.46 (2×s, 2H), 4.51 (t, J =6.7 Hz, 4H), 4.35 (m, 8H), 2.12–2.08 (m, 12H), 1.75–1.71 (m, 12H), 1.45–1.20 (m, 72H), 0.93–0.83 (m, 18H); ^{13}C NMR (CDCl_3 , 75 MHz) δ = 144.43, 144.28, 144.25, 135.92, 135.91, 135.63, 135.60, 131.03, 130.15, 139.48, 129.42, 129.29, 139.27, 129.14, 129.12, 128.77, 127.61, 126.17, 125.80, 124.45, 123.47, 123.42, 123.19, 123.12, 119.79, 119.45, 119.37, 119.09, 119.00, 74.15, 73.99, 73.94, 32.14, 32.11, 30.94, 30.82, 29.96, 29.87, 29.80, 29.87, 29.80, 29.78, 29.60, 29.55, 26.63, 26.52, 22.91, 22.88, 14.31, 14.30, 14.28 ppm; HRMS [APPI(+)], calcd for $\text{C}_{108}\text{H}_{146}\text{O}_6$ ($[\text{M}]^+$): 1539.1119, found: 1539.1109.

Method B (using diiodide **21**) – Using the procedure described above, (4,5-didecoxy-pyren-1-yl)-4,4,5,5-tetramethyl-1,3,2-dioxaborolane (**22**) (2.51 g, 3.91 mmol), 1,8-diiodo-4,5-didecoxy-pyrene (**21**) (1.00 g, 1.30 mmol), anhydrous $\text{Ba}(\text{OH})_2$ (4.47 g, 26.1 mmol), toluene (80 mL), ethanol (20 mL), water (10 mL) and $\text{Pd}(\text{PPh}_3)_4$ (0.015 g, 0.013 mmol) were used to afford 4,5-didecoxy-1,8-bis(4,5-didecoxy-pyren-1-yl)pyrene (**11a**) (1.83 g, 91%) as a bright yellow viscous oil.

1,8-Bis(8-bromo-4,5-didecoxy-pyren-1-yl)-4,5-didecoxy-pyrene (23): To a solution of 4,5-didecoxy-1,8-bis(4,5-didecoxy-pyren-1-yl)pyrene (**11a**) (0.050 g, 0.032 mmol) in CH_2Cl_2 (3 mL) was added a solution of bromine (0.010 g, 0.065 mmol) in CH_2Cl_2 (3 mL) and the reaction was stirred at room temperature for 5 min. Excess bromine was quenched by the addition of

was then resealed with a rubber septum and heated at 80 °C in an oil bath for 24 h. After cooling to room temperature, the solvent was removed under reduced pressure and the resulting brown oil was dissolved in CH₂Cl₂ (2×35 mL). The resulting solution was washed with H₂O (50 mL), dried over anhydrous MgSO₄ and the solvent was removed under reduced pressure. The resulting yellow oil was subjected to column chromatography (1:1:10 toluene/CH₂Cl₂/hexanes) to afford 1,8-bis(8-(4,5-didecoxyphenyl)-4,5-didecoxyphenyl)-4,5-didecoxyphenyl (13a) (0.127 g, 84%) as a bright yellow viscous oil. R_f (7.5:7.5:85, toluene/CH₂Cl₂/hexanes) = 0.50; ¹H NMR (CDCl₃, 300 MHz) δ = 8.66–8.33 (m, 10H), 8.11–7.89 (m, 12H), 7.79–7.30 (m, 10H), 4.46–4.18 (m, 20H), 2.03–1.81 (m, 20H), 1.66–1.44 (m, 20H), 1.44–1.07 (m, 120H), 0.88–0.63 (m, 30H); ¹³C NMR (75 MHz, CDCl₃) δ = 144.17, 144.11, 144.11, 135.50, 135.47, 130.87, 129.89, 129.87, 129.14, 128.89, 128.81, 128.57, 128.05, 127.41, 126.07, 126.02, 125.91, 125.83, 125.79, 125.72, 125.12, 124.54, 124.33, 124.30, 123.28, 123.26, 123.23, 123.17, 123.15, 122.93, 122.16, 121.78, 121.39, 120.36, 119.08, 118.99, 118.85, 77.46, 77.04, 76.62, 74.03, 74.00, 73.95, 73.92, 73.87, 31.96, 31.91, 30.73, 30.70, 30.67, 29.76, 29.74, 29.68, 29.67, 29.41, 29.36, 26.42, 26.37, 22.74, 14.16; HRMS [APPI(+)], calcd for C₁₈₀H₂₄₂O₁₀ ([M]⁺): 2563.8428, found: 2566.8658.

1,1'-Bi(4,5-didecoxyphenyl) (10a): Method A (Suzuki-Miyaura cross-coupling) – A 250 mL round-bottomed flask equipped with a side arm and capped with a rubber septum was charged with 2-(4,5-didecoxyphenyl)-4,4,5,5-tetramethyl-1,3,2-dioxaborolane (**22**) (1.46 g, 2.27 mmol), 1-bromo-4,5-didecoxyphenyl (**20**) (0.450 g, 0.758 mmol), anhydrous Ba(OH)₂ (2.60 g, 15.2 mmol), toluene (40 mL), ethanol (10 mL) and water (5 mL). The resulting slurry was subjected to three freeze-pump-thaw cycles before Pd(PPh₃)₄ (0.009 g, 0.008 mmol) was added

under a positive pressure of N₂. The flask was then resealed with a rubber septum and heated at 80 °C in an oil bath for 24 h. After cooling to room temperature, the solvent was removed under reduced pressure and the resulting brown oil was dissolved in CH₂Cl₂ (2×100 mL). The resulting solution was dried over anhydrous MgSO₄ and the solvent was removed under reduced pressure to afford a yellow oil. The residue was subjected to column chromatography (1:1:10 toluene/CH₂Cl₂/hexanes) to afford 1,1'-bi(4,5-didecoxyppyrenyl) (**10a**) (0.498 g, 64%) as a bright yellow viscous oil, which crystallized over 60 d. R_f (20% CH₂Cl₂/hexanes) = 0.35; ¹H NMR (CDCl₃, 300 MHz) δ = 8.66 (d, J=8.0 Hz, 2H), 8.55 (dd, J=7.5 Hz, 1.4 Hz 2H), 8.15 (d, J=8.0 Hz, 2H), 8.08 (d, J=7.2 Hz, 2H), 8.03 (t, J=7.7 Hz, 2H), 7.85 (d, J=9.3 Hz, 2H), 7.62 (d, J=9.3 Hz, 2H), 4.42 (m, 8H), 2.07–2.00 (m, 8H), 1.79–1.54 (m, 8H), 1.46–1.26 (m, 48H), 0.92–0.81 (m, 12H); ¹³C NMR (CDCl₃, 75 MHz) δ = 144.18, 135.62, 130.93, 130.07, 129.21, 128.98, 128.66, 127.47, 126.14, 125.75, 124.37, 123.00, 119.69, 118.99, 73.95, 73.90, 31.96, 31.94, 30.71, 30.68, 29.74, 29.66, 29.39, 26.39, 22.73, 22.71, 14.15, 14.13 ppm (only 14 of the 16 expected aromatic signals and only 14 of the 20 expected aliphatic signals observed); HRMS [APPI(+)], calcd for C₇₂H₉₈O₄ ([M]⁺): 1026.7465, found: 1026.7466.

Method B (Feringa homocoupling) –A 2-necked pear-shaped flask equipped with a calcium chloride drying tube and a rubber septum was charged with 1-bromo-4,5-didecoxyppyrene (**20**) (0.250 g, 0.421 mmol), *n*-hexane (5 mL), PEPPSI-*i*PrTM (0.003 g, 0.004 mmol) and the mixture was stirred at room temperature for 15 min. *t*-Butyllithium (0.3 M, 1.00 mL, 0.3 mmol) was then added dropwise over a period of 10 min via syringe through the rubber septum. The excess *t*-butyllithium was quenched by the addition of aqueous NH₄Cl solution (1 mL). The water and *n*-hexane were removed under reduced pressure and the resulting brown solid was

dissolved in CH₂Cl₂ (15 mL) and passed through a plug of Celite® and silica gel (*ca.* 1:1). The solvent was removed under reduced pressure to afford 4,5-didecoxy-1-(4,5-didecoxypyren-1-yl)pyrene (**10a**) as a bright yellow viscous liquid (0.203 g, 94%).

Method C (Scholl reaction) – To a solution of 4,5-didecoxypyrene (**8a**) (0.100 g, 0.194 mmol) in CH₂Cl₂ (10 mL) and methanesulfonic acid (1 mL) was added DDQ (0.022 g, 0.097 mmol). The deep green solution was stirred at room temperature for 1 min and then quenched by the addition of aqueous 10% sodium bicarbonate solution (10 mL). The layers were separated and the organic phase was dried over anhydrous MgSO₄. The solvent was removed under reduced pressure and the resulting red solid was subjected to column chromatography (5% CH₂Cl₂/hexanes) to afford 1,1'-bi(4,5-didecoxypyrenyl) (**10a**) as a bright yellow viscous oil (0.037 g, 37%) and 4,5-didecoxy-1,8-bis(4,5-didecoxypyren-1-yl)pyrene (**11a**) as a bright yellow viscous oil (0.017 g, 17%).

1,1'-Bi(8-bromo-4,5-didecoxypyrenyl) (24): To a solution of 1,1'-bi(4,5-didecoxypyrenyl) (**10a**) (0.125 g, 0.122 mmol) in CH₂Cl₂ (10 mL) was added a solution of bromine (0.039 g, 0.24 mmol) in CH₂Cl₂ (10 mL) and the reaction was stirred at room temperature for 5 min. Excess bromine was quenched by the addition of saturated sodium thiosulfate solution (25 mL). The layers were separated and the aqueous phase was extracted with CH₂Cl₂ (3×25 mL). The organic phase was dried over anhydrous Na₂SO₄ and the solvent was removed under reduced pressure. The resulting brown solid was subjected to column chromatography (10% CH₂Cl₂/hexanes) to afford 1,1'-bi(8-bromo-4,5-didecoxypyrenyl) (**24**) (0.127 g, 88%) as a pale yellow solid. *R*_f (20% CH₂Cl₂/hexanes) = 0.60; mp=39.1–41.1 °C (crystallized from hexanes); ¹H NMR (CDCl₃, 300 MHz) δ = 8.70 (d, *J*=8.0 Hz, 2H), 8.40 (d, *J*=8.5 Hz, 2H), 8.27 (d, *J*=8.5

Hz, 2H), 8.23 (d, $J=9.5$ Hz, 2H), 8.17 (d, $J=8.0$ Hz, 2H), 7.73 (d, $J=9.5$ Hz, 2H), 4.43 (t, $J = 6.7$ Hz, 4H), 4.39 (t, $J = 6.7$ Hz, 4H), 2.08–1.96 (m, 8H), 1.72–1.59 (m, 8H), 1.50–1.24 (m, 48H), 0.93– 0.88 (m, 12H); ^{13}C NMR (CDCl_3 , 75 MHz) $\delta = 144.18, 143.90, 135.79, 130.36, 129.96, 129.56, 129.37, 128.97, 128.83, 127.21, 126.19, 124.21, 122.45, 120.49, 119.74, 119.56, 73.99, 31.96, 31.94, 30.67, 30.63, 29.73, 29.66, 29.63, 29.39, 26.37, 22.73, 22.71, 14.15, 14.13$ ppm (only 14 of the 20 expected aliphatic signals observed); HRMS [APPI(+)], calcd for $\text{C}_{72}\text{H}_{96}^{81}\text{Br}^{79}\text{BrO}_4$ ($[\text{M}]^+$): 1182.5675, found: 1182.5669.

1,1'-Bi(8-(4,5-didecoxyphenyl)-4,5-didecoxyphenyl) (12a): A 250 mL round-bottomed flask equipped with a side arm and capped with a rubber septum was charged with 2-(4,5-didecoxyphenyl)-4,4,5,5-tetramethyl-1,3,2-dioxaborolane (**22**) (0.227 g, 0.354 mmol), 1,1'-bi(8-bromo-4,5-didecoxyphenyl) (**24**) (0.140 g, 0.118 mmol), anhydrous $\text{Ba}(\text{OH})_2$ (0.404 g, 2.36 mmol), toluene (16 mL), ethanol (4 mL) and water (2 mL). The resulting slurry was subjected to three freeze-pump-thaw cycles before $\text{Pd}(\text{PPh}_3)_4$ (0.014 g, 0.012 mmol) was added under a positive pressure of N_2 . The flask was then resealed with a rubber septum and heated at 80 °C in an oil bath for 24 h. After cooling to room temperature, the solvent was removed under reduced pressure and the resulting brown oil was dissolved in CH_2Cl_2 (2×35 mL). The resulting solution was washed with H_2O (50 mL), dried over anhydrous MgSO_4 and the solvent was removed under reduced pressure. The resulting yellow oil was subjected to column chromatography (1:1:10 toluene/ CH_2Cl_2 /hexanes) to afford 1,1'-bi(8-(4,5-didecoxyphenyl)-4,5-didecoxyphenyl) (**12a**) (0.172 g, 71%) as a bright yellow viscous oil. R_f (7.5:7.5:85, toluene/ CH_2Cl_2 /hexanes) = 0.55; ^1H NMR (CDCl_3 , 300 MHz) $\delta = 8.70\text{--}8.46$ (m, 8H), 8.16–7.94 (m, 10H), 7.86–7.40 (m, 8H), 4.51– 4.30 (m, 16H), 2.13–1.92 (m, 16H), 1.74–1.53 (m,

16H), 1.54–1.17 (m, 96H), 0.95–0.78 (m, 24H); ^{13}C NMR (75 MHz, CDCl_3) δ = 144.21, 144.20, 144.15, 144.12, 135.65, 135.56, 135.53, 135.47, 130.89, 130.01, 129.89, 129.28, 129.15, 128.95, 128.87, 128.56, 127.45, 126.09, 126.05, 125.91, 125.88, 125.71, 124.34, 123.28, 123.20, 123.12, 122.99, 122.95, 119.66, 119.14, 118.94, 118.83, 74.01, 73.92, 73.89, 31.97, 30.73, 30.68, 29.75, 29.68, 29.42, 26.42, 26.39, 22.74, 14.16; HRMS [APPI(+)], calcd for $\text{C}_{144}\text{H}_{194}\text{O}_8$ ($[\text{M}]^+$): 2051.4774, found: 2051.4704.

Acknowledgements

Financial support of this work from the Natural Sciences and Engineering Research Council (NSERC) of Canada (G.J.B., Y.Z. and B.D.W.) and the National Science Foundation (R.P.J., CHE1362519) is gratefully acknowledged. Compute Canada is acknowledged for the use of their facilities for the DFT studies. This research used the Extreme Science and Engineering Discovery Environment (XSEDE), supported by NSF Grant No. OCI-1053575 (R.P.J.). The authors thank Prof. Jeff Dahn, Dalhousie University, for acquisition of the SWAXS data.

References

1. T. M. Figueira-Duarte, K. Müllen, *Chem. Rev.* **2011**, *111*, 7260–7314.
2. T. M. Figueira-Duarte, S. C. Simon, M. Wagner, S. I. Druzhinin, K. A. Zachariasse, K. Müllen, *Angew. Chem. Int. Ed.* **2008**, *47*, 10175–10178.

3. a) D. Lorbach, A. Keerthi, T. M. Figueira-Duarte, M. Baumgarten, M. Wagner, K. Müllen, *Angew. Chem. Int. Ed.* **2016**, *55*, 418–421. b) K. Ikemoto, S. Sato, H. Isobe, *Chem. Lett.* **2015**, *45*, 217–219.
4. M. Kreyenschmidt, M. Baumgarten, N. Tyutyulkov, K. Müllen, *Angew. Chem. Int. Ed. Engl.* **1994**, *33*, 1957–1959.
5. M. V. Ivanov, K. Thakur, A. Boddeda, D. Wang, R. Rathore, *J. Phys. Chem. C* **2017**, *121*, 9202–9208.
6. a) T. M. Figueira-Duarte, P. G. Del Rosso, R. Trattnig, S. Sax, E. J. W. List, K. Müllen, *Adv. Mater.* **2010**, *22*, 990–993. b) R. Trattnig, T. M. Figueira-Duarte, D. Lorbach, W. Wiedemair, S. Sax, S. Winkler, A. Vollmer, N. Koch, M. Manca, M. A. Loi, M. Baumgarten, E. J. W. List, K. Müllen, *Optics Express* **2011**, *19*, A1281–A1293. c) Y. Gao, H. Bai, G. Shi, *J. Mater. Chem.* **2010**, *20*, 2993–2998. d) G. Lu, G. Shi, *J. Electroanal. Chem.* **2006**, *586*, 154–160. e) G. Lu, L. Qu, G. Shi, *Electrochim. Acta* **2005**, *51*, 340–346. f) L. Qu, G. Shi, *Chem. Commun.* **2004**, 2800–2801. g) X.-G. Li, Y.-W. Liu, M.-R. Huang, S. Peng, L.-Z. Gong, M. G. Mahoney, *Chem. Eur. J.* **2010**, *16*, 4803–4813. h) J.-Y. Hu, X. Feng, H. Tomiyasu, N. Seto, U. Rayhan, M. R. J. Elsegood, C. Redshaw, T. Yamato, *J. Mol. Struct.* **2013**, *1047*, 194–203.
7. F. Lu, T. Takaya, K. Iwata, I. Kawamura, A. Saeki, M. Ishii, K. Nagura, T. Nakanishi, *Sci. Rep.* **2017**, *7*, 3416.
8. a) B. Narayan, T. Nakanishi in *Functional Organic Liquids* (Ed. T. Nakanishi), *Wiley-VCH, Weinheim*, **2019**, pp. 1–20. b) S. S. Babu, T. Nakanishi, *Chem. Commun.* **2013**, *49*, 9373–9382. c)

A. Ghosh, T. Nakanishi, *Chem. Commun.* **2017**, 53, 10344–10357. d) F. Lu, K. Jang, I. Osica, K. Hagiwara, M. Yoshizawa, M. Ishii, Y. Chino, K. Ohta, K. Ludwichowska, K. J. Kurzydowski, S. Ishihara, T. Nakanishi, *Chem. Sci.* **2018**, 9, 6774–6778. e) S. S. Babu, J. Aimi, H. Ozawa, N. Shirahata, A. Saeiki, S. Seki, A. Ajayaghosh, H. Möhwald, T. Nakanishi, *Angew. Chem. Int. Ed.* **2012**, 51, 3391–3395.

9. a) E. A. Younes, K.-L. M. Williams, J. C. Walsh, C. M. Schneider, G. J. Bodwell, Y. Zhao, *RSC Adv.* **2015**, 5, 23952–23956. b) M. Khadem, J. C. Walsh, G. J. Bodwell, Y. Zhao, *Org. Lett.* **2016**, 18, 2403–2406. c) Z. A. Tabasi, E. A. Younes, J. C. Walsh, D. W. Thompson, G. J. Bodwell, Y. Zhao, *ACS Omega* **2018**, 3, 16387–16397.

10. There does not appear to be a published experimental barrier to rotation for 1,1'-bipyrene. It would, however, be expected to be close to that of 1,1'-binaphthyl, for which energy barriers of 24.1 kcal/mol (44 °C in benzene) and 23.5 kcal/mol (55 °C in DMF) have been measured. See: a) A. K. Colter, L. M. Clemens, *J. Phys. Chem.* **1964**, 68, 651-654. b) A. S. Cooke, M. M. Harris, *J. Chem. Soc.* **1963**, 2365-2373. Our calculated (M06-2X/6-31G*) barriers (see Supporting Information) for 1,1'-binaphthyl (26.2 kcal/mol) and 1,1'-bipyrene (25.8 kcal/mol) are indeed similar.

11. G. Venkataramana, P. Dongare, L. N. Dawe, D. W. Thompson, Y. Zhao, G. J. Bodwell, *Org. Lett.* **2011**, 13, 2240–2243.

12. J. C. Walsh, K.-L. M. Williams, D. Lungerich, G. J. Bodwell, *Eur. J. Org. Chem.* **2016**, 5933–5936. [13] A. M. Dmytrejchuk, S. N. Jackson, R. Meudom, J. D. Gorden, B. L. Merner, *J. Org. Chem.* **2018**, 83, 10660–10667.

14. a) E. B. Pinxterhuis, P. Visser, I. Esser, J.-B. Gualtierotti, B. L. Feringa, *Angew. Chem. Int. Ed.* **2018**, *57*, 9452–9455. b) E. B. Pinxterhuis, M. Giannerini, V. Hornillos, B. L. Feringa, *Nat. Commun.* **2016**, *7*, 11698.

15. L. Zhai, R. Shukla, R. Rathore, *Org. Lett.* **2009**, *11*, 3474–3477.

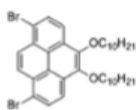
16. Assignment of the electronic transitions for **8a** can be made by analogy to closely related systems described by Hynes based on the extensive studies of Thulstrup. The assignments of four π - π^* transitions using Platt notation are: (a) a forbidden $S_0 \rightarrow 1L_b$ transition aligned across the short axis of the pyrenyl skeleton ($E_{\text{abs}}(\text{pyrene}) = 26800 \text{ cm}^{-1}$; $E_{\text{abs}}(\mathbf{8a}) = 26667 \text{ cm}^{-1}$); (b) a higher energy allowed $S_0 \rightarrow 1L_a$ (check the superscripts and subscripts that are appropriate here – and elsewhere in this reference) transition that lies on the long axis of pyrene skeleton ($E_{\text{abs}}(\text{pyrene}) = 29500 \text{ cm}^{-1}$; $E_{\text{abs}}(\mathbf{8b}) = 28820 \text{ cm}^{-1}$). Depending on the substituent pattern and the solvent, the $S_0 \rightarrow 1L_b$ may gain intensity through vibronic coupling with the $S_0 \rightarrow 1L_a$ transition. The vibronic coupling depends on the energy gap between the $1L_b$ and $1L_a$ electronic states ($\Delta E_{\text{abs}}(\text{pyrene}) = 2700 \text{ cm}^{-1}$; $\Delta E_{\text{abs}}(\mathbf{8b}) = 2150 \text{ cm}^{-1}$). The two major higher lying transitions are assigned to $S_0 \rightarrow 1B_b$ ($E_{\text{abs}}(\text{pyrene}) = 36200 \text{ cm}^{-1}$; $E_{\text{abs}}(\mathbf{8b}) = 35590 \text{ cm}^{-1}$) and a $S_0 \rightarrow 1B_a$ ($E_{\text{abs}}(\text{pyrene}) = 41000 \text{ cm}^{-1}$; $E_{\text{abs}}(\mathbf{8b}) = 41152 \text{ cm}^{-1}$) transitions respectively. a) T.-H. Tran-Thi, C. Prayer, P. Uznanski, J. T. Hynes, *J. Phys. Chem. A* **2002**, *106*, 2244–2255. b) E. W. Thulstrup, J. W. Downing, J. Michl, *Chem. Phys.* **1977**, *23*, 307–319.

17. J. A. Simon, S. L. Curry, R. H. Schmechl, T. R. Schatz, P. Piotrowiak, X. Jin, R. P. Thummel, *J. Am. Chem. Soc.* **1997**, *119*, 11012–11022.

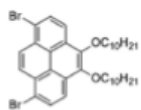
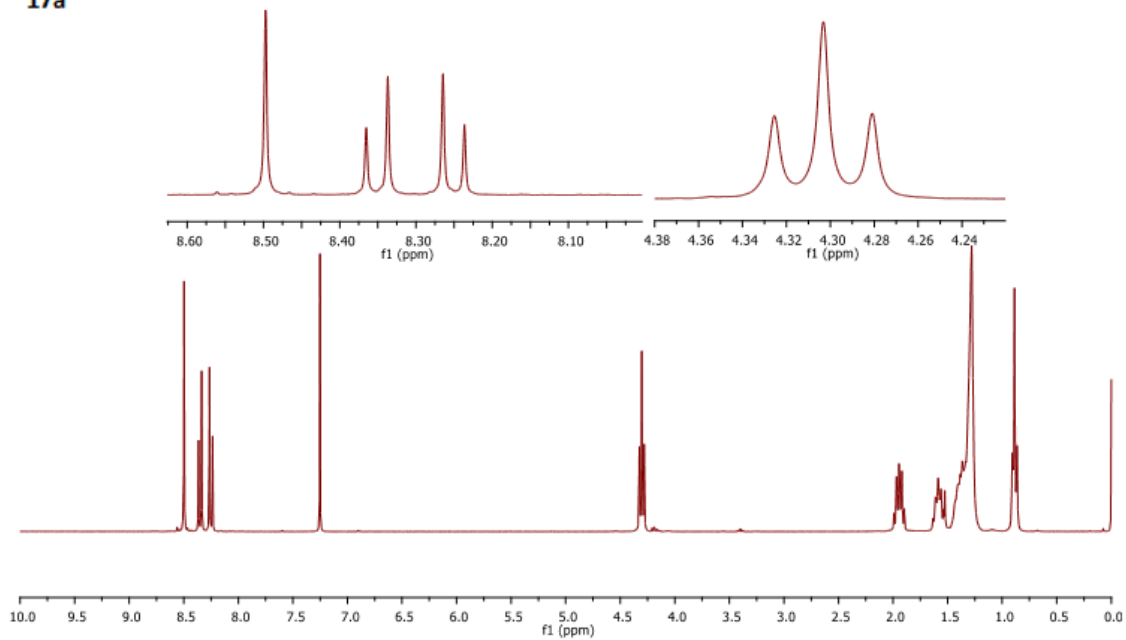
18. P. Chen, M. Curry, T. J. Meyer, *Inorg. Chem.* **1989**, *28*, 2271–2280.

19. M. V. Ivanov, M. R. Talipov, A. Boddeda, S. H. Abdelwahed, R. Rathore, *J. Phys. Chem C* **2017**, *121*, 1552–1561.
20. D. R. Coulson, L. C. Satek, S. O. Grim, *Inorg. Synth.* **1972**, *13*, 121–124.
21. D. F. Eaton *Pure Appl. Chem.* **1988**, *60*, 1107–1114.
22. D. R. James, A. Siemiarczuk, W. R. Ware, *Rev. Sci. Instr.* **1992**, *63*, 1710–1716.
23. M. J. Frisch, G. W. Trucks, H. B. Schlegel, G. E. Scuseria, M. A. Robb, J. R. Cheeseman, G. Scalmani, V. Barone, G. A. Petersson, H. Nakatsuji, X. Li, M. Caricato, A. V. Marenich, J. Bloino, B. G. Janesko, R. Gomperts, B. Mennucci, H. P. Hratchian, J. V. Ortiz, A. F. Izmaylov, J. L. Sonnenberg, D. Williams-Young, F. Ding, F. Lipparini, F. Egidi, J. Goings, B. Peng, A. Petrone, T. Henderson, D. Ranasinghe, V. G. Zakrzewski, J. Gao, N. Rega, G. Zheng, W. Liang, M. Hada, M. Ehara, K. Toyota, R. Fukuda, J. Hasegawa, M. Ishida, T. Nakajima, Y. Honda, O. Kitao, H. Nakai, T. Vreven, K. Throssell, J. A. Montgomery, Jr., J. E. Peralta, F. Ogliaro, M. J. Bearpark, J. J. Heyd, E. N. Brothers, K. N. Kudin, V. N. Staroverov, T. A. Keith, R. Kobayashi, J. Normand, K. Raghavachari, A. P. Rendell, J. C. Burant, S. S. Iyengar, J. Tomasi, M. Cossi, J. M. Millam, M. Klene, C. Adamo, R. Cammi, J. W. Ochterski, R. L. Martin, K. Morokuma, O. Farkas, J. B. Foresman, and D. J. Fox, Gaussian, Inc., Wallingford CT, 2016

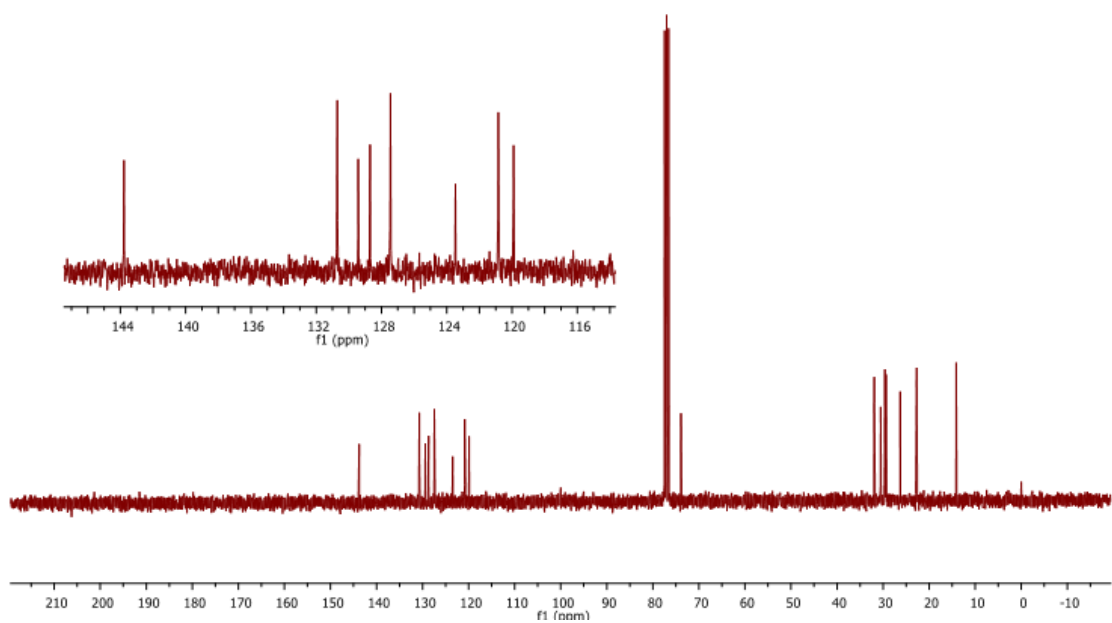
Appendix

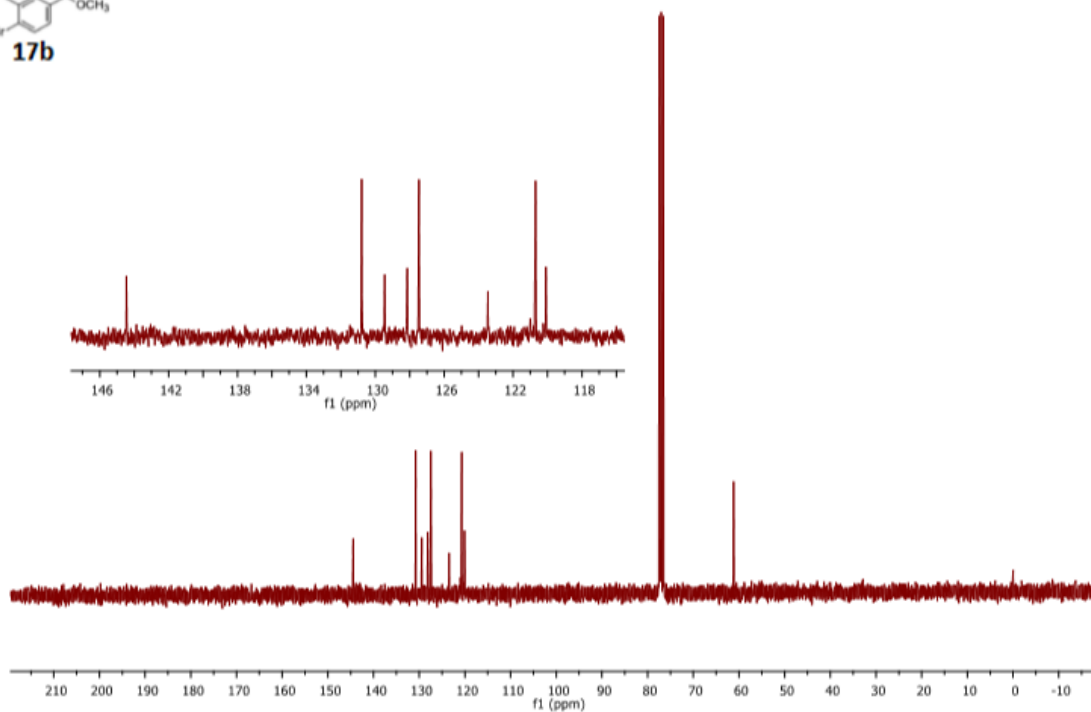
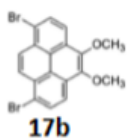
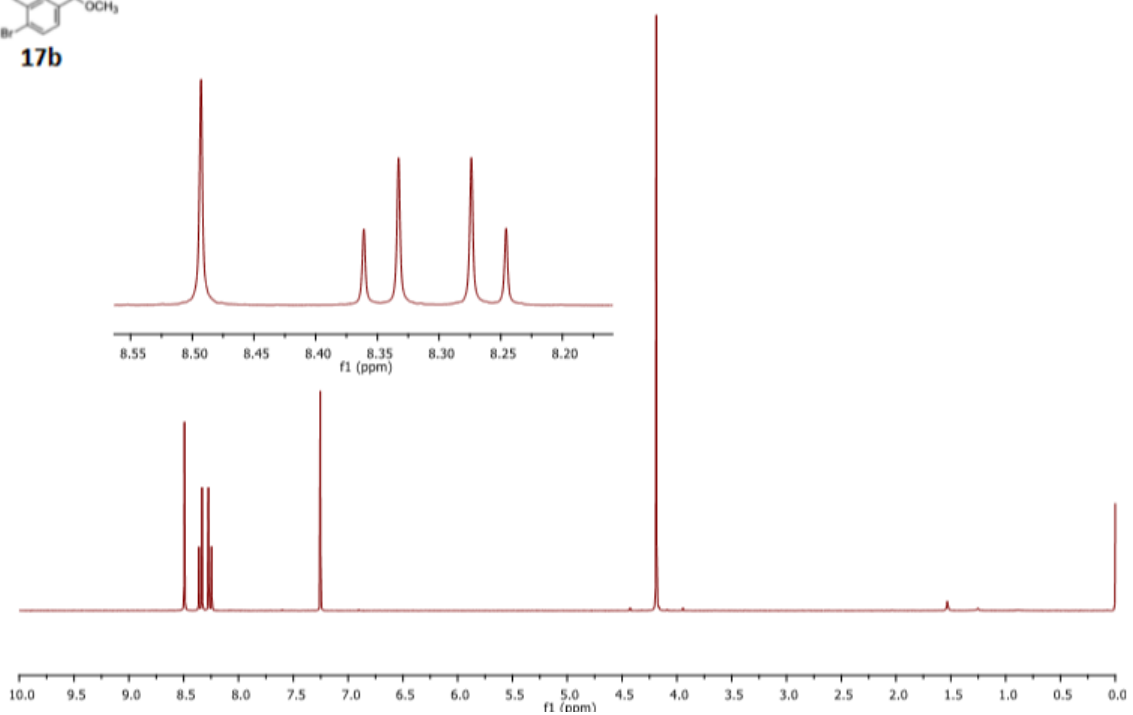
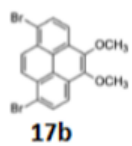


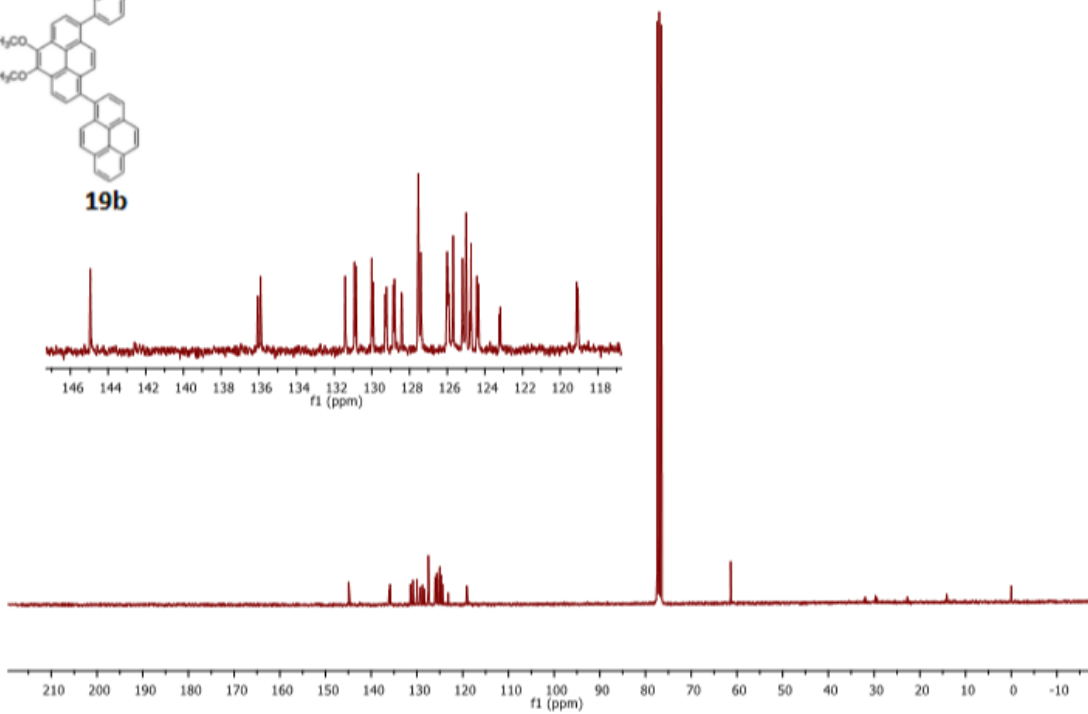
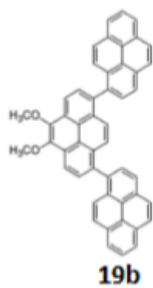
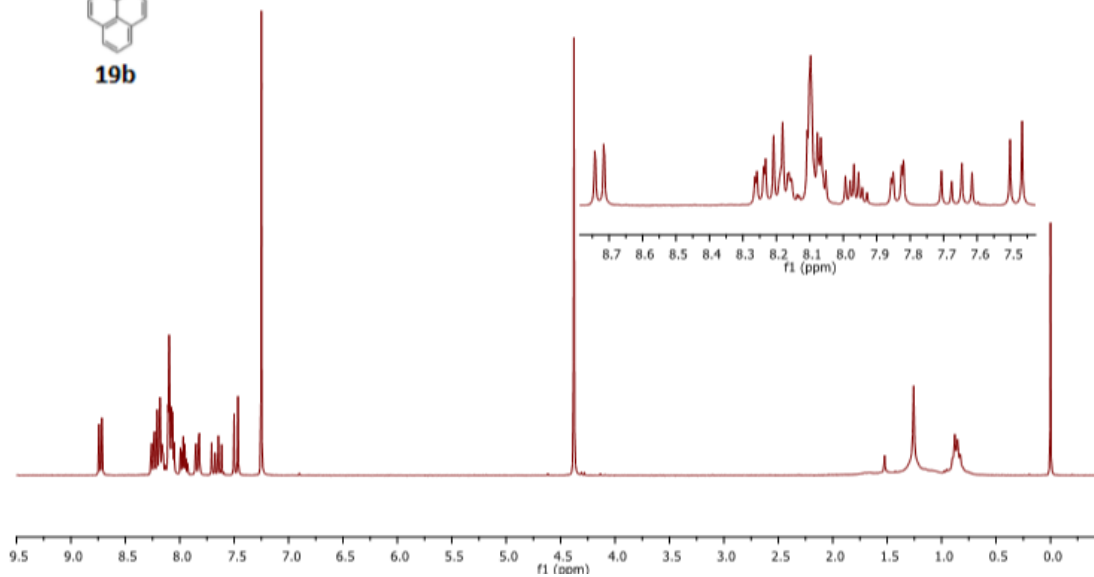
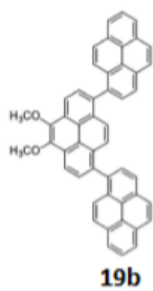
17a

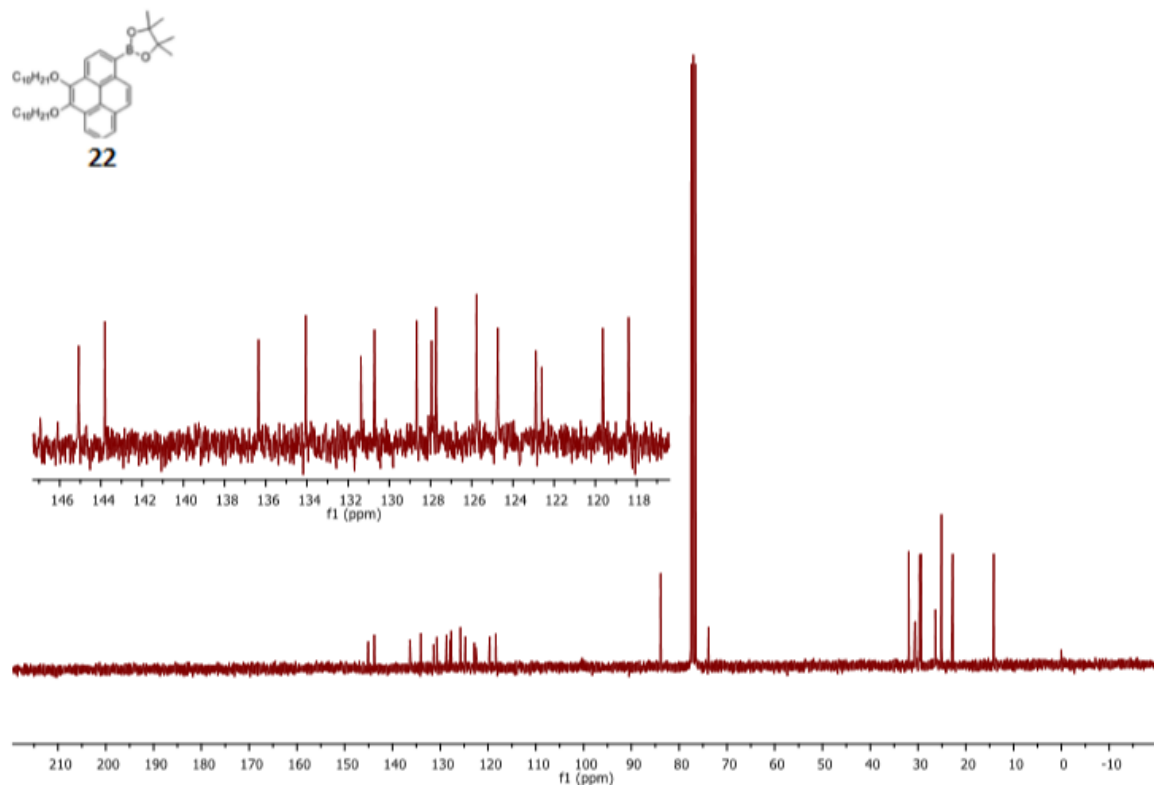
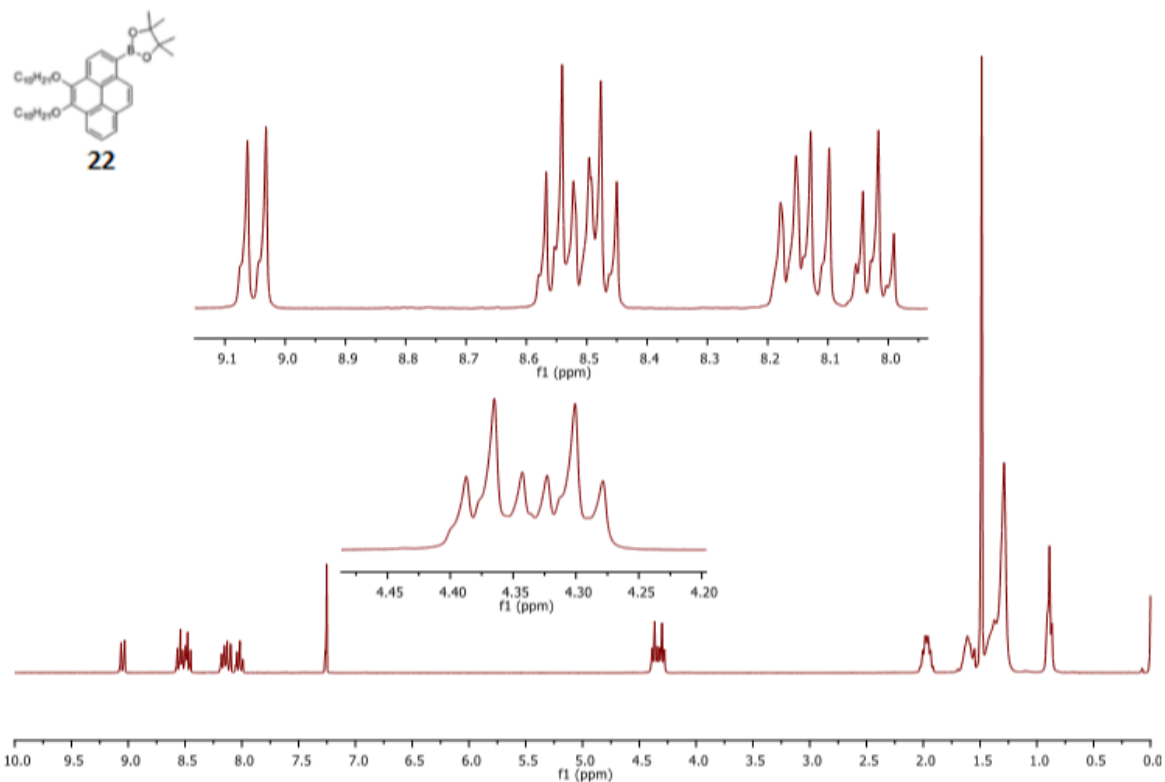


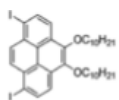
17a



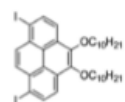
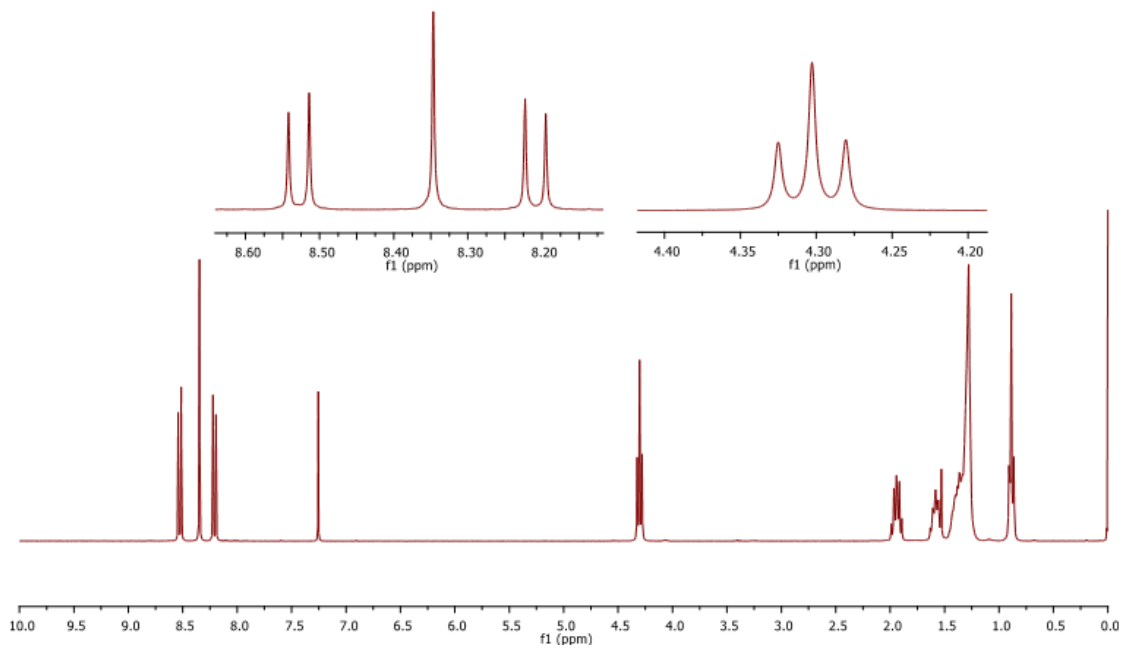




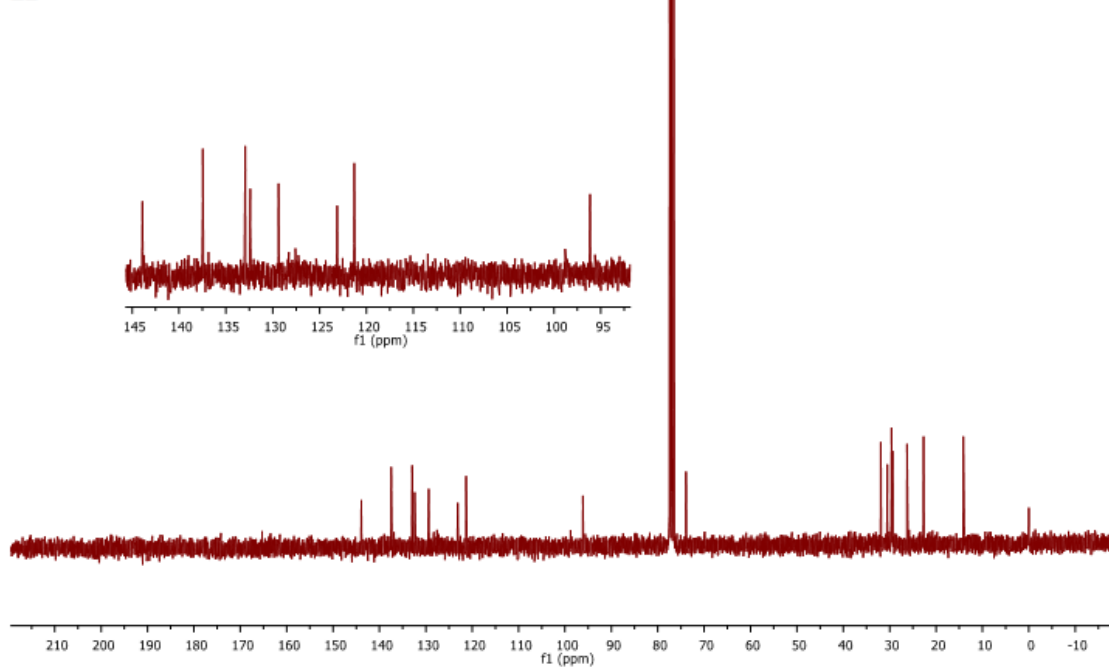


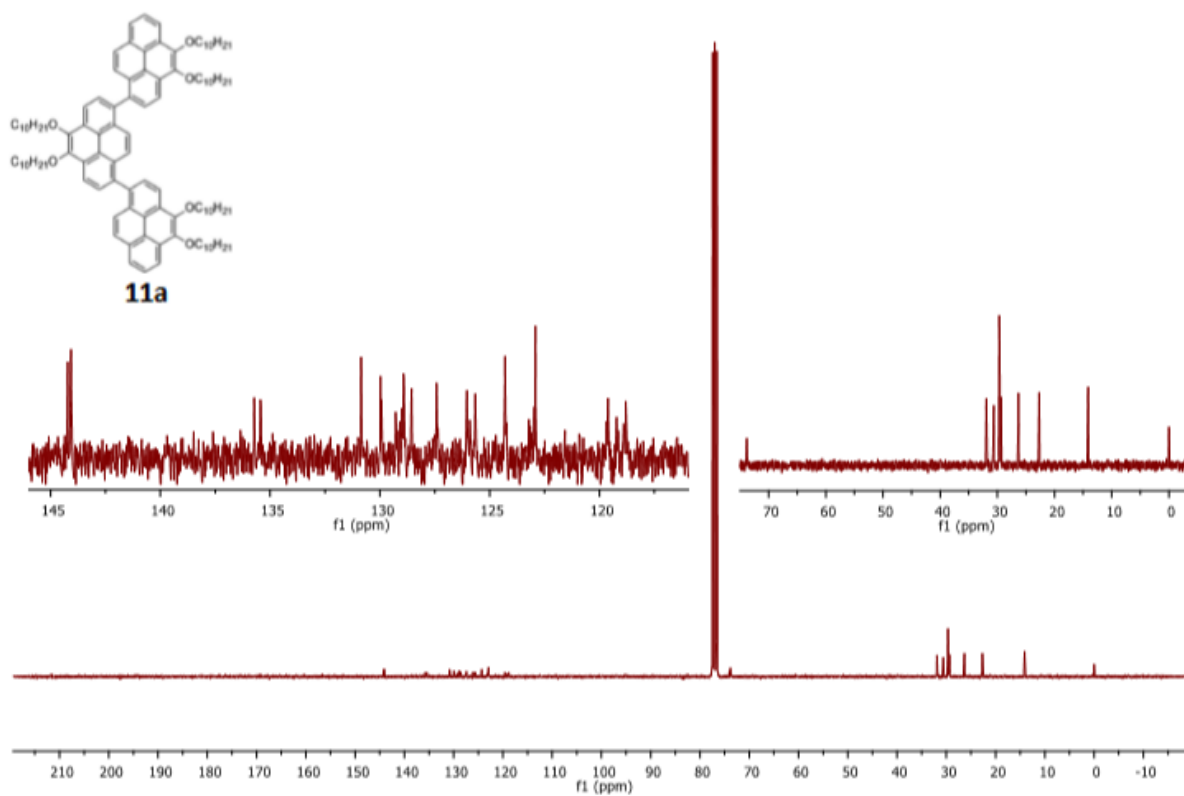
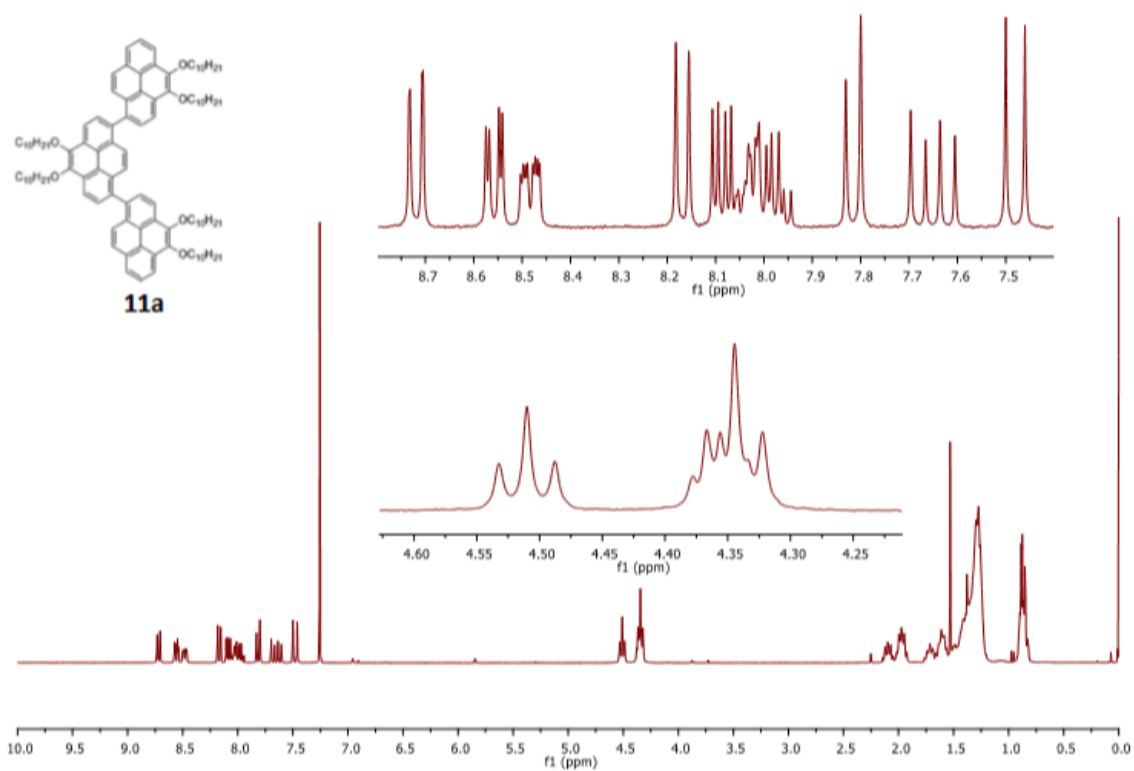


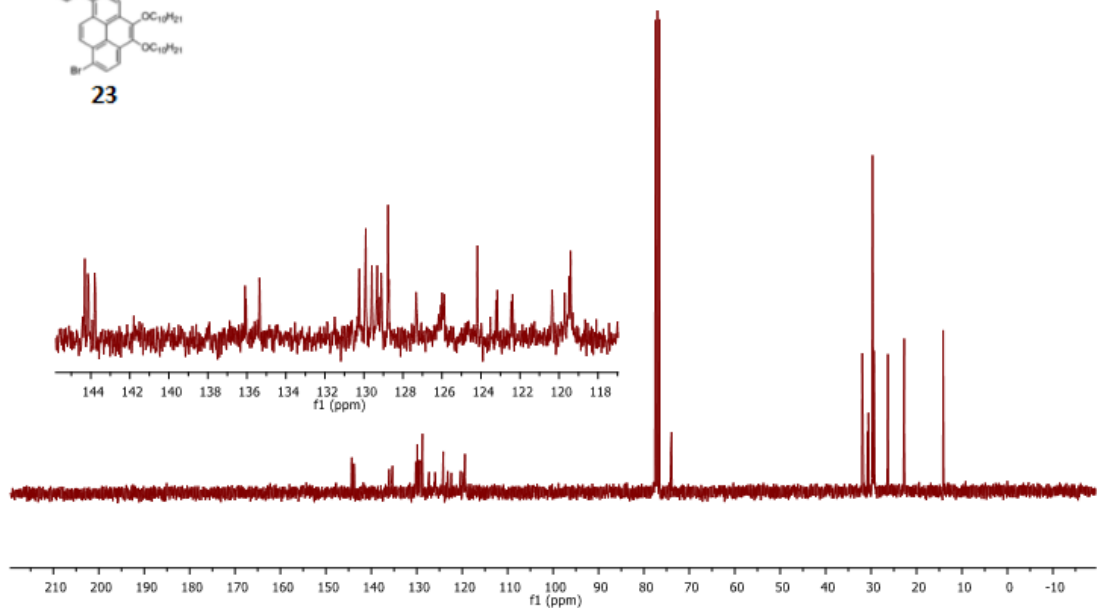
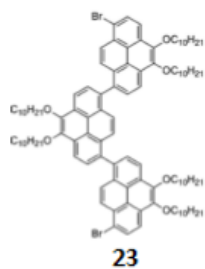
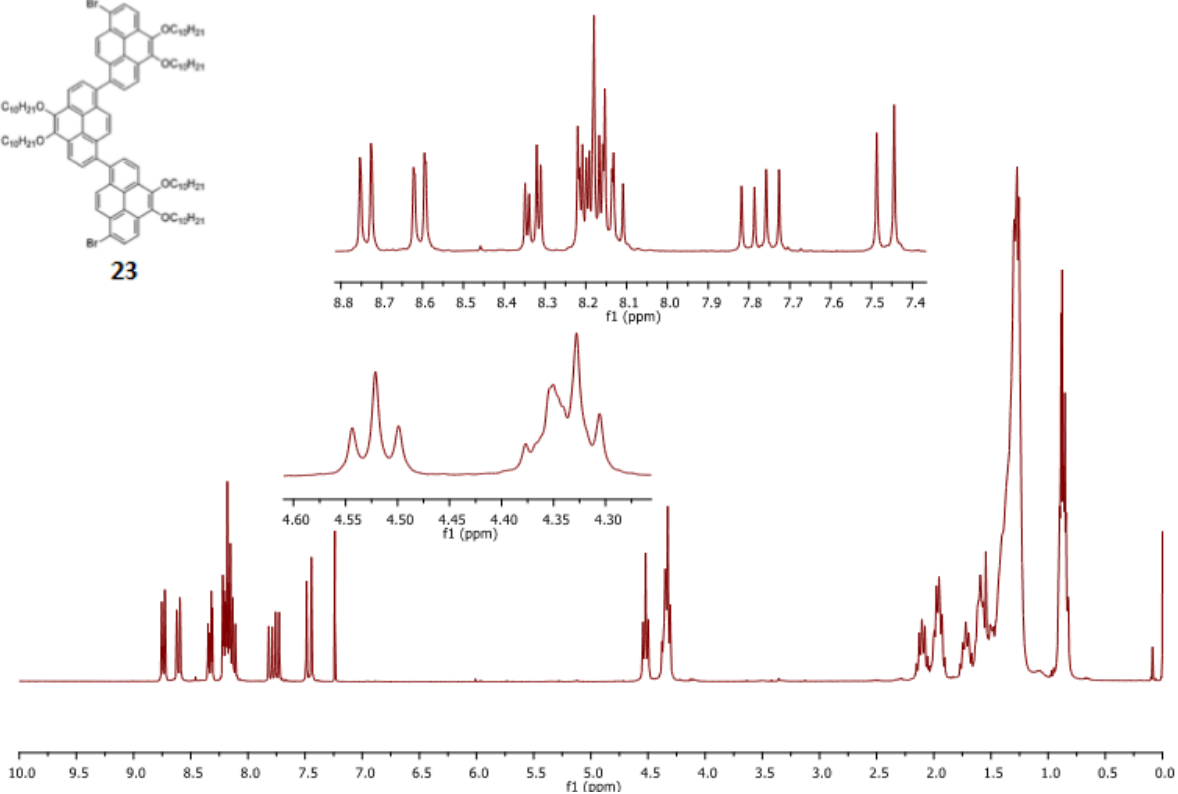
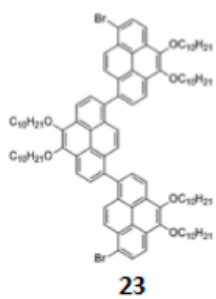
21

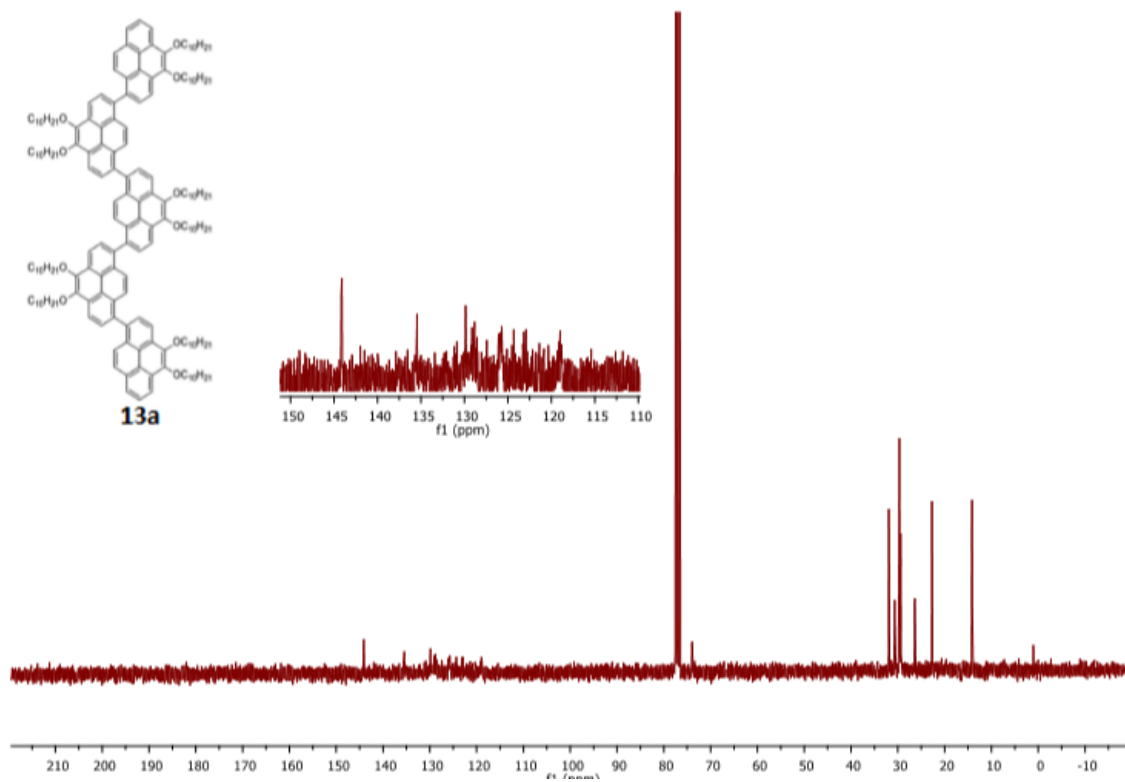
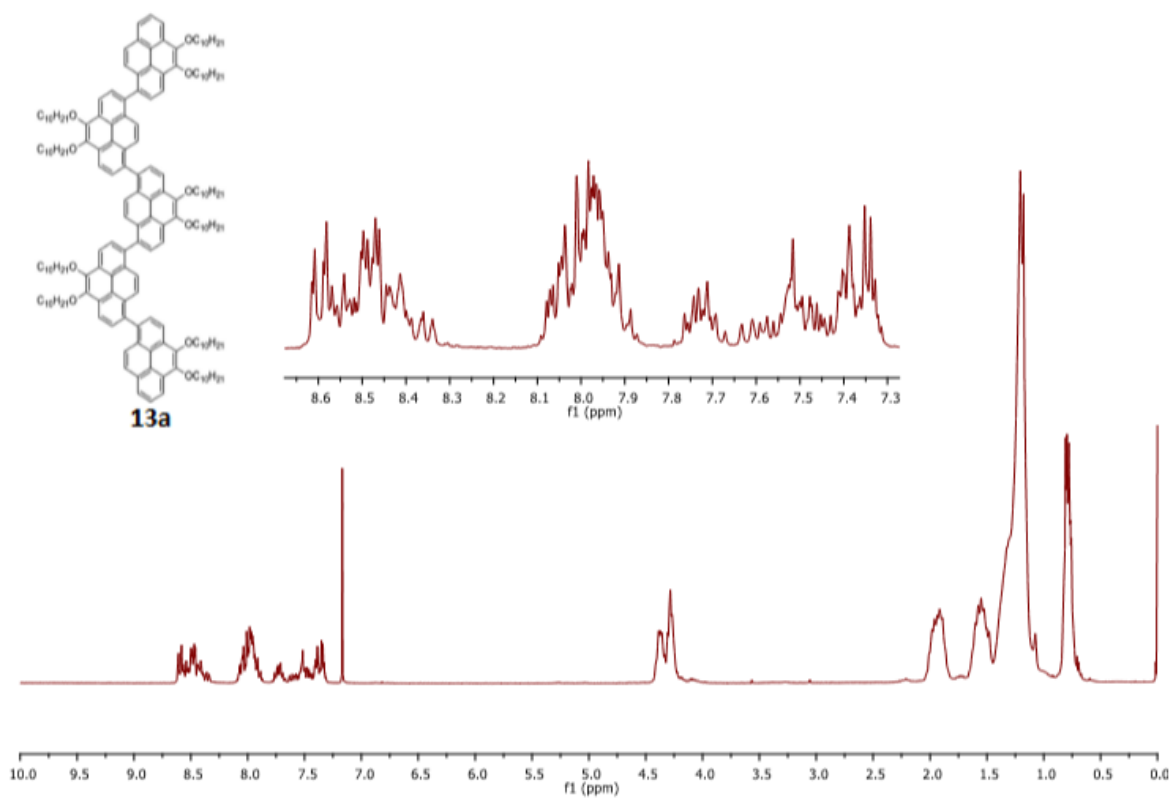


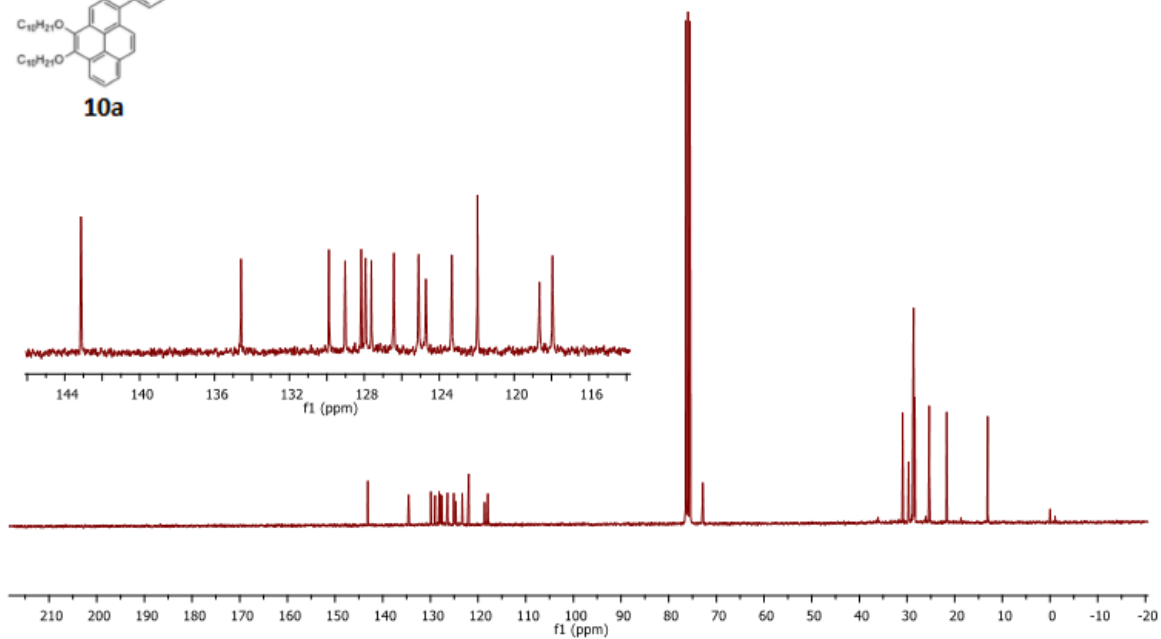
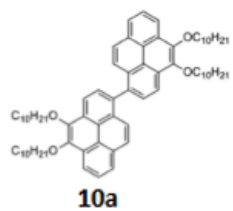
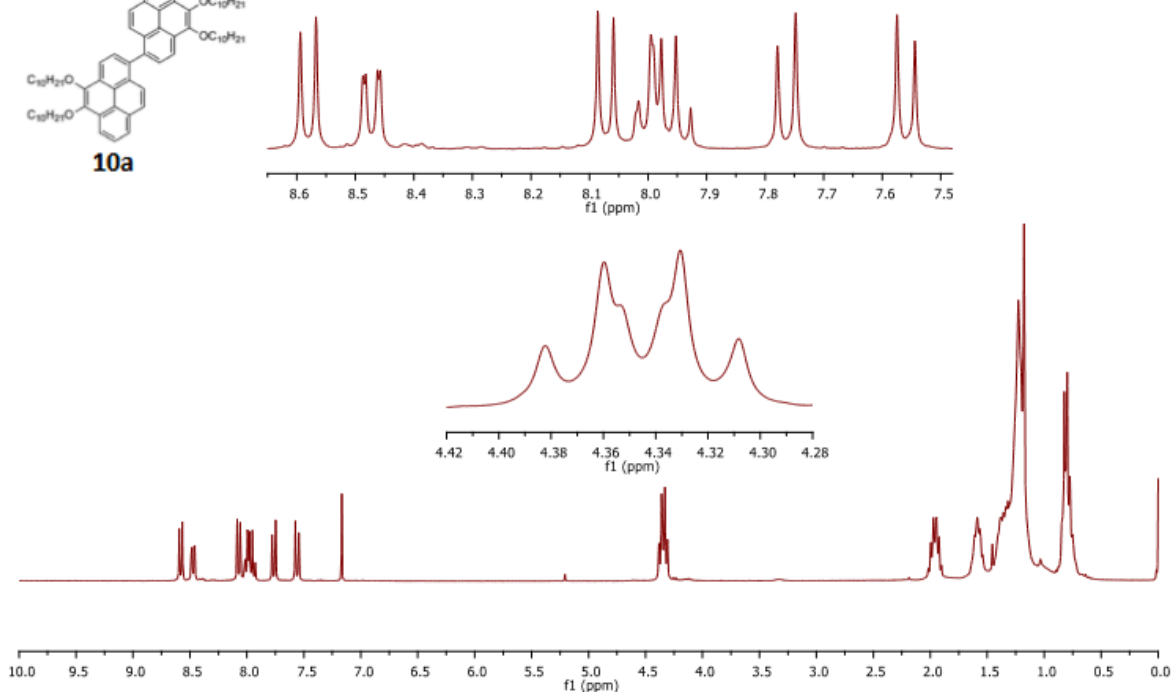
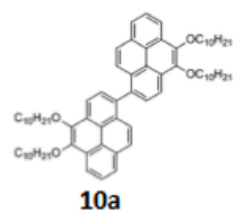
21

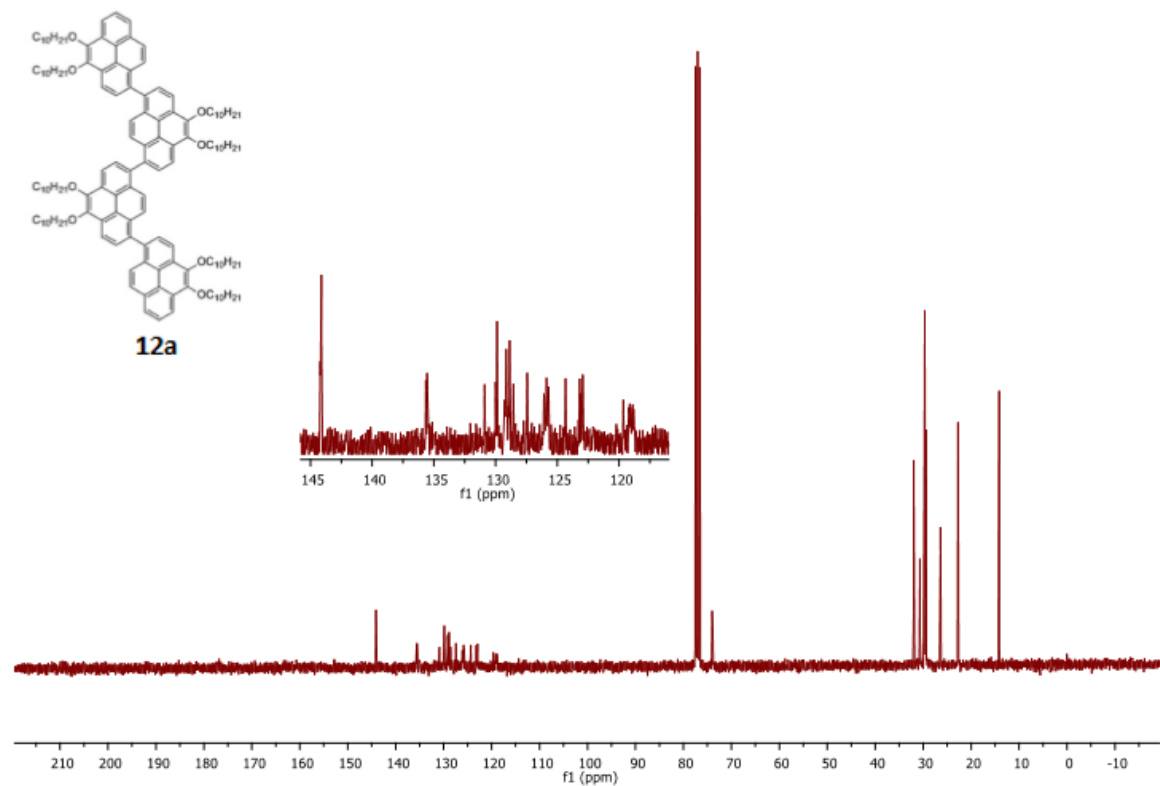
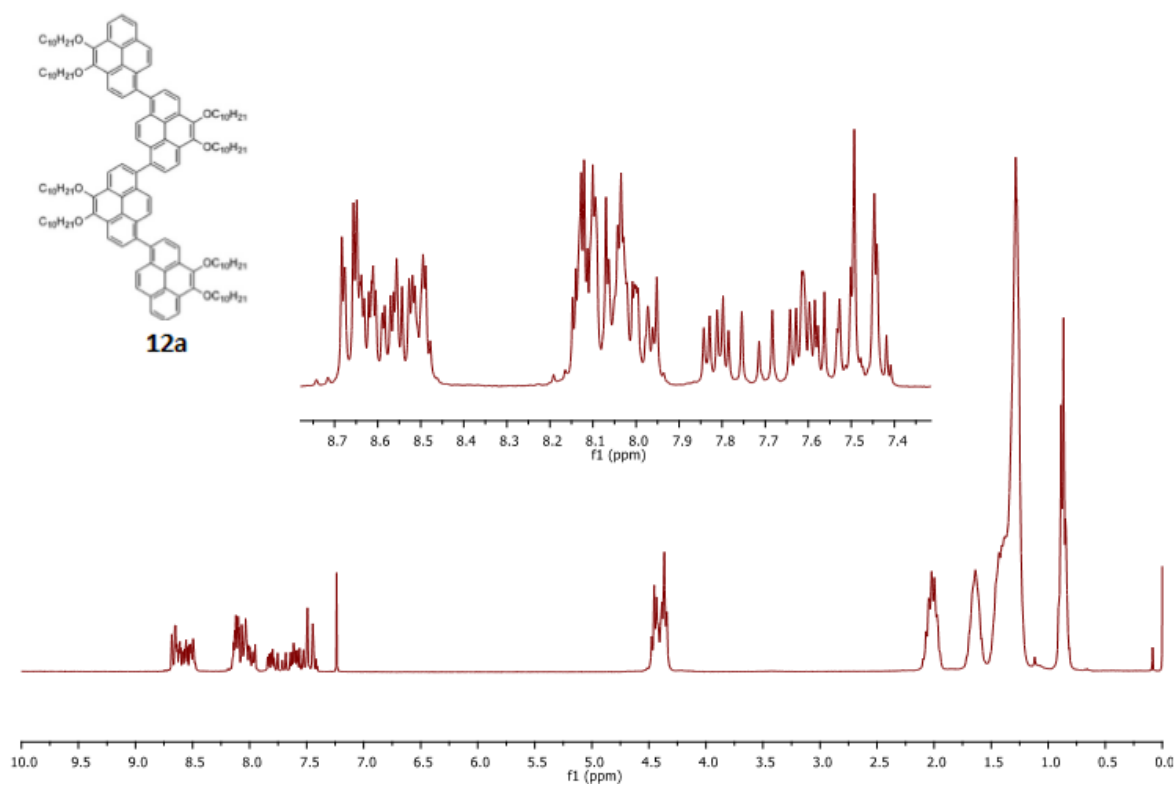


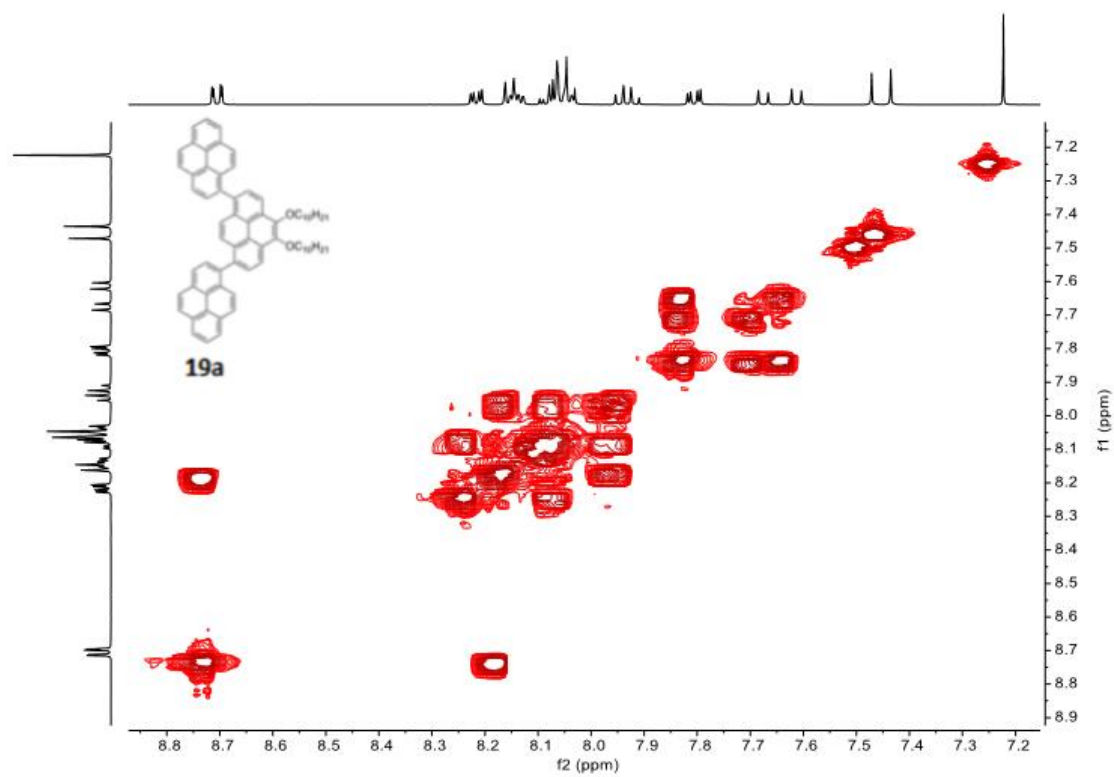
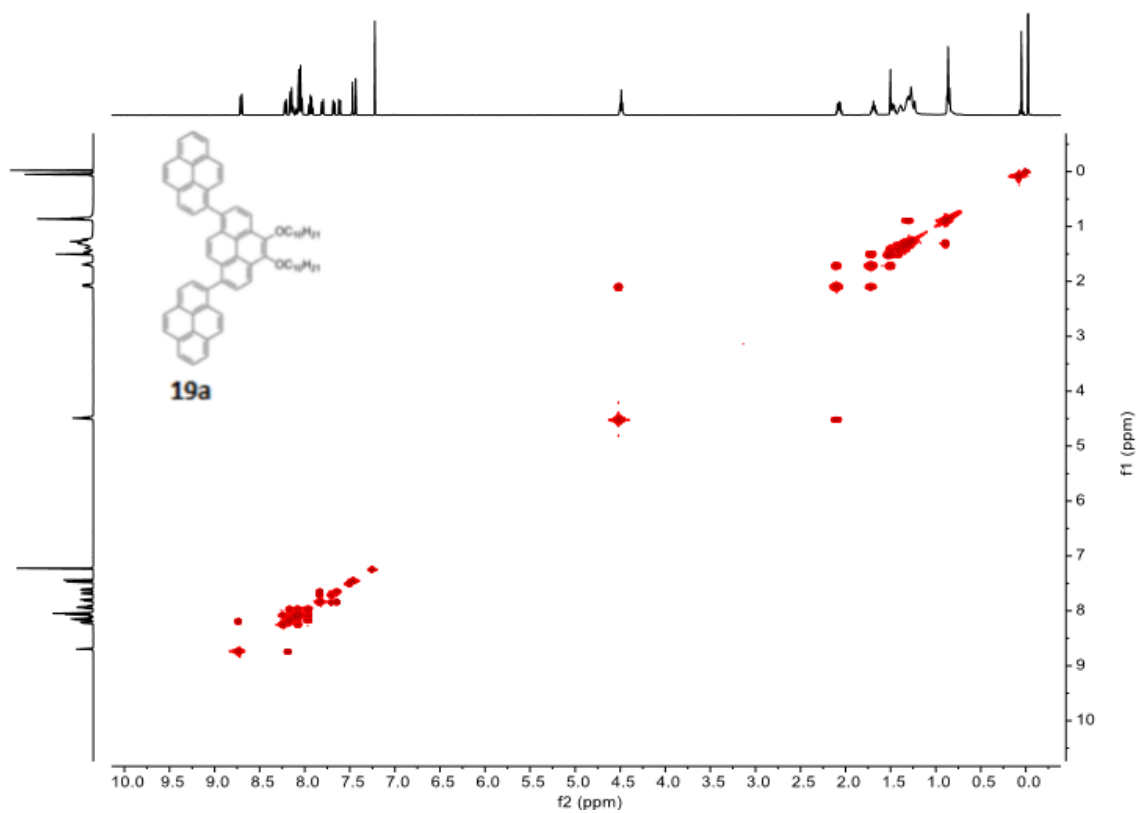


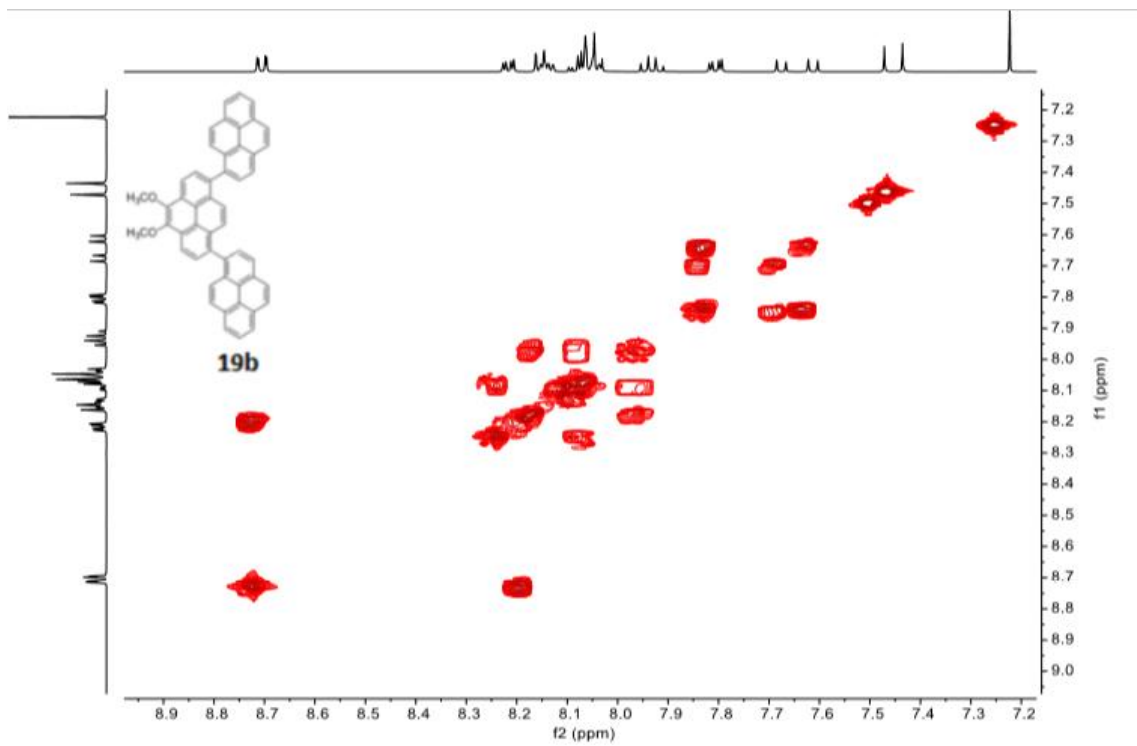
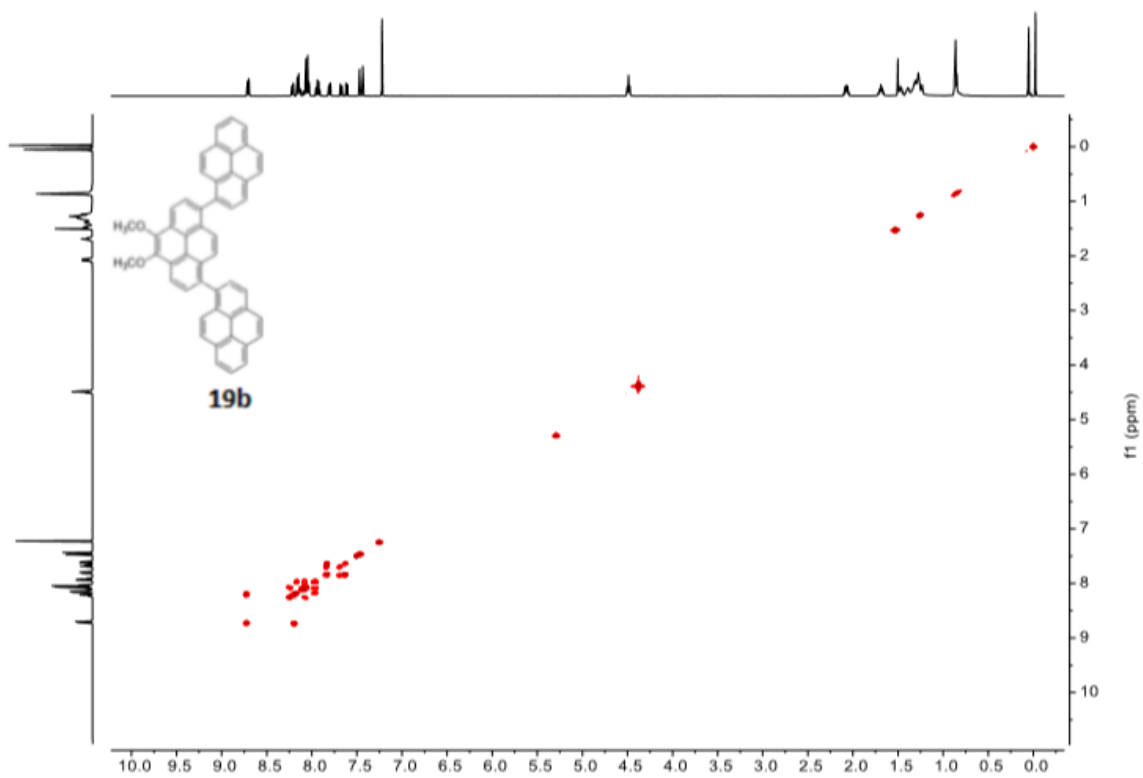












Stereoisomers of 10a–13a and 6b.

a) Compounds 10a–13a

Dimer 10a	R S	Pair of enantiomers
Trimer 11a	RR SS Diastereomer 1 (\pm)	1 : 1
	RS SR Diastereomer 2 (meso)	
Tetramer 12a	RRR SSS Diastereomer 1 (\pm)	1 : 1 : 1 : 1
	RrS SrR Diastereomer 2 (\pm) (meso)	
	RSR SRS Diastereomer 3 (\pm)	
	RsS SsR Diastereomer 4 (\pm) (meso)	
Diastereomers 2 and 4 have a pseudo chiral axis, which is designated with a lower-case descriptor.		
Pentamer 13a	RRRR SSSS Diastereomer 1 (\pm)	1 : 2 : 2 : 1 : 1 : 1
	RRRS SSSR Diastereomer 2 (\pm)	
	RRSR SSRS Diastereomer 3 (\pm)	
	RRSS SSRR Diastereomer 4 (meso)	
	RSRR SRSS Diastereomer 3 (\pm)	
	RSRS SRSR Diastereomer 5 (meso)	
	RSSR SRRS Diastereomer 6 (\pm)	
	RSSS SRRR Diastereomer 2 (\pm)	

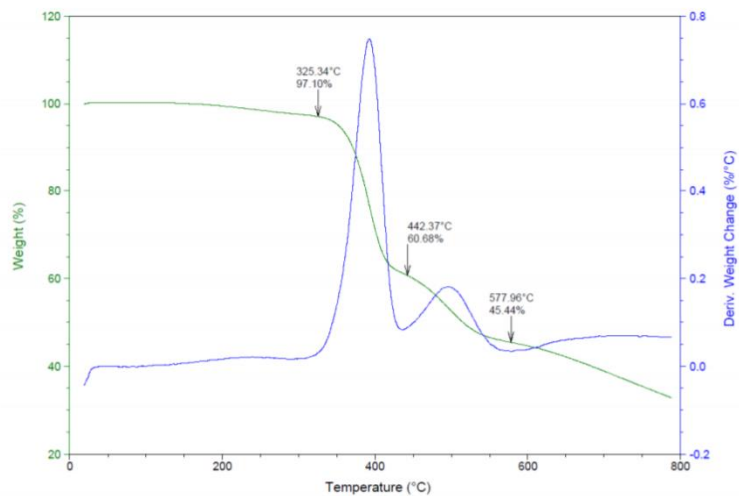


Figure 2.12 TGA Thermogram of tetramer **12a**

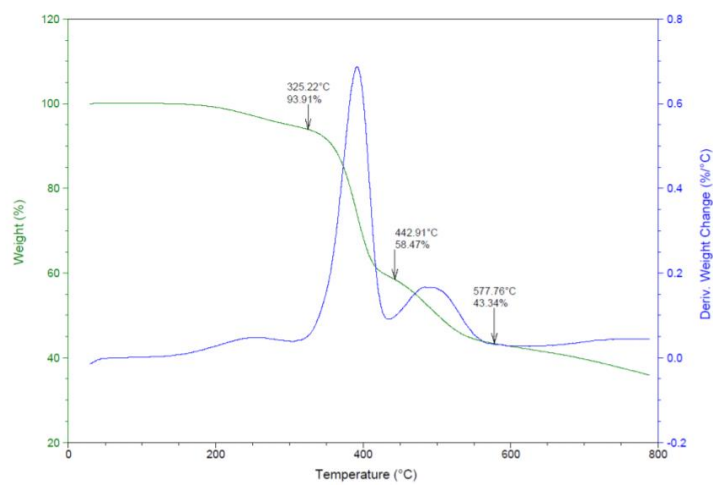


Figure 2.13 TGA thermogram of pentamer **13a**

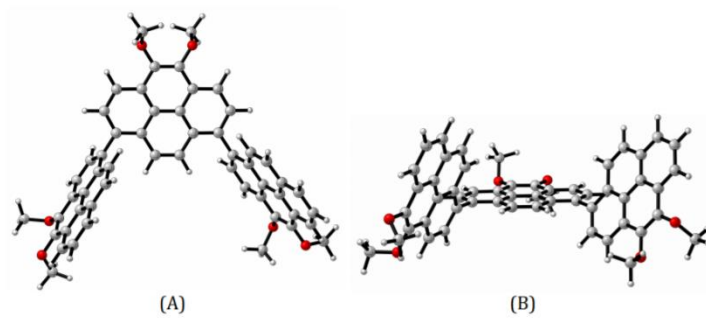


Figure 2.14 Optimized geometry of *meso*-S1 calculated at the B3LYP/6-31G(d) level of theory

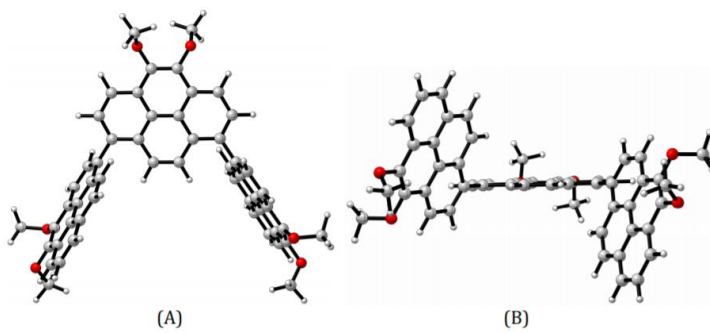


Figure 2.15 Optimized geometry of (±)-S1 calculated at the B3LYP/6-31G(d) level of theory.

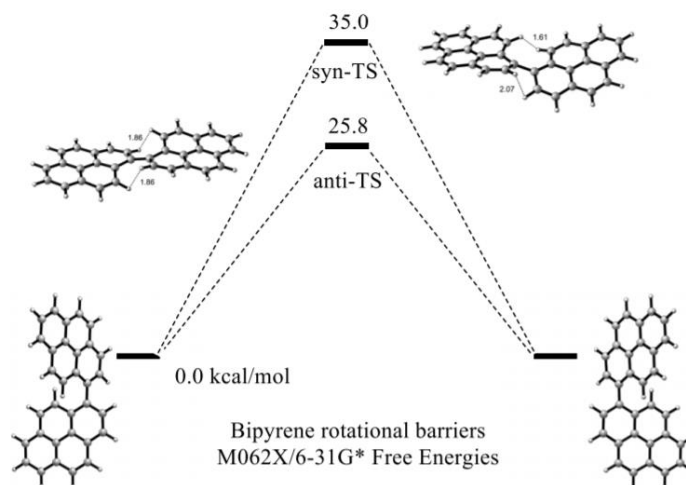


Figure 2.16 Interconversion of 1,1'-bipyrene enantiomers through *syn* and *anti*-transition states. Structures are similar to those reported earlier for 1,1'-binaphthyl, showing substantial distortion of the aromatic rings from planarity. Calculated barriers are similar for the binaphthyl and bipyrenyl rings.

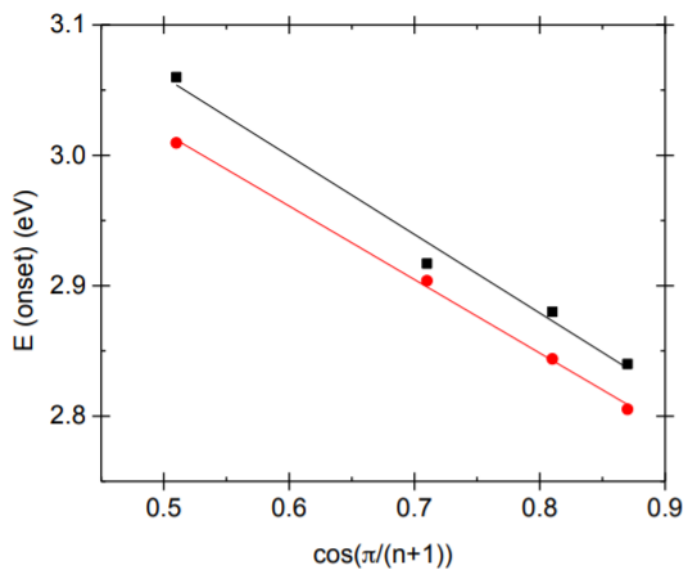


Figure 2.17 A plot of the onset energies for transition (centered at 360 nm) *vs.* $\cos[\pi/(n+1)]$ for **10a-13a** (black; slope = -0.60 , intercept = 3.36 ; $R^2 = 0.98$) and (red) the onset energies *vs.* $\cos[\pi/(n+1)]$ for oligo(1,6-pyrenylene)s **5** (slope = -0.56 , intercept = 3.30 ; $R^2 = 0.99$).

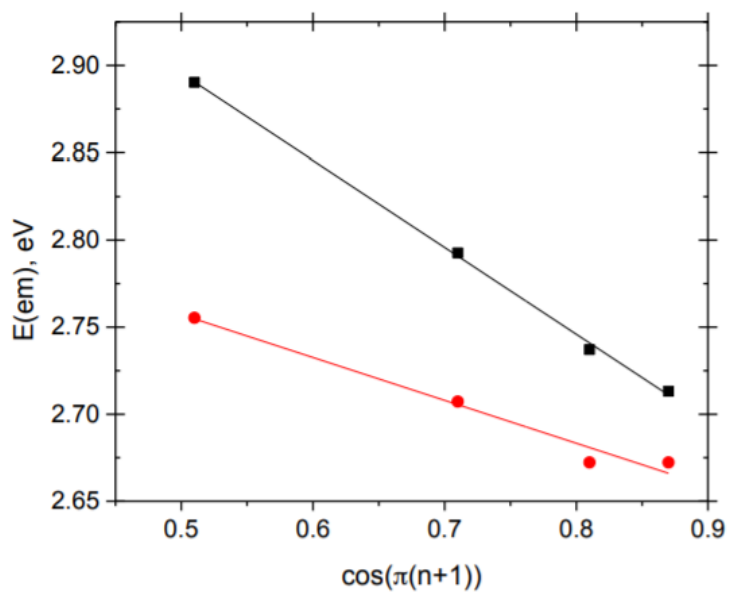


Figure 2.18 A plot of the emission energies vs $\cos[\pi/(n+1)]$ for compounds **10a-13a** (black; slope = -0.50 , intercept = 3.14 ; $R^2 = 0.98$) and (red) the onset energies vs $\cos[\pi/(n+1)]$ for oligo(1,6-pyrenylene)s **5** (slope = -0.25 , intercept = 2.88 ; $R^2 = 0.99$).

Chapter 3

From Functional Molecular Liquids to Functional Materials

Synthetic Macrocycles

Synthetic macrocyclic chemistry is generally agreed to have arrived with Pederson's accidental discovery of the crown ethers in 1967,^{[1][2]} the first of which was dibenzo-18-crown-6 (**1**). Pederson's discovery spawned the now huge fields of host-guest chemistry and supramolecular chemistry, which were led in their infancy by D. J. Cram and J.-M. Lehn, respectively. Pederson,^[3] Cram^[4] and Lehn's^[5] work culminated in sharing the 1987 Nobel prize in chemistry for, in the Nobel committee's words "...their development and use of molecules with structure-specific interactions of high selectivity".

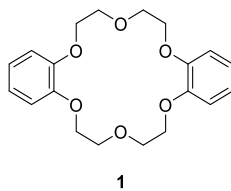


Figure 3.1 Pederson's macrocyclic dibenzo-18-crown-6 (**1**).

Shape-Persistent Macrocycles

Distinct from the Pederson's crown ethers, the family of macrocycles known as shape-persistent macrocycles (SPMs) have rigid, non-collapsible backbones. SPMs have been more rigorously defined by Grosberg and Khoklov as having an interior (known as a lumen) where the internal diameter (d) is, on average, equal to the contour length (l) of the molecular backbone divided by π ^[6] (Figure 3.2).

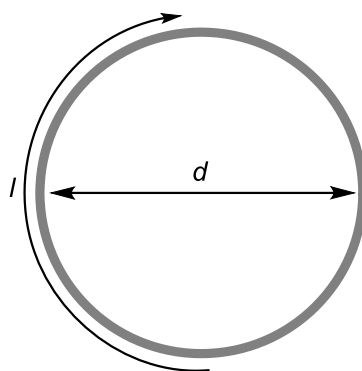


Figure 3.2 The formal definition of a shape-persistent macrocycle as described by Grosberg and Khoklov (when $d \approx l/\pi$).

Cyclophenylenes

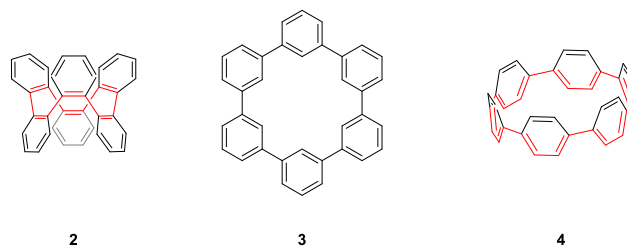


Figure 3.3 The three substitution patterns of [6]cyclophenylenes **2-4** with internal annulenes highlighted in red.

The cyclophenylenes are a subclass of SPMs composed of only benzene units (Figure 3.3). The symmetry and molecular beauty of molecules with this architecture have both been driving forces for work aimed at their synthesis and the plethora of chemical means to furnish biaryl bonds has been crucial to many of the successes in this area. Pictured in Figure 3.3 are examples of cyclophenylenes with differing substitution patterns, *ortho*-, *meta*- and *para*-substituted [6]cyclophenylenes **2-4**. Each arene in a cyclophenylene need not have the same substitution pattern and many systems bearing mixed-linkages are known. Most of these have been recently reviewed by Fujioka.^[7] It is, however, instructive to consider the cases which display unmixed substitution patterns.

The *ortho* and *para* substituted cyclophenylenes **2** and **4** display strong electronic communications around the macrocycle and, as highlighted in Figure 3.4, they contain uninterrupted annulene substructures. The [*n*]cycloorthophenylenes ([*n*]COPs) can be considered fully benzannulated all-*cis*-annulenes and the cycloparaphenylenes (CPP), as

benzannulated all-*trans*-annulenes. The COPs and CPPs are fully conjugated and, despite these two classes of cyclophenylenes sharing the property of resonance delocalization, the amount of attention they have received is very one-sided, with most of it having been directed toward the *para*-motif.

In contrast to the *ortho*- and *para*-cyclic oligomers, the *meta*-cyclophenylenes (CMP) display much larger band gaps and better thermal stability (*vide infra*) and they often act as insulators or high-bandgap materials owing to the lack of electronic communications between the rings (Figure 3.4).

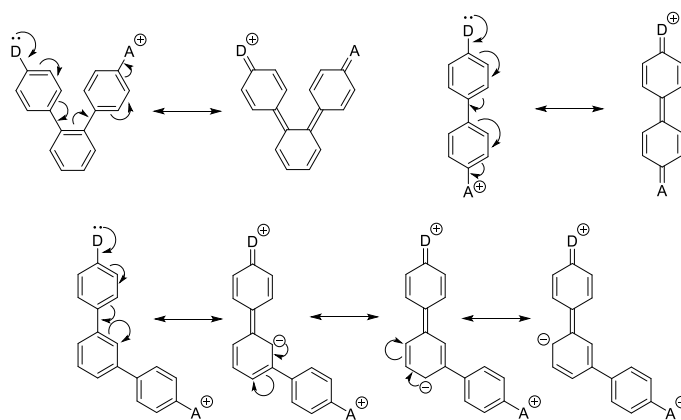


Figure 3.4 Illustration of the electronic communications in *para*- and *ortho*-substitutions and the lack of communication in *meta* substituents (D=donor, A=acceptor).

[*n*]Cycloorthophenylenes (COPs)

The class of [*n*]cycloorthophenylenes has received very little attention in the literature. The smallest two members of the series, biphenylene **5** and triphenylene **6** and are not usually seen in this light since they are also planar polycyclic aromatic hydrocarbons (PAH).

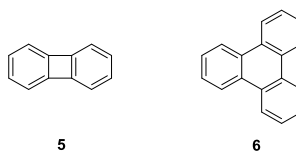
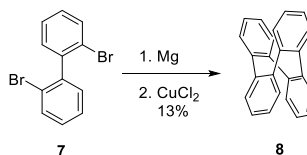


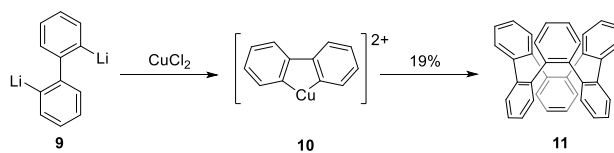
Figure 3.5 The first two members of the [*n*]COP family: **5** and **6**.

The first member of the series that can be considered a COP, distinct from the family of PAHs, is [4]COP (**8**). The first synthesis of this oligomer was reported in 1940 by Rapson and Shuttleworth, whose synthesis relied upon dimerization of 1,1'-dibromobiphenyl **7** using magnesium and cupric chloride (Scheme 3.1).^[8]



Scheme 3.1 Rapson and Shuttleworth's synthesis of [4]COP.

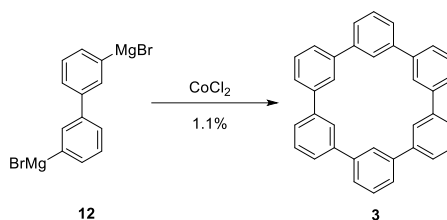
Wittig^[9] and Staab^[10] turned their attention towards the [*n*]COPs in the 1950s and 1960s. Wittig, through various metal salts of biphenyl, furnished and characterized a number of [*n*]cycloorthophenylenes such as [6]COP (hexabenz[12]annulene) (**8**), which can be seen as a segment of a (3,3)carbon nanotube (Scheme 3.2).



Scheme 3.2 Wittig's 1957 synthesis of hexabenz[12]annulene ([6]COP) **11**.

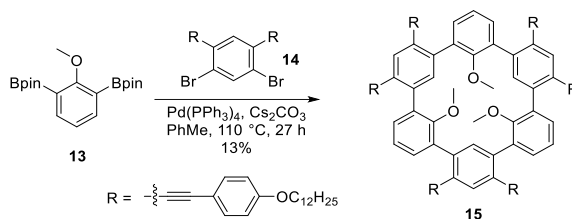
[*n*]Cyclometaphenylenes (CMPs)

The first [*n*]CMP, [6]CMP (**3**), was reported in 1968 by Staab,^[11] who synthesized it in 1.1% yield by treating the double Grignard reagent prepared from 3,3'-dibromobiphenyl with a dilute solution of cobalt(II) chloride (Scheme 3.3). [6]CMP displayed remarkable thermal stability. It was found to have a melting point of 509-511 °C and the compound could even be distilled under vacuum (10^{-4} mmHg) at 650 °C. While this property was noteworthy at the time, today it is a highly desired property for materials applications, not only in the context of high temperature devices, but also to allow purification by sublimation, which generally yields high purity samples.^[12]



Scheme 3.3 Staab's 1964 synthesis of [6]CMP (**3**).

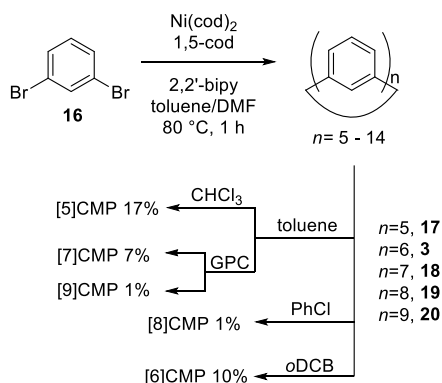
Before 2014, the highest yield reported for the construction of the [6]CMP skeleton was 13%. This was achieved by the Swager group through Suzuki macrocyclization from advanced intermediates **13** and **14** (Scheme 3.4).^[13] While this method allows for some fine tuning of the substituents on [6]CMP, methods to produce a range of CMPs in higher yield remained elusive until recently.



Scheme 3.4 Swager's synthesis of a highly decorated [6]CMP derivative.

[*n*]CMP chemistry experienced a revival in 2014 when Isobe and coworkers published an improved synthesis that took advantage of the Yamamoto coupling of 1,3-dibromobenzene (**16**). The reaction not only yielded [6]CMP (**3**) in a higher overall yield (10%), but also delivered [5]CMP (**17**) as the major product (17%) along with isolable amounts of previously unknown [*n*]CMPs **18-20**, where *n* = 7 to 9 (Scheme 3.5).^[14] At first blush, it is surprising that [5]CMP is the major product since it possesses by far the highest strain energy of any compound the reaction produces (Table 3.1). However, when the organometallic intermediate

that precedes the last bond closure is considered, i.e., the one that involves a [5]CMP with a nickel atom between two benzene rings, the overall strain energy before demetallation is likely closer to that of [6]CMP. Likewise, the cyclic precursor to [6]CMP is expected to be more strained than the product.



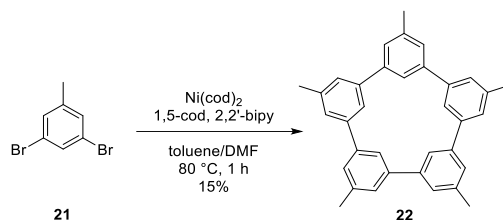
Scheme 3.5 Isobe’s synthesis of [5]-[9]CMP on a gram scale.

Owing to its increased strain energy, [5]CMP (**17**) has significantly lower thermal stability than the other members of the series. Nevertheless, the temperature of decomposition is still very high (358 °C) and this still lends itself well to high temperature device applications (Table 3.1).

Table 3.1 Measured absorption, temperature of decomposition and calculated strain energy of Isobe’s CMPs.^[14]

	λ_{max} (nm)	$T_{\text{dec.}}$ (°C)	Strain energy (kcal/mol)
[5]CMP	252	358	23
[6]CMP	250	451	1.3
[7]CMP	250	440	3.6
[8]CMP	246	449	1.6
[9]CMP	248	480	6.3

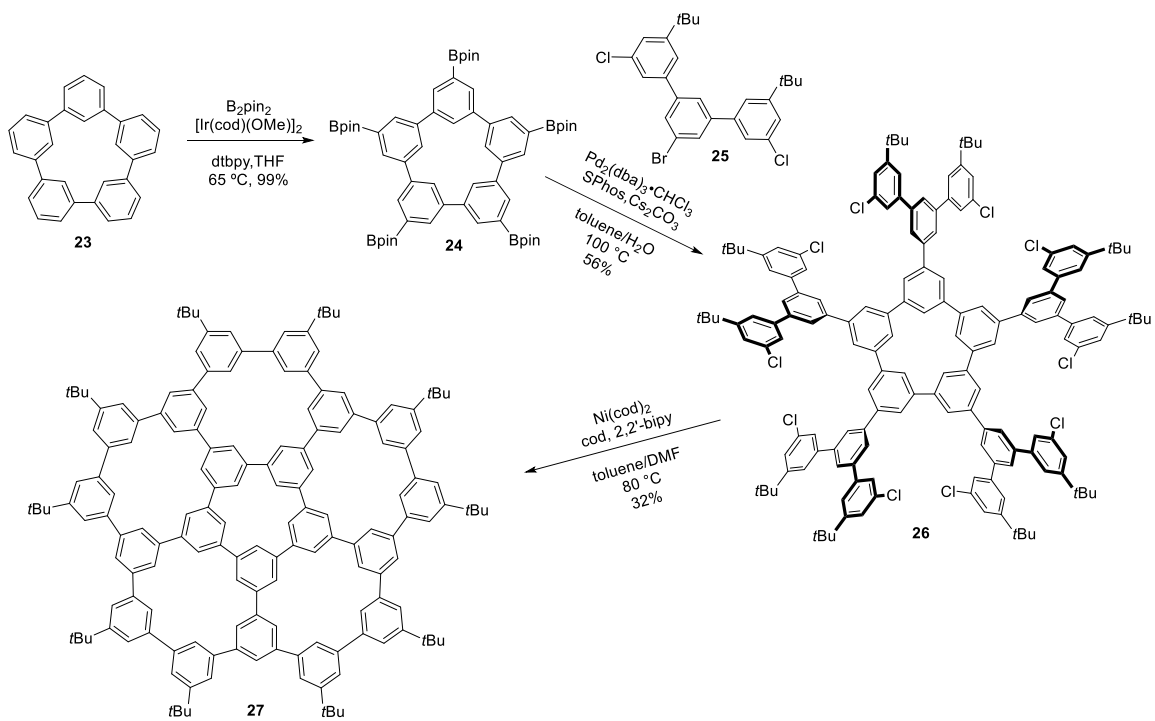
Isobe's work has lifted the [*n*]CMPs from being mainly of theoretical interest to being worthy of device application. Only two years after reporting the gram scale synthesis of several CMPs (*vide infra*), Isobe *et al.* achieved another landmark in CMP chemistry.^[15] By screening a number of alkylated derivatives of CMP, it was found that a pentamethyl derivative of [5]CMP, 5Me-[5]CMP (**22**) displayed remarkable efficiency in single layer OLED devices. Mirroring the previous synthesis of [*n*]CMPs, Isobe utilized a Yamamoto type coupling to deliver **22** in 15% yield, in a single step from commercially available 5-methyl-1,3-dibromobenzene (**21**) (Scheme 3.6).



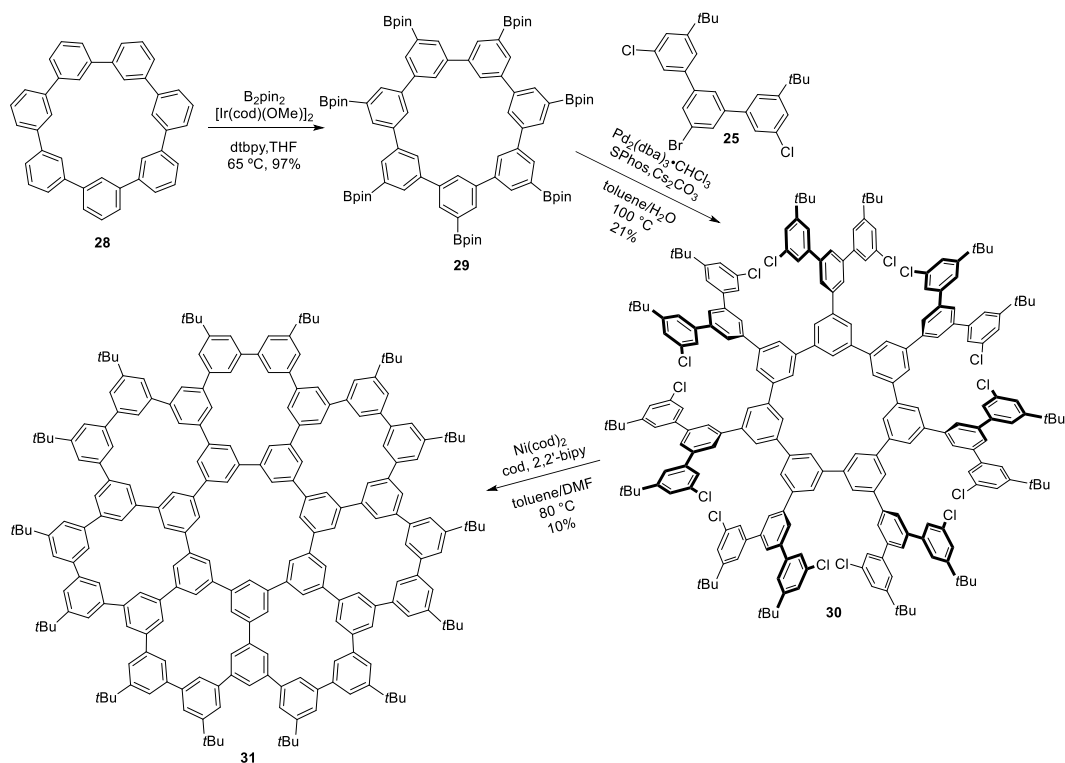
Scheme 3.6 Isobe's synthesis of 5Me-[5]CMP (**22**).

Astonishingly for a molecule of such a simple structure, OLED devices fabricated from **22** displayed similar efficiency to top-of-the-line multi-layer OLEDs, with 21% conversion of solar to electrical energy. This discovery hammers home the fact that exotic and/or difficult-to-synthesize molecules are not always necessary for impactful performance and that small changes in molecular structure can have massive effects on the bulk properties of materials. Isobe *et al.* have rationalized that the alkyl groups provide insulation from pi-pi conductivity and the molecular flexibility of 5Me-[5]CMP versus the [6]CMP derivatives also has some effect on energy conversion efficiency.

Isobe's revival of the $[n]$ CMP chemistry and the efficacy of his Yamamoto type coupling in the formation of *meta*-substituted biaryls has spawned a fresh idea in organic chemistry – that of the phenine unit. The crux of this idea is to use a 1,3,5-substituted benzene ring in place of an sp^2 carbon atom as a basic building block. Building on this idea, Isobe and coworkers have made massive leaps in phenine chemistry, brushing over the lower hanging fruit and diving into some truly impressive structures. Using two powerful tools in CMP chemistry, the highly effective Yamamoto-type coupling that they optimized for CMP synthesis and the Marder borylation, which faithfully installs functionality in the required 1,3,5-motif, Isobe *et al.* constructed phenine equivalents of corannulene (**23**) (Scheme 3.7),^[16] and [7]circulene (**28**) (Scheme 3.8).^[17] Perborylation of the starting $[n]$ CMPs was achieved in extraordinarily high yields and this was followed by Suzuki coupling with a dichlorinated bromo-*m*-terphenyl unit (**25**) to set the stage for a Yamamoto type coupling that produced phenine derivatives of the circulenes, or, through the eyes of this section a highly decorated CMP (Scheme 3.7 and 3.8).



Scheme 3.7 Isobe's synthesis of phenine-[5]circulene (**27**).

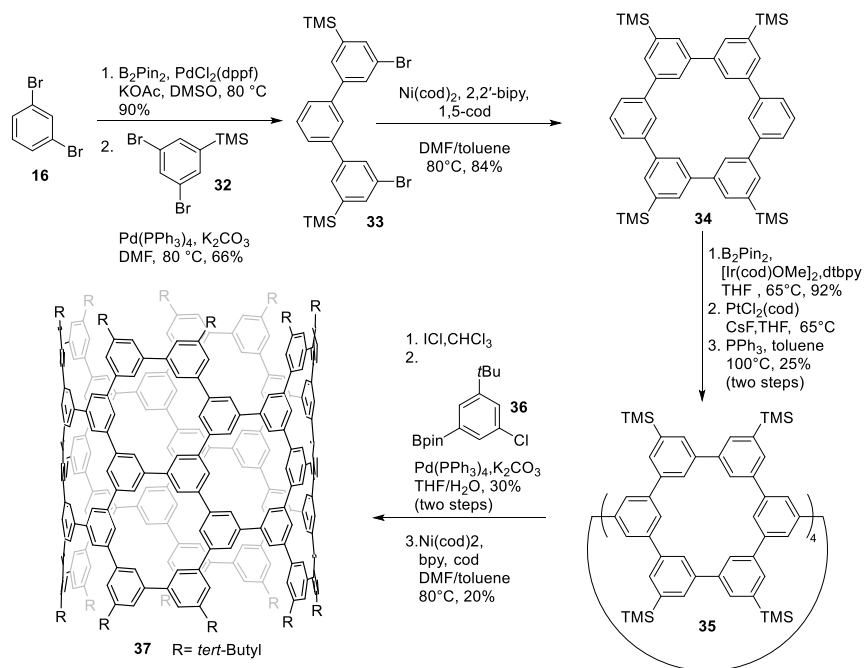


Scheme 3.8 Isobe's synthesis of phenine-[7]circulene.

Having made the phenine equivalents of [5]circulene (**27**) (corannulene) and [7]circulene (**31**), Isobe *et al.* set out to emphasize the power of their methodology by synthesizing a phenine nanotube. While this chemistry is on the verge of being outside the scope of simple [*n*]CMPs, it is useful to show the current state of the arts in this field of 1,3,5-trisubstituted phenylenes. The synthesis began with the Miyaura borylation of 1,3-dibromobenzene (**16**) and subsequent Suzuki coupling with 1,3-dibromo-5-trimethylsilylbenzene (**32**) to afford *m*-terphenyl **33**. This compound was then dimerized under Isobe's Yamamoto-type coupling to give a [6]CMP with 4 placed TMS units (Scheme 3.9). Again taking advantage of the tremendous selectivity and high yields of the Marder

borylation in these types of *meta*-substituted systems, the [6]CMP derivative was borylated at the only remaining unsubstituted *meta*-positions. Utilizing the difference in reactivity between Bpin and TMS, Isobe then constructed a platinacycle (*à la* Yamago, *vide infra*), which after ligand exchange and reductive elimination yielded a cyclic tetramer of [6]CMP. In the context of Isobe's work, this can also be thought of as the phenine equivalent of an unknown cycloparaphenylene, [4]CPP. The utility of the aryl-TMS functionality was then revealed by a two-step iododesilylation followed by Suzuki coupling with another 1,3,5-substituted benzene system, which set the stage for the final Yamamoto-type coupling leading to an "atom defective carbon nanotube segment". This is a tremendously impressive molecule, regardless of whether it is viewed through the lens of [*n*]CMP chemistry or any other lens (Scheme 3.9).^[18]

A more recent synthesis of a nitrogen doped analogue of the phenine nanotube has been published and it again highlighted the considerable power and potential of Isobe's methodology in the construction of CMP systems. This paper was the subject of an invited commentary coauthored by the author of this thesis for *Communications Chemistry*.^{[19][20]} A side by side comparison of Staab's initial synthesis of the first isolated [6]CMP (**3**) and Isobe's gargantuan nitrogen doped phenine nanotube (**31**) shows just how far the field has come in the 56 years since its inception (Figure 3.5).



Scheme 3.9 Isobe's synthesis of phenine-nanotube, or the most complex CMP known.

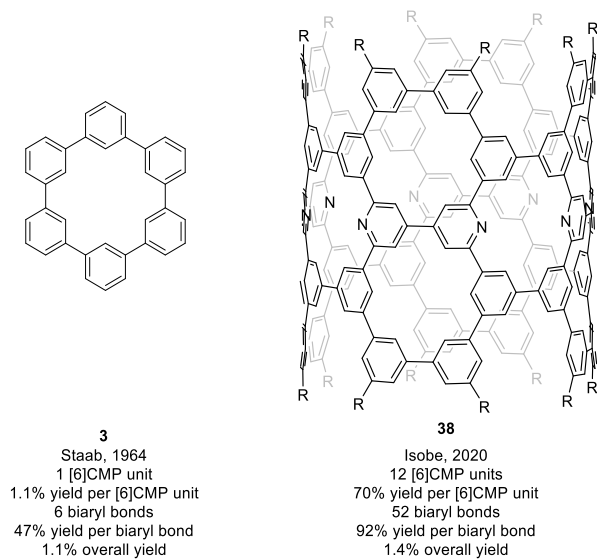
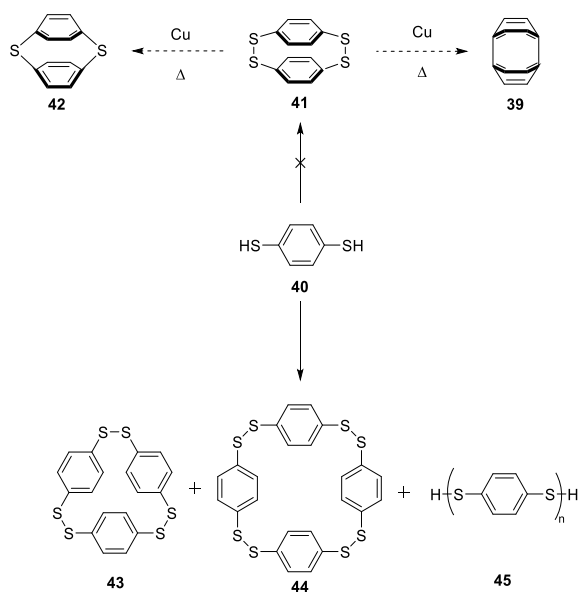


Figure 3.6 The current state of affairs in $[n]$ CMP chemistry *versus* the first synthesis. R = *t*-Bu

[*n*]Cycloparaphenylenes (CPPs)

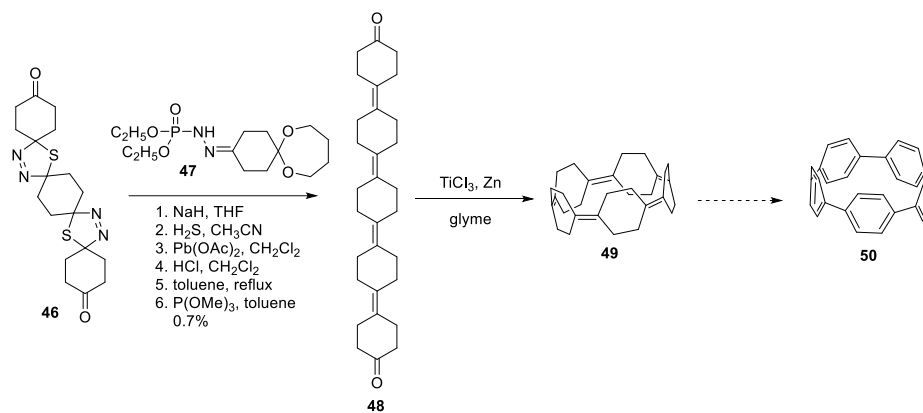
CPPs, which are also referred to as nanorings and nanohoops, can be thought of as the smallest possible arene-containing segments of armchair carbon nanotubes. Interestingly, looking at the oldest literature involving CPPs, the targets the pioneers in this field were attempting to synthesize are still and likely always will be out of reach. Nearly 90 years ago, Parekh and Guha attempted the synthesis of [2]CPP (**39**) by copper-mediated sulfur extrusion from bis-disulfide (**40**).^[21] Armed with today's knowledge about the limits of CPP synthesis (see below), any chemist today would know instantly that any attempt to access the smallest possible CPP was doomed to fail. Parekh and Guha believed they had succeeded in extruding two of the four sulfurs leading to the highly strained dithia[1.1]paracyclophane (**42**), while the [2]CPP (**39**) unsurprisingly remained elusive (Scheme 3.10). Parekh and Guha noted that the product of this reaction was highly insoluble in organic solvents, which would be surprising for a molecule of its size and structure. Indeed, only having characterized the cyclophane **42** by elemental analysis, it was later shown that the reaction yields a mixture of trimer (**43**), tetramer (**44**) and polymeric material (**45**), even under higher dilution conditions than those employed by Parekh and Guha.^{[22][23]} Given the insolubility of Parekh and Guha's material, it is highly likely they only isolated polymeric material.



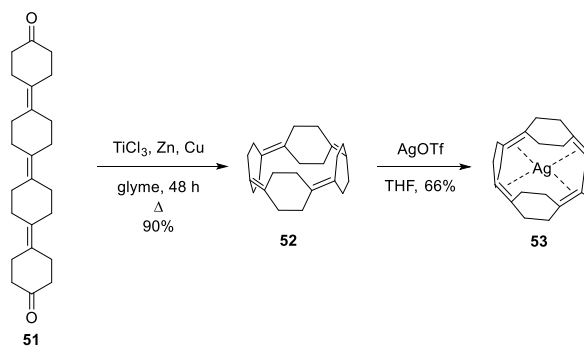
Scheme 3.10 Parekh and Guha's attempt at the assuredly impossible target **39**.

CPP chemistry fell into an era of neglect until the early 1990s when Fritz Vögtle, counted among the founding fathers of supramolecular chemistry,^[24] took an interest in the macrocyclic carbon rings. Through a route that was anticipated to circumvent solubility issues encountered with planar polyphenylenes, Vögtle and coworkers synthesized diketone **48** in 0.7% yield with the intention of cyclizing it to afford **49**. Intramolecular McMurry coupling of **48**, however, only yielded traces of **49**, as detected by HRMS. Due to the unexpected insolubility of **49** and the low yielding and laborious synthesis of diketone **48**, attempts at inducing the requisite loss of 20 hydrogen atoms to form [5]CPP (**50**) went untested (Scheme 3.11).^[25] Seven years earlier, McMurry himself had already accomplished similar cyclizations in much higher yields, but was apparently not working towards CPPs.^[26] Instead McMurry was seeking to use the cyclic tetraene **52** as a ligand and he easily accomplished this using silver

triflate. The metal complex **53** was isolated in 66% yield and was characterized by single crystal X-ray crystallography (Scheme 3.12).



Scheme 3.11 Vögtle's progress towards [5]CPP.



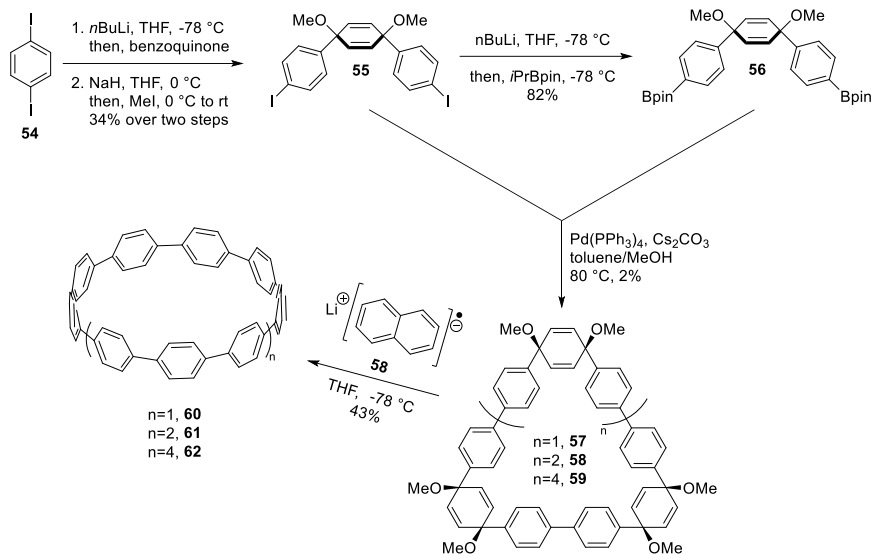
Scheme 3.12 McMurry's synthesis of square planar silver complex **53**.

Table 3.2 Strain energy of [n]CPPs calculated by Itami *et al.*^[29]

[n]CPP	Strain energy (kcal/mol)	Strain per <i>n</i> (kcal/mol/ <i>n</i>)
5	119.0	23.8
6	96.0	16.0
7	84.0	12.0
8	72.2	9.0
9	65.6	7.3
10	57.7	5.8
11	53.7	4.9
12	48.1	4.0
13	45.5	3.5
14	41.0	2.9
15	39.2	2.6
16	35.6	2.2
17	33.7	2.0
18	31.7	1.8
19	30.0	1.6
20	28.4	1.4

It was not until 2008 when the cycloparaphenylenes were realized. During Ramesh Jasti's stay as a postdoctoral fellow in Carolyn Bertozzi's lab, he came up with a route that drew upon Vögtle's approach, but it featured a few important differences. A main reason why the yield of Vögtle's macrocyclization of pentacyclohexylidendione (**48**) was vanishingly low was that it had to populate an *all-boat* conformation to allow the formation of macrocycle **49**. Jasti circumvented this issue by taking advantage of the inherent bend induced by the 1,4-*syn*-substituted-1,4-cyclohexadienes, which served to promote macrocyclization over polymerization. Jasti's new approach also had the tremendous advantage of being closer in oxidation state to the subsequent CPPs, requiring only the injection of two electrons per benzene precursor to afford the fully aromatic product. As such, the ultimate aromatization

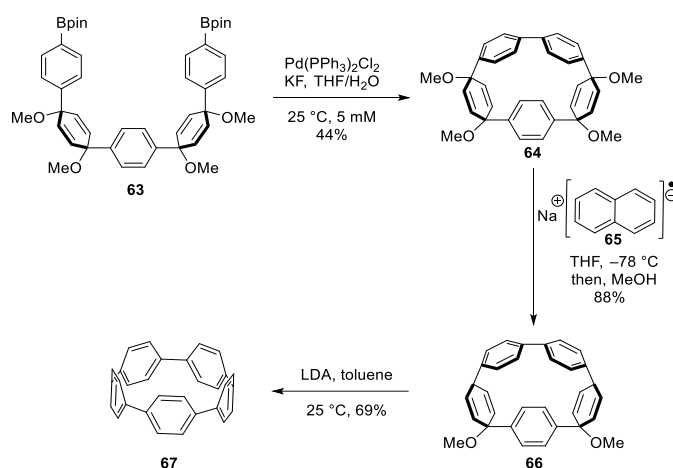
utilizing lithium naphthalenide (**58**) as a source of electrons not only occurred as planned, but proceeded smoothly at $-78\text{ }^{\circ}\text{C}$ (Scheme 3.13).^[27]



Scheme 3.13 Jasti's synthesis of [9], [12] and [18]CPP.

In Jasti's initial publication, he and Bertozzi reported the synthesis of [9]-, [12]- and [18]CPP, taking full advantage of the easily synthesized 3-ring units **55** and **56** to make ring systems where [*n*] is divisible by 3. Jasti later developed modifications to this strategy as an independent researcher and was thereby able to achieve the synthesis of several other CPPs. At first blush, [9]CPP (**60**) appears to be an impossible result of the original CPP-forming reaction. It was surmised that [9]CPP must be a result of some degree of homocoupling between ArBpin units at some point in the reaction. This notion was revisited by Jasti in the synthesis of the smallest known [*n*]CPP, [5]CPP (**67**) (Scheme 3.14)^[28] The key step in this synthesis was the Bpin homocoupling of **63**, which afford CPP precursor **64** under very mild

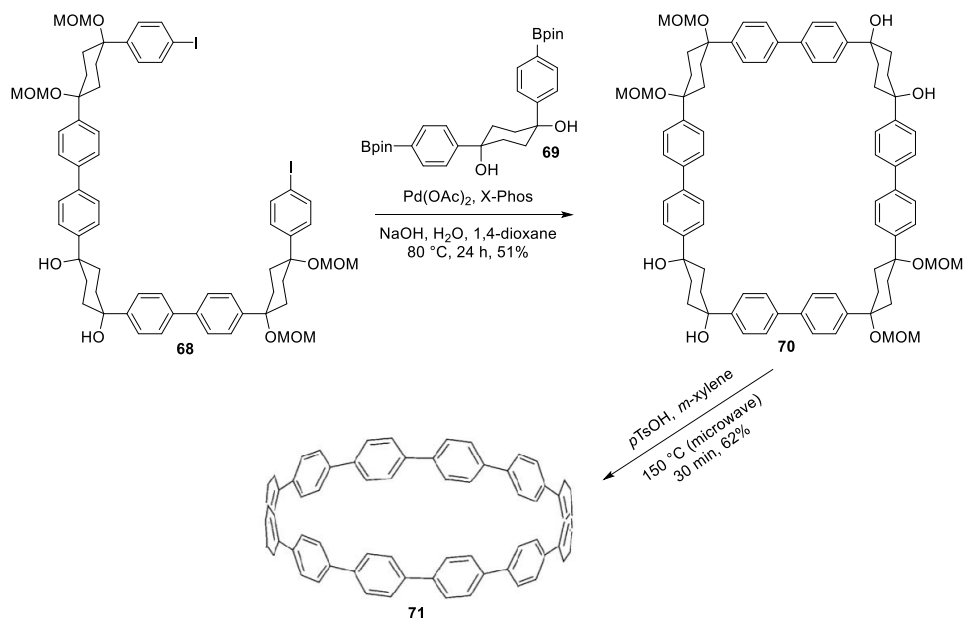
conditions in a remarkably good 44% yield. Unlike the previous CPPs, the reductive elimination methodology started showing signs of reaching the limits of what it can deliver. With **64**, the reaction with sodium naphthalenide did not fully aromatize the nanoring, but instead gave diether **66** after quenching of a presumed dianionic intermediate. Fortunately, [5]CPP precursor **66** underwent a twofold elimination of methanol upon treatment with LDA to yield [5]CPP (**67**).



Scheme 3.14 Jasti's synthesis of [5]CPP (**67**).

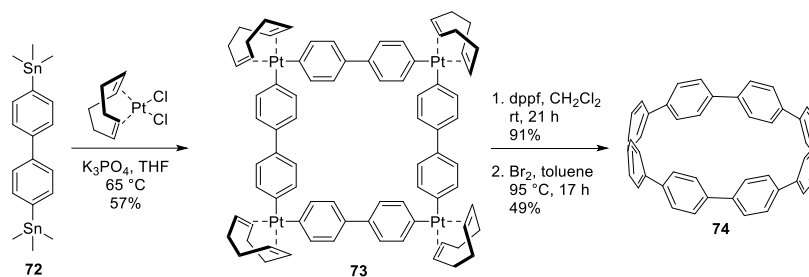
Several other groups around the world have succeeded in making CPPs. A year after Jasti and Bertozzi's original publication, Itami and coworkers used similar chemistry, but utilizing a different pre-aromatic unit: 1,4-disubstituted bis(MOM-protected) cyclohexanes (Scheme 3.15).^[29] Itami's pre-aromatic unit could be constructed in a similar manner to Jasti's. Suzuki partners **68** and **69** underwent macrocyclization in 51% yield setting the stage for Itami's aromatization step. Macrocycle **70** was then heated with *p*-toluenesulfonic acid under microwave irradiation to yield, selectively [12]CPP. It is interesting that the cyclohexandiols

aromatize under these conditions since elimination of two molecules of water can only produce cyclohexadienes and the loss of two hydrogen atoms to gain aromaticity is still required.



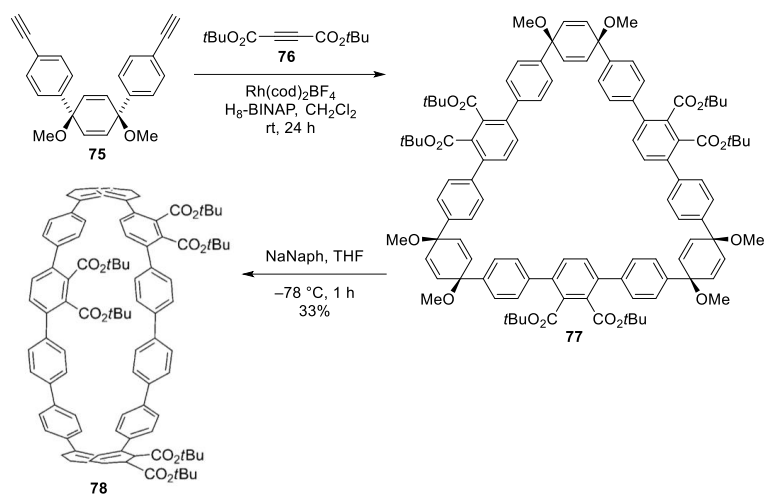
Scheme 3.15 Itami's selective synthesis of [12]CPP (**71**).

In a much different vein, Yamago and coworkers achieved the synthesis of a number of CPPs using the formation of platinacycles as a key step.^[30] The long C–Pt bonds and favorable C–Pt–C angles (*ca.* 90 °) allow for the easy formation of square-shaped macrocycles such as **73**, which upon ligand exchange and reductive elimination complete the synthesis of a variety of CPPs. The formation of biaryl bonds in the final step sharply contrasts the approaches of Jasti and Itami, where aromatization fills this role (Scheme 3.16).



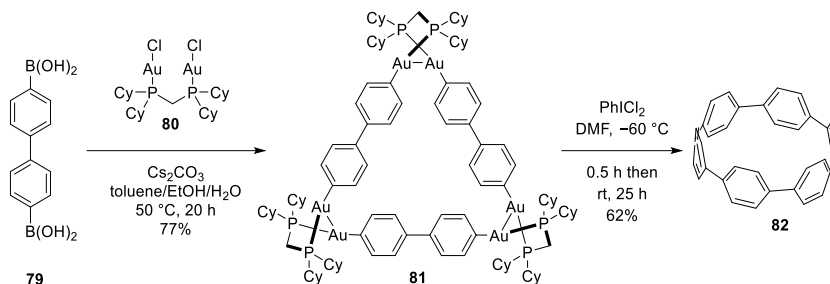
Scheme 3.16 Yamago's synthesis of [8]CPP through platinacycle (**73**).

Much more recently, new methods have emerged. Tanaka has produced a [12]CPP using rhodium-mediated alkyne trimerization, which has the large advantage of bringing functionality to the CPP skeleton. Doing so remains surprisingly difficult to achieve as evidenced by the great lengths and/or harsh conditions required to put even the simplest functional groups on CPP frameworks. It is a testament to the aromatization conditions that sodium naphthalenide undergoes electron injection to the dimethoxycyclohexadiene rings rather than performing a Birch-type reduction of the diester-bearing rings (Scheme 3.17).^[31]



Scheme 3.17 Tanaka's synthesis of [12]CMP-hexaester **78**.

In a dramatic advancement this year, Osakada reported the synthesis of [6]CPP (**82**) in only two synthetic steps from the commercially available 4,4'-biphenylbis(boronic acid) (**79**) in 47% overall yield from triangular complex (**81**) featuring gold-gold bonds at the corners (Scheme 3.16).^[32]



Scheme 3.18 Osakada's two-step, high-yielding synthesis of [6]CPP.

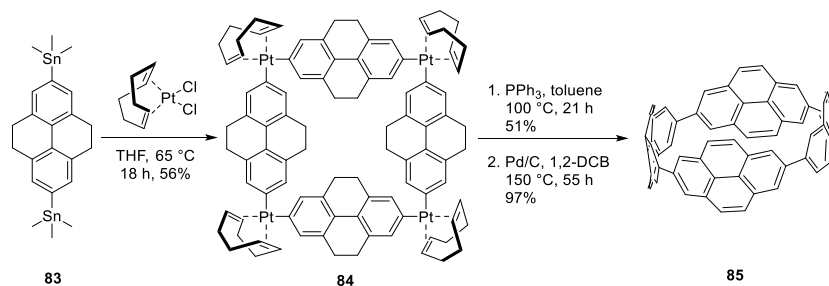
Osakada's synthesis is a tremendous achievement in CPP chemistry, made only sweeter by the fact that in the final step, the digold complex used in the first step is regenerated in 65% yield.

From the seminal work of Jasti, which allowed the synthesis of CPPs from [18] to [5], to the current state of affairs where [6]CPP can be produced in 48% yield in two steps from commercially available materials, it may seem like the field is coming to an end. However, when looking at the recent work of Jasti, Itami and others, it is clear that functionalization and elaboration of these interesting substrates promises to bring new and interesting properties as well as opportunities to build molecules that would have been scarcely imaginable only 20 years ago. Now with multiple sets of robust methodology, many of the CPPs that were once pie-in-the-sky molecules are commercially available and can conceivably serve as starting points for bigger and better things.

[*n*]Cyclopyrenylenes (CPys)

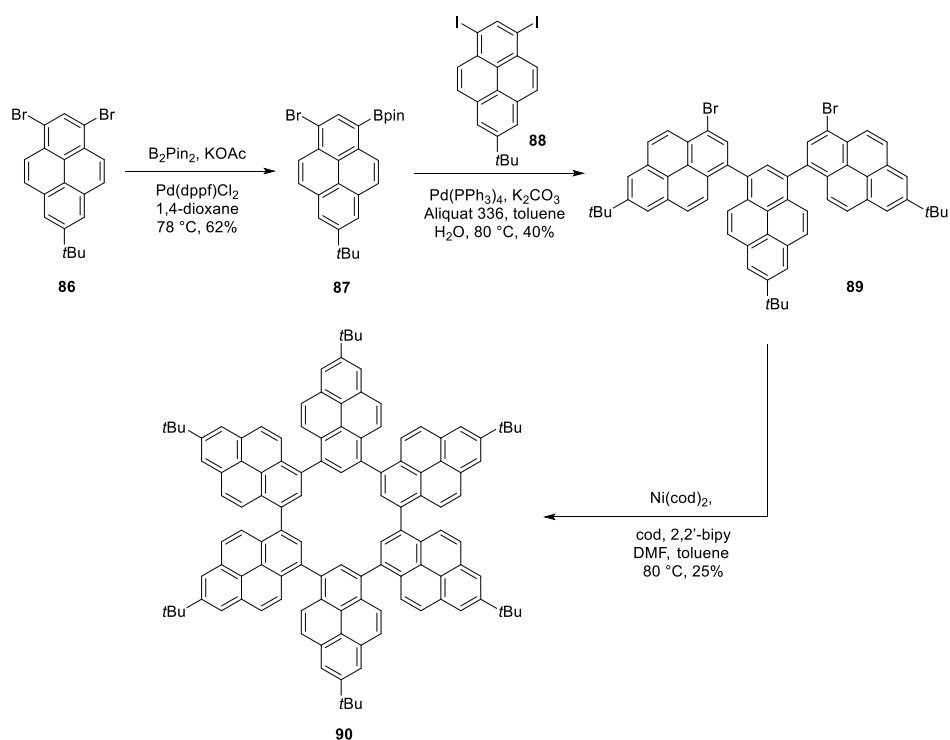
Cyclopyrenylenes are very scarce in the literature and this is in part attributable to the difficulty in working with pyrene derivatives on a large scale, due mainly to solubility problems. The first all-pyrene cycloarylene was reported by Yamago. The synthesis was achieved in much the same manner as his CPP synthesis (*vide supra*), but it was found to be advantageous to carry the pyrene units through as 4,5,9,10-tetrahydropyrenes. Doing so was advantageous because tetrahydropyrene undergoes bromination efficiently at the 2- and 7-positions and the resulting dibromide is more soluble than the very poorly soluble 2,7-dibromopyrene, which is not directly accessible from pyrene. With the 2,7-dibromotetrahydropyrene in hand, the required trimethyl stannyl groups could be installed through halogen-metal exchange with *n*-BuLi and quenching with Me₃SnCl. Using an improved methodology over the earlier CPP

synthesis (*cf.* Scheme 3.16 – two-step biaryl bond formation) the platinumacycle (**84**) was formed in 56%. Ligand exchange and reductive elimination of platinum yielded the [4]cyclo-4,5,9,10-tetrahydropyrenylene in 51% yield, which was ultimately fully aromatized to give [4]CPPy (**85**) in 97% yield (Scheme 3.19).^[33]



Scheme 3.19 Yamago's synthesis of the first cyclopyrenylene, [4]-2,7-CPy.

Other substitution patterns of cyclopyrenylenes are as scarce as Yamago's 2,7-pyrenylenes. Müllen reported a cyclo-1,3-pyrenylene, but this substitution pattern allows the product to be viewed as a highly decorated [6]CMP.^[34] Müllen's strategy involved the bromination of 2-*tert*-butylpyrene to give the 1,3-dibromide (**86**). This compound was then used as a point of divergence, furnishing Suzuki coupling partners **87** and **88** by a halogen-metal exchange / iodination sequence and a Miyaura borylation respectively. In the penultimate step, the two units were coupled to give a symmetric dibromide (**89**), which could be dimerized under Yamamoto-type coupling conditions (Scheme 3.20) to yield [6]cyclo-1,3-pyrenylene **90**.



Scheme 3.20 Müllen's synthesis of [6]cyclo-1,3-pyrenylene.

An early and attractive target of this thesis that remained elusive through cyclization of dibromo oligomers produced in Chapter 2 is cyclic tetramer [4]-1,8-CPy (**91**), which has been recently reported by Yamada *et al.*^[35](Figure 3.7). This saddle-shaped molecule forms 1:1 columnar complexes with I_h -C₆₀ fullerene, each side of the molecule acting as an acceptor. The synthesis of **91** was achieved through a blunderbuss approach, which afforded a long series of [*n*]-1,8-CPPys ([*n*]=3-15) (Scheme 3.21), albeit in vanishingly small yields. Individual members of the series were only isolated after extended and repeated flash column chromatography and gel-permeation chromatography. Clearly, there is room for improvement in the synthesis of these compounds.

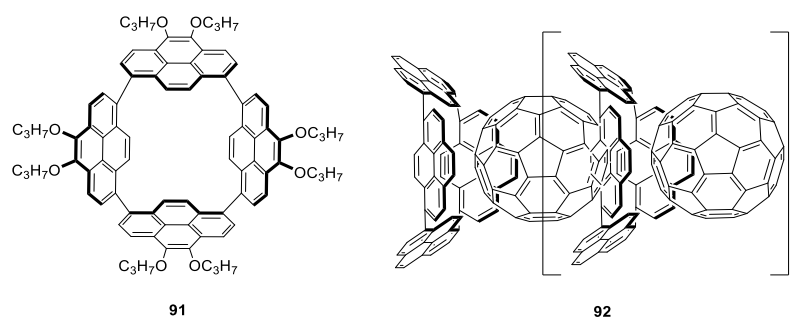
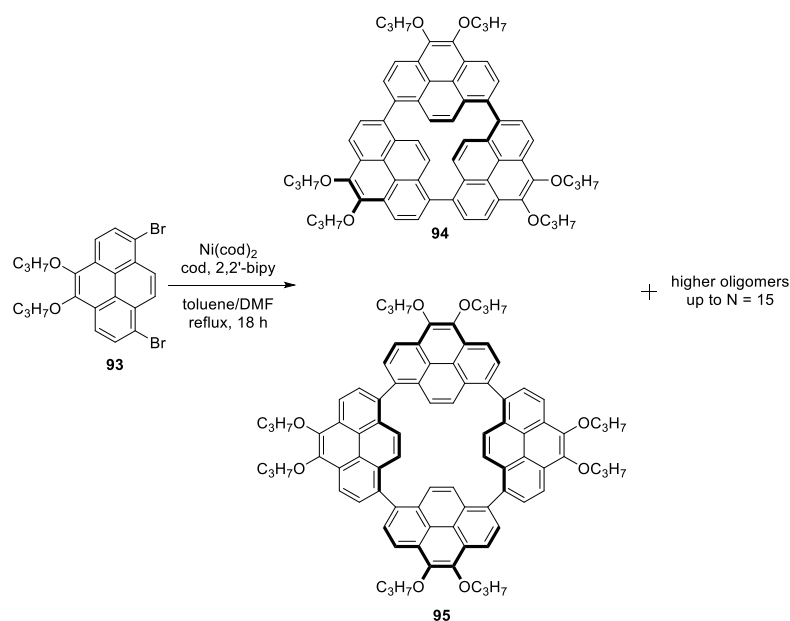


Figure 3.7 Yamada's cyclotetramer **91** and the end-to-end C_{60} supramolecular complex observed (propoxy groups omitted for clarity).



Scheme 3.21 Yamada's synthesis of cyclic pyrenylene oligomers.

Taking the top spot among Yamada's $[n]$ -1,8-CPPy family is cyclotrimer (**94**),^[36] which was isolated in 3.6% yield from direct Yamamoto cyclization of **93**. For a compound with only pyrene as chromophore, the absorption and emission maxima appear at remarkably low

energy ($\lambda_{\text{max}}=505$ nm, $\lambda_{\text{em}}=599$ nm). The quantum yield is 0.34 at 298 K. Compared to pyrene, the red shift is drastic indeed, with an emission at much longer wavelength than pristine pyrene's excimer emission (460 nm). In solution and in the crystal, the compound adopts D_{3h} symmetry and is significantly strained (not "remarkably" strained like the authors state) with a calculated strain energy of 60 kcal/mol. To put this number into perspective, using the same basis set, the cyclotrimer has intermediate strain to [9] and [10]CPP (Table 3.2).

While certainly this cyclotrimer is a beautiful compound in and of itself, the strained pyrenylene displays a bizarre reactivity with synthetic implications. To preface this, as the authors outline in their paper, the synthesis of biaryl ethers has changed little since 1901, when Cook prepared a number of diaryl ethers by nucleophilic aromatic substitution on nitro- and dinitrobenzene halides with the potassium salts of various phenols, neat at 137 °C (Figure 8).^[37] A somewhat newer and more relevant example is the transition metal mediated oxidation of biphenylenes, whereby the two C–O bonds of the diaryl ether arise from the formal insertion of an O atom into a biaryl bond (Figure 3.8).^[38]

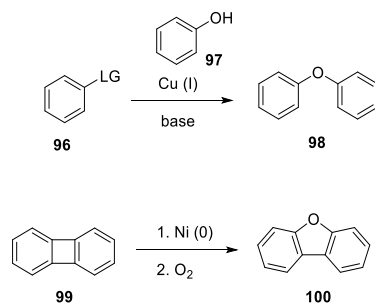
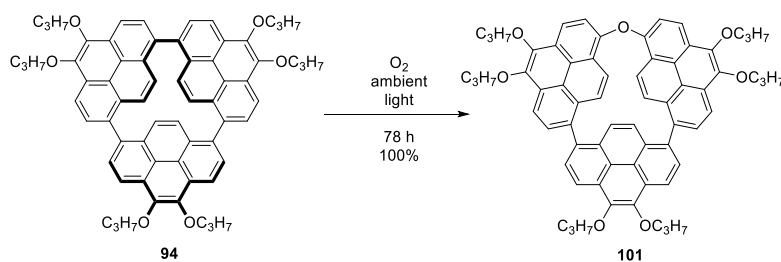


Figure 3.8 Previous methods to produce biaryl ethers.

Cyclotrimer **94**, however, offers another route towards biaryl ether formation through a process analogous to biphenylene, but the reaction proceeds without a transition metal catalyst. Remarkably, the cyclotrimer reacts with molecular oxygen resulting in the insertion of a single oxygen atom, presumably with strain relief as the main driving force. The reaction proceeds at room temperature under ambient pressure and concentration of oxygen with a half-life of 18 hours. Complete consumption of starting material (by absorption spectroscopy) occurs after 78 hours (Scheme 3.19). The authors stated that progress of the reaction was not affected by the nature of the solvent, but only dichloromethane and chloroform were tested. It appears that the compound acts as its own sensitizer in the reaction, generating the required singlet oxygen from photoexcitation. Pristine pyrene can also act as a photosensitizer (with a much higher quantum yield than cyclotrimer **94**), but pyrene only absorbs in the UV region while cyclotrimer **94** can sensitize oxygen through photoexcitation by ambient room light thanks to its longer wavelength (>600 nm) absorptions.

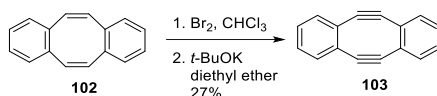


Scheme 3.22 Oxygen insertion and biaryl ether formation in **94** under ambient conditions.

[*n*]Cyclophenyleneacetylenes (CPPAs)

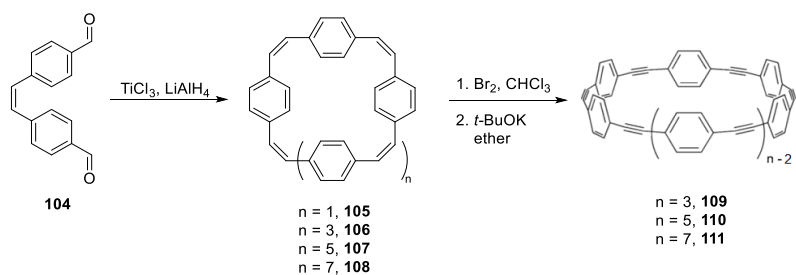
Starting with CPPs, the formal insertion of an acetylene unit between each ring of a cyclophenylene gives rise to the class of molecules known as the cyclophenyleneacetylenes (CPPA).

Kawase and Oda introduced a series of *para*-substituted oligomers of phenylacetylene between the years of 1996 and 2006. Kawase's CPPAs were the first fully conjugated pi systems with radially oriented *p* orbitals to be isolated.^[39] To synthesize the series of radially conjugated rings, Kawase utilized methodology that was shown to be extraordinarily powerful in the facile synthesis of angle-strained alkynes. Using a bromination / double dehydrobromination protocol, Sondheimer was able to synthesize dibenzocycloocta-4,6-diene-5,11-diyne (**103**) in 27% yield over two steps at room temperature.^[40] The ability to generate such an exotic molecule under these seemingly mild conditions is interesting indeed.



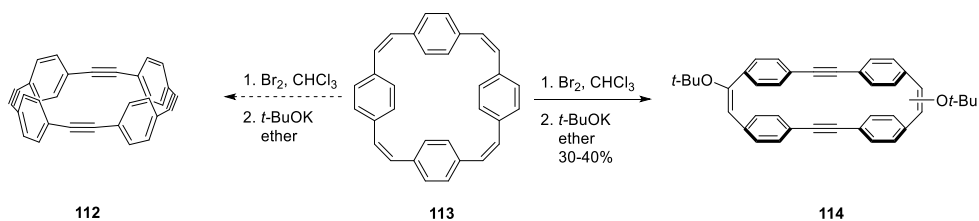
Scheme 3.23 Sondheimer's extraordinary cyclooctadiyne **103**.

For the synthesis of a series of CPPAs (Scheme 3.24), Kawase and Oda employed McMurry reactions to form the alkene-containing macrocycles **105-108** necessary to apply Sondheimer's chemistry.



Scheme 3.24 Kawase's general synthesis for [6]-[10]CPPAs **109-111**.

Sondheimer's methodology proved to be general and proceeded efficiently at room temperature to afford the series of CPPAs **109-111**. The methodology finally failed in the attempted synthesis of [4]CPPA (**112**). In this case, it is clear that the alkynes were generated in the reaction, but the system is too strained to coexist at room temperature with the nucleophile *t*-BuOK (Scheme 3.25) (Table 3.3).^[41]



Scheme 3.25 The limits of Sondheimer's methodology in Kawase's failed synthesis of [4]CPPA **112**.

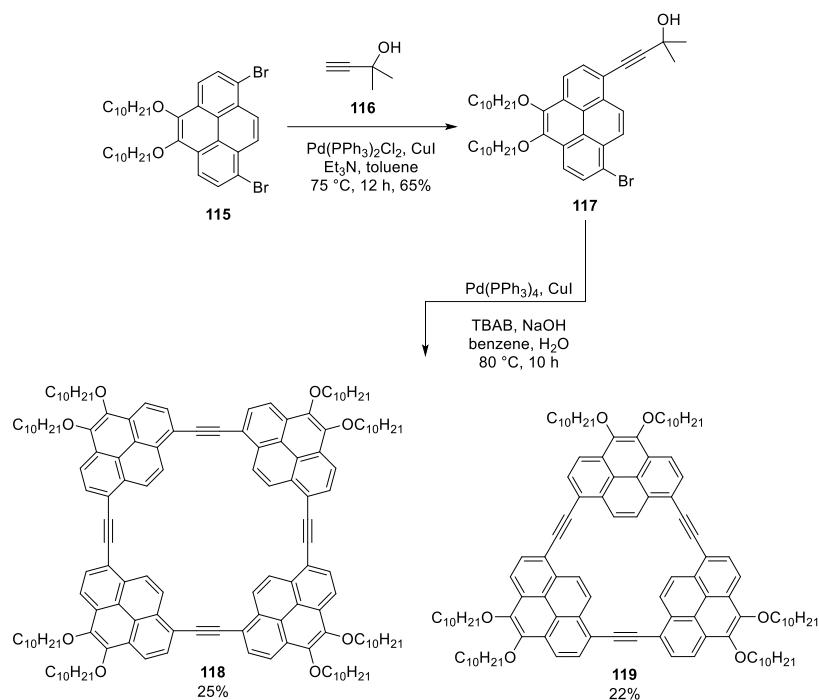
Table 3.3 Calculated strain energies and bend angles of [4]-[10]CPPA.^[42]

	Strain (kcal/mol)	Strain/ <i>n</i> (kcal/mol/ <i>n</i>)	Calculated bend (°)
[4]CPPA	64	16	160.0
[5]CPPA	49	10	162.8
[6]CPPA	39	6.5	165.3
[7]CPPA	32	4.6	167.7
[8]CPPA	26	3.3	169.2

[9]CPPA	22	2.4	170.6
[10]CPPA	17	1.7	171.4

[n]Cyclopyrenylene acetylenes (CPyAs)

If the cyclopyrenes can be considered scarce in the literature, then cyclopyrenylene acetylenes are extremely rare. Only two such examples can be found in the literature and both were produced in the Bodwell lab. Starting with 1,8-dibromo-4,5-didecapyrenes **115**, which was easily prepared as described in Chapter 2, a mono-Sonogashira coupling with a protected acetylene equivalent set the stage for an *in situ* deprotection and Sonogashira macrocyclization yielding cyclotetramer **118** and cyclotrimer **119** in respectable yields (Scheme 3.26).^[43] An interesting conclusion was drawn from the NICS values calculated for **118** and **119**. A dummy atom in the middle of the macrocycle was calculated to have a NICS_{zz} value of 17.98, which appeared to speak to high antiaromatic character. However, removal of the triple bonds (computationally) resulted in only a minor reduction in the magnitude of the NICS value (NICS_{zz} = 14.08), which led to the conclusion that there was actually very little delocalization between the three pyrene systems. (**119** NICS_{zz} = 17.98; excluding alkynes NICS_{zz} = 14.08, excluding pyrenes NICS_{zz} = 1.26). The lack of delocalization was attributed to the large aromatic stabilization energy of pyrene (74.6 kcal/mol, as calculated by Cyrański in collaboration with Schleyer and Bodwell),^[44] which would be severely disrupted by macrocyclic delocalization. Indeed, as the UV/vis spectra corroborated, the molecules can be thought of as isolated pyrenes bridged by nearly non-participating triple bonds.



Scheme 3.26 Bodwell's synthesis of [4]- and [3]-1,8-CPPy by Sonogashira macrocyclization.

Intermediate CPP/CPPA Hybrids

While the CPPAs are certainly fully conjugated, the electronic communications between benzene rings through the acetylene linkers is significantly diminished in comparison to the CPPs^[45] Between the two well-characterized groups of compounds lies a grey area of shape-persistent macrocycles incorporating a mix of biaryl and acetylene spaced rings. For example, from [4]CPP to [4]CPPA there are four possible hybrids: one containing three acetylene units (**124**), two isomers containing two acetylene units (**122** and **123**) and finally one hybrid containing only a single acetylene unit (**121**). The number of possible hybrids grows

quickly as the number of arenes increases, so even though none of these compounds are known, they nicely illustrate the point.

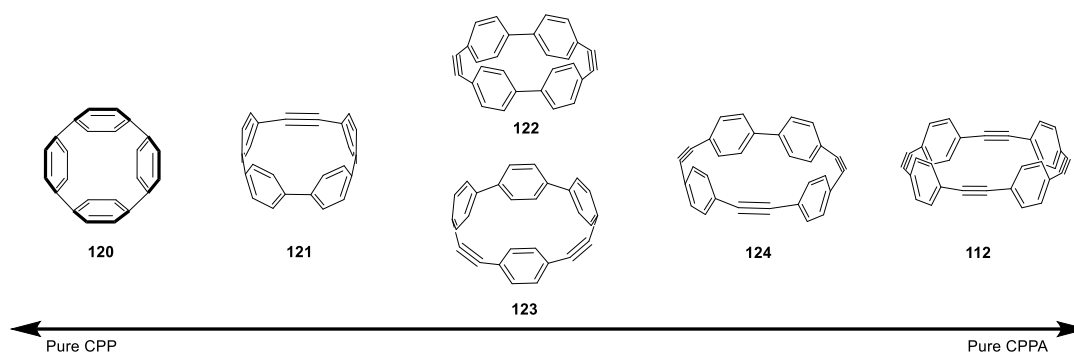
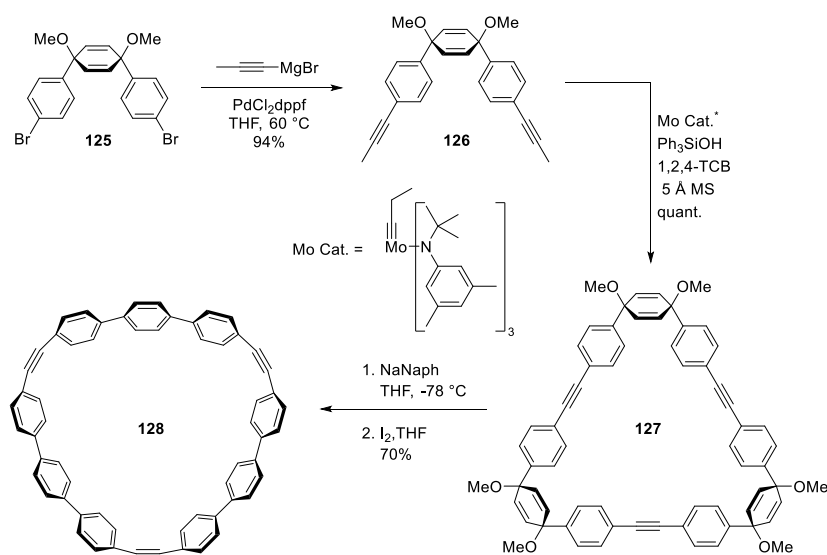


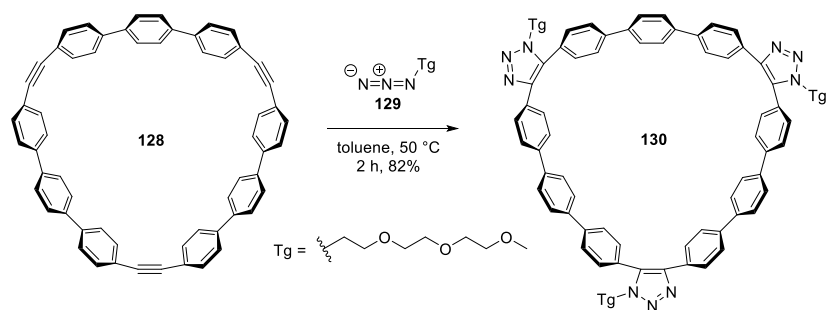
Figure 3.9 The hybrids that lie between the structures of [4]CPP and [4]CPPA.

One such hybrid between a CPP and a CPPA, macrocycle **128**, was published by Jeffrey Moore in 2016 (Scheme 3.27).^[46] This hybrid system is notable not only for its beautiful structure, but also the inclusion complexes it forms, the strain promoted azide/alkyne cycloaddition (SPAAC) reactivity it exhibits, and the brevity/elegance of its synthesis. With regard to the latter point, Moore’s synthetic approach differs drastically from those used previously for the synthesis of CPPAs, which have relied heavily on the tried and tested methods of bromination-elimination of alkene intermediates derived from Wittig or McMurry reactions or by Sonogashira reactions and/or Glaser coupling. Mirroring Jasti’s and Itami’s approaches, which utilize “pre-aromatic” structures that are inherently bent and thus predisposed towards macrocyclization, Moore started off by constructing what Jasti would call an L-shaped precursor. The first L-shaped precursor **125** underwent Kumada coupling with propynylmagnesium bromide to give diyne **126**, which was subjected to an alkyne metathesis

reaction. In the broader context of CPPA synthesis, this step is quite remarkable. Benefiting from both the very low solubility of macrocycle **127** (even in hot 1,2,4-trichlorobenzene) as well as the reversible nature of alkyne metathesis under the reaction conditions, arene precursor **127** was produced in quantitative yield on a gram scale without the need for purification. Borrowing from Jasti's CPP synthesis, the pre-arene unit could be induced to undergo reductive elimination using sodium naphthalenide to afford hybrid [3]CPP³A **128** in 70% yield. It is worth noting here that again (*vide supra*) other parts of the molecule are unreactive towards the sodium naphthalenide, and the bent alkynes do not undergo Birch type reduction (Scheme 3.24). This structurally interesting compound was shown to easily undergo SPAAC reactions, e.g. with azide **129** to afford macrocycle **130** as the major isomer (Scheme 3.27). Three years later, Lee *et al.* succeeded in applying Moore's approach in the synthesis of [3]CPP⁴A (**131**) and [3]CPP⁵A (**132**) (Figure 3.10).^[47]



Scheme 3.27 Moore's synthesis of CPP/CPA hybrid **128**.



Scheme 3.28 SPAAC reaction of Moore's CPP/CPPA hybrid **128** with Tg-azide **129**.

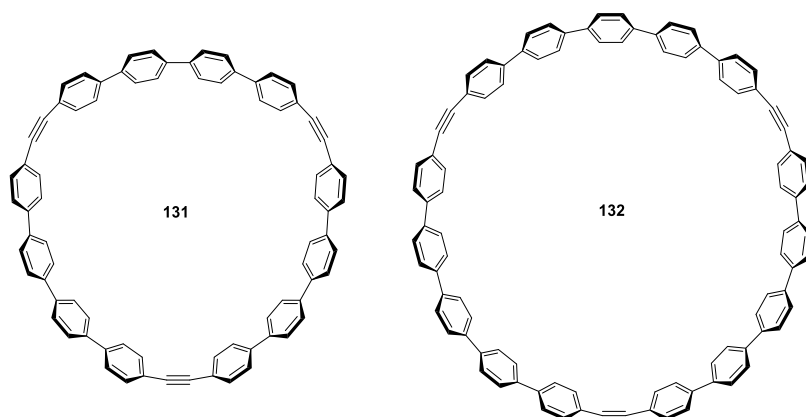
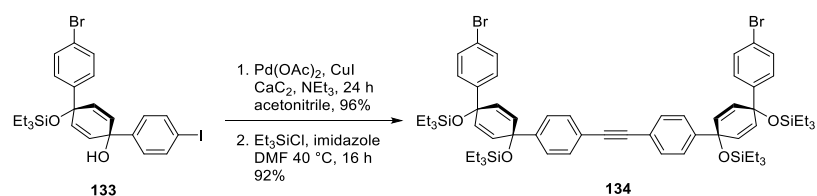
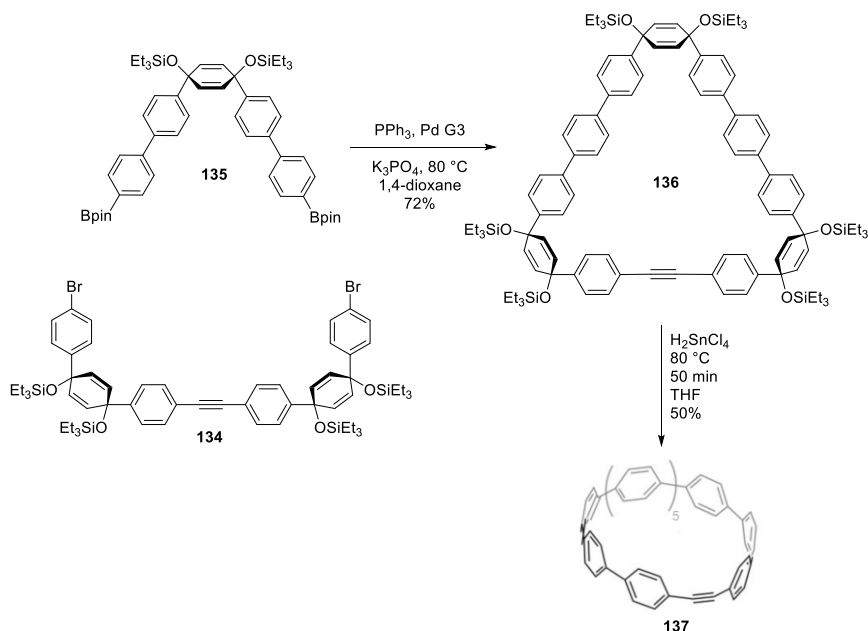


Figure 3.10 [3]CPP⁴A (**131**) and [3]CPP⁵A (**132**).

In 2018, Jasti published a hybrid CPP/CPPA with just one alkyne moiety.^[48] The synthesis of this molecule followed closely the previous syntheses of CPPs while efficiently incorporating the alkyne unit using a double Sonogashira using calcium carbide, as developed by Cheng in 2006 (Schemes 3.29, 3.30).^[49] Under Cheng's conditions, Jasti was able to achieve an iodo-selective double Sonogashira of iodobromide **133** to furnish alkyne containing dibromide **134** in 96% yield. This was followed by protection of the remaining alcohols with triethylsilyl chloride in 92% yield.



Scheme 3.29 Jasti's application of Cheng's double Sonogashira utilizing calcium carbide as acetylene equivalent.

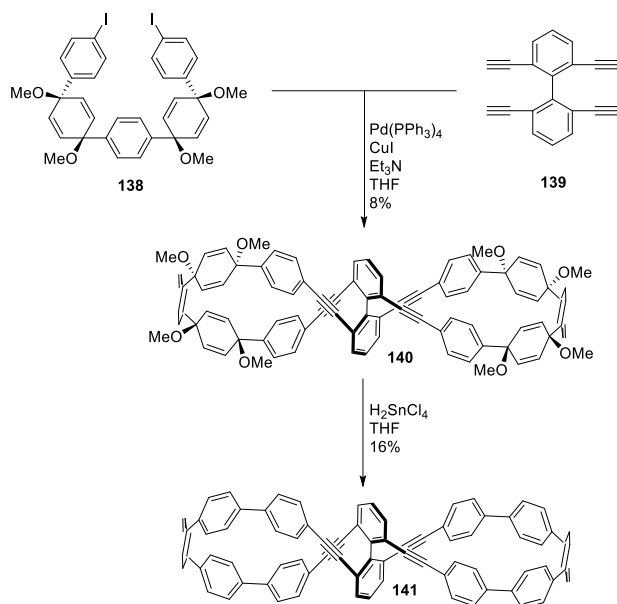


Scheme 3.30 Jasti's synthesis of CPP/CPPA hybrid **137**. (Pd G3 = 2-dicyclohexylphosphino-2',6'-dimethoxybiphenyl) [2-(2'-amino-1,1'-biphenyl)]palladium(II) methanesulfonate.

A very recent contribution to CPP/CPPA hybrids came from Tanaka's lab.^[50] Jasti's methodology was used to build U-shaped fragment **138** and this building block was subjected to an extremely productive fourfold Sonogashira coupling to yield macrocycle **140** in 8% yield. The low yield should be weighed against what was accomplished in the reaction: 4 carbon-

carbon bonds were formed (two intramolecularly and two intermolecularly) to yield a structurally novel bicycle **140**, which can be viewed as a molecular lemniscate.[‡] The 8% yield is certainly acceptable and can even be viewed as a testament to the Sonogashira reaction's utility in forming macrocycles (Scheme 28). Aromatization to afford **141** was achieved using the ate-complex, H₂SnCl₄. The remarkable hybrid **141** displays both helical and axial chirality by virtue of the connectivity of the CPP fragments to the twisted biphenyl system. Calculated HOMO and LUMO coefficients show that there is electronic communication between the benzene rings of the internal biphenyl moiety despite a 96.4 ° torsion angle between them. Separation of the *P* and *M* helicates was achieved at room temperature using chiral HPLC, and due to high rigidity of the molecular skeleton, the enantiomers are configurationally stable. Bicyclic compound **141** displayed much larger Cotton effects than those observed for comparable monocyclic molecules of its size,^[51] which demonstrated that aligning more than one helical structure (two in this case) has a pronounced and non-linear effect on the molecule's interaction with light.

[‡]In algebraic geometry, a lemniscate is any figure-eight shaped curve.



Scheme 3.31 Tanaka's synthesis of CPP/CPPA hybrid **141**, which displays both helical and axial chirality.

Only the surface of the field of CPP/CPPA hybrids appears to have been scratched. With the large number of hybrids available, even while limiting the arene to benzene, there appears to be a lot of room for the design of novel and useful hybrid systems.

Results

The concept of hybrid CPP/CPPA structures can of course be extended to systems containing aromatic systems other than benzene. Pyrene is an attractive aromatic system to consider due to the photophysical properties it brings to the table. Focussing on the 1,8-substitution pattern, the ends of the structural spectrum are represented by Yamada's cyclotrimer **94** and Bodwell's cyclotrimer **144** (Figure 3.11). The two possible hybrids between them are **142** and **143**, which contain one and two alkynes, respectively. While **143** is certainly

an attractive target, **142** features a trimeric oligopyrene unit, which was found to be the oligomer size where the changes in the photophysical properties of the 1,8-oligopyrene series level out (Chapter 2). For example, the fluorescence quantum yield of the acyclic trimer reaches the maximum value in the series of 0.80 ± 0.04 .

Considering that pyrene units in Bodwell's pyrenylene-ethynylene macrocycles (**118**) and (**119**) (*vide supra*) remained essentially as isolated pyrene systems, it is not unreasonable to expect that the trimer moiety in **142** will behave much like the acyclic pyrene trimer. In the context of reactive triple bonds that may have applications in sensing, **142** is a much more interesting molecule. Diyne **143**, which contains a dimeric pyrene unit and a monomeric pyrene unit, would be expected to have significantly less fluorescence intensity and the presence of more than 1 alkyne complicates possible applications such as useful click chemistry. It is nevertheless a target that warrants attention. An advantage of these types of systems over some of the classical strained alkynes such as cyclooctyne is that the fluorophore is part and parcel of it.

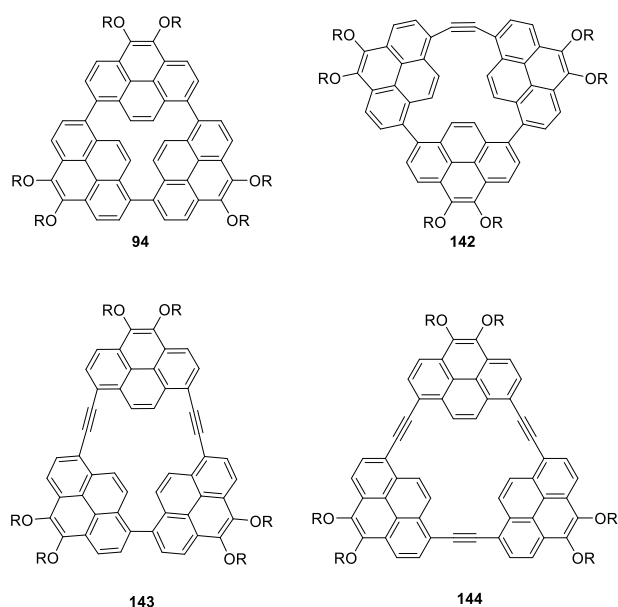
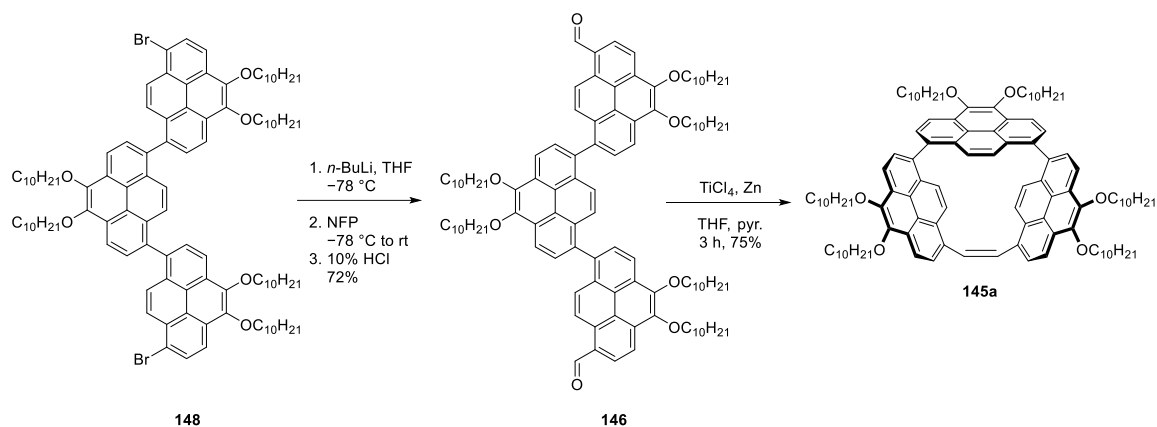


Figure 3.11 Yamada's CPy **94** to Bodwell's CPyA **144** and the hybrids **142-143** in between.

Trimer **147**, the first member of the porphyrin oligomers that can rightly be called a functional molecular liquid, is an interesting substrate due to its molecular architecture. It exists as two slowly interconverting atropisomers. When incorporated into macrocycle **142**, it would appear at first glance to necessarily be held in the *syn* conformation. This would not, however, be expected to have any meaningful effect on the photophysical properties. From a synthetic perspective, an approach to **142** could conceivably mirror that of Kawase's CPPA synthesis, where alkyne formation would come from bromination and double dehydrobromination of the corresponding alkene **145** (Scheme 3.32). This alkene would be the product of an intramolecular McMurry reaction of dialdehyde **146**, which could come from the known dibromide **148** (Chapter 2).

reported synthesis of 4,5-dihexyloxy pyrene-1,8-dialdehyde,^[53] treatment of dibromide **148** with *n*-BuLi brought about halogen-metal exchange and quenching of the dilithiate with *N*-formylpiperidine afforded dialdehyde **146** in 72% yield. In stark contrast to trimer **147** and dibromide **148**, which are both *ca.* 1:1 mixtures of atropisomers that present themselves as one tight spot upon TLC analysis in a variety of solvent systems, the two atropisomers of dialdehyde **146** are easily separable. The difference in R_f value in 50% dichloromethane/hexanes is 0.4. Although the diastereomers are indeed easily separable by column chromatography, the barrier to isomerization does not appear to be significantly different from that of the trimer (calculated value = 25.8 kcal/mol).^[52] The trimer dialdehyde (**146**) offers some interesting synthetic opportunities, the aldehyde being one of the most versatile groups in the organic chemist's toolkit. These possibilities aside, attention was turned to using them as handles for construction of an alkyne that would furnish cycloalkyne **142** using an approach akin to Kawase's CPPA synthesis. The first step in this direction was to generate an alkene and the McMurry coupling was identified as the most direct methodology. McMurry coupling on pyrene aldehydes has been well-documented, both in intermolecular^[54] and intramolecular settings, the latter of which has been demonstrated to be quite powerful.^{[55][56]} Satisfyingly, the reaction of both diastereomers of trimer dialdehyde **146** under McMurry conditions resulted in the consumption of the starting material and the formation of a single mobile spot (TLC analysis)(Scheme 3.33). The new, less polar compound eluted as a single tight spot and material with a mass corresponding to a 75% yield of cyclic alkene **145** was obtained.

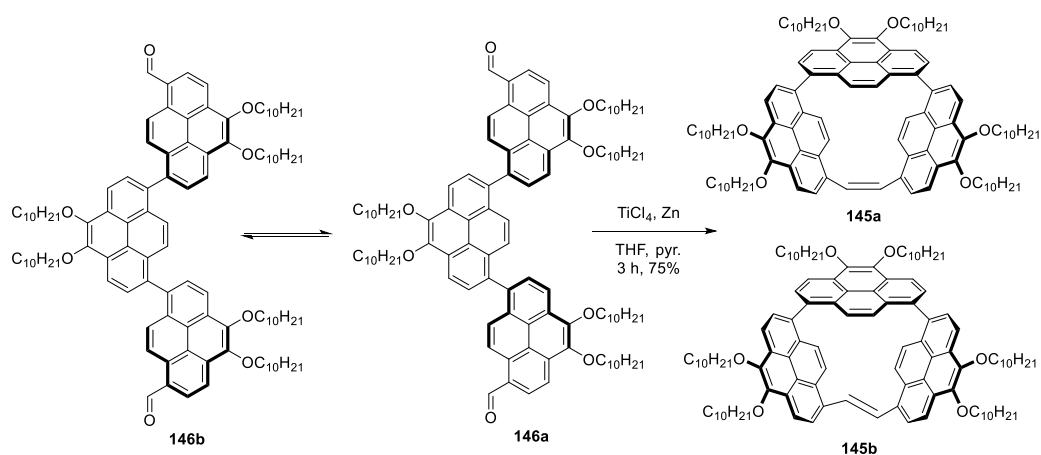


Scheme 3.33 Synthesis of cycloalkene **145**.

The ^1H NMR of the isolated material contained a clear set of signals that could be reasonably matched to cyclic alkene **145**, but a substantial amount (*ca.* 25%) of what appeared to be a second compound was also present. LCMS analysis showed a single signal at $m/z = 1564$, which was consistent with **145**. This being the case, the possibility of the minor product being a double bond geometric isomer was considered. The atropisomerism in the starting dialdehyde **146** and the mechanism of the McMurry reaction were also brought into play.

Dialdehyde **146** exists as a *ca.* 1:1 mixture of *syn* and *anti* atropisomers (Scheme 3.34). Reductive coupling of the *syn* isomer can lead to the formation of an *E* or a *Z* alkene, depending upon whether a *threo* or *erythro* dialkoxide forms in the first step of the McMurry reaction. The relative energies of (*Z*)-*syn*-**145** and (*E*)-*syn*-**145** were calculated the B3LYP/6-31G(d) level of theory; the former was found to be 8.48 kcal/mol lower in energy than the latter (Figure 3.12).^[57] The rather large energy difference between the two isomers does not necessarily rule out the formation of (*E*)-*syn*-**145** because it is likely the relative energies of the

dialkoxide intermediates (or more likely the transition states leading to them) that would dictate the product distribution.



Scheme 3.34 Dialdehyde diastereomers **146a** and **146b** leading to two cyclic alkene products, **145a** and **145b**.

If the minor product is indeed (*E*)-*syn*-**145** (**145b**), then it would be expected to have a more complicated ^1H NMR spectrum than (*Z*)-*syn*-**145** (**145a**) because the presence of the *E*-configured alkene would lower the molecular symmetry to the C_1 point group. On the other hand, a pedal-like motion of the *E*-alkene would interconvert enantiomeric species that on average would return the point group to C_s . The NMR spectra of (*Z*)-*syn*-**145** and (*E*)-*syn*-**145** were calculated at the B3LYP/6-311+G(2d,p) level of theory using the polarizable continuum model (PCM) to take the solvent (Chloroform) effect into consideration, and the predicted chemical shifts of the (*Z*)-*syn*-**145** closely match those of the major product (Figure 3.12). On the other hand, it is more difficult to match the calculated chemical shifts of (*E*)-*syn*-**145** to the observed signals of the minor compound. In particular, there is no doublet with a *ca.* 16 Hz coupling constant. However, this only really speaks against a static structure for (*E*)-*syn*-**145**.

If the pedal-like motion is rapid on the NMR time scale, then a singlet at roughly 7.26 ppm would be expected, and this region of the spectrum is quite congested. On the other hand, a rapid pedal-like motion would simplify the rest of the spectrum and this is not what is observed.

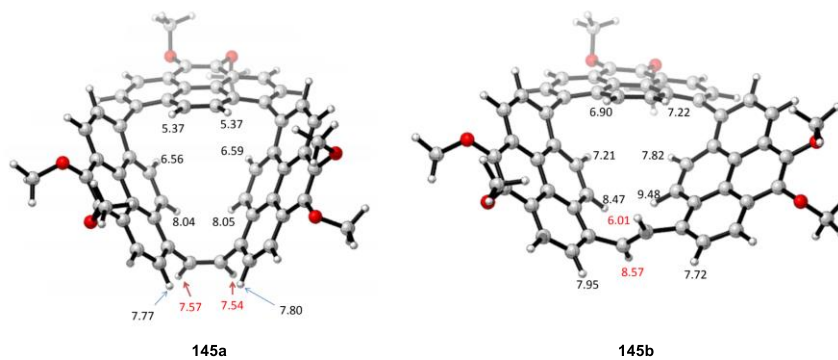


Figure 3.12 Calculated NMR shifts of two cycloalkene isomers **145a** and **145b** (B3LYP/6-311+G(2d,p) in CHCl_3).

It was initially thought that only *syn*-**146** could undergo intramolecular McMurry reaction, but inspection of molecular models suggested that this may not be the case. To probe this possibility, the structures of (*E*)-*anti*-**145** and (*Z*)-*anti*-**145** were calculated (Figure 3.13). These structures were found to be much higher in energy than (*Z*)-*syn*-**145**, by 25.0 and 38.6 kcal/mol, respectively. The diol models for the McMurry intermediates (**149c** and **149d**) were also found to be far too high in energy (23.0 and 24.6 kcal/mol higher than diol **149a**) to warrant any further consideration of the *anti* conformers. This left (*E*)-*syn*-**145** (**145b**) as the most likely structure for the minor product.

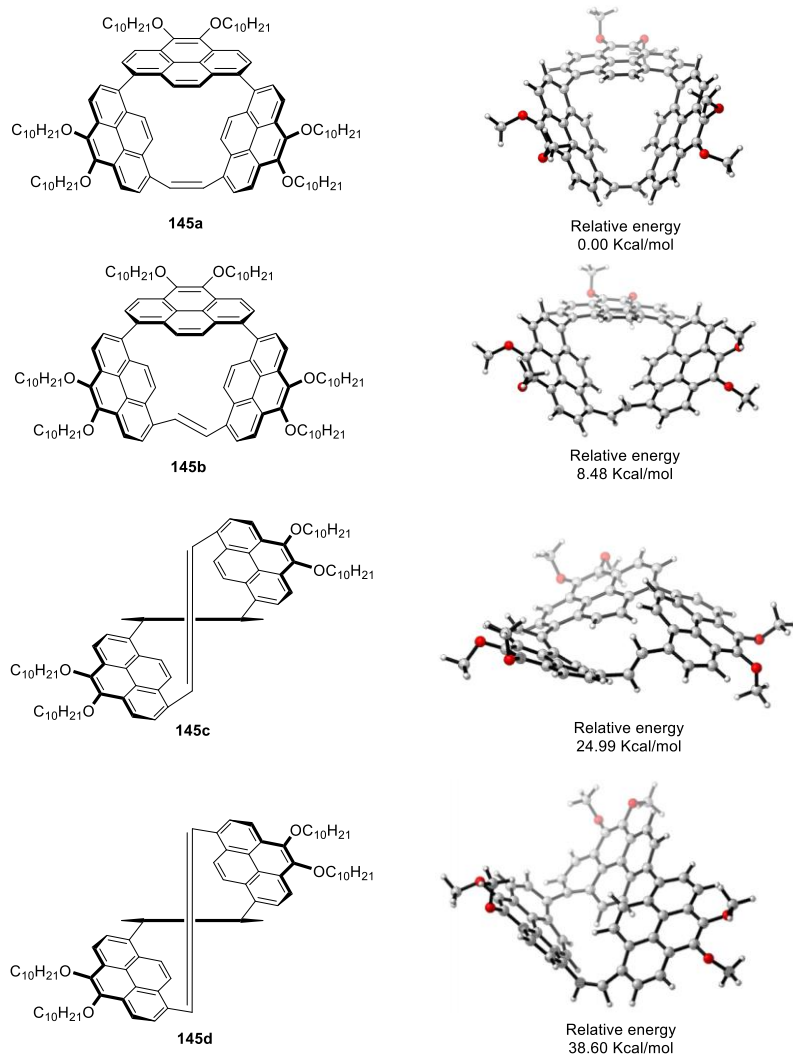


Figure 3.13 Calculated isomers and conformations available to alkene 145.

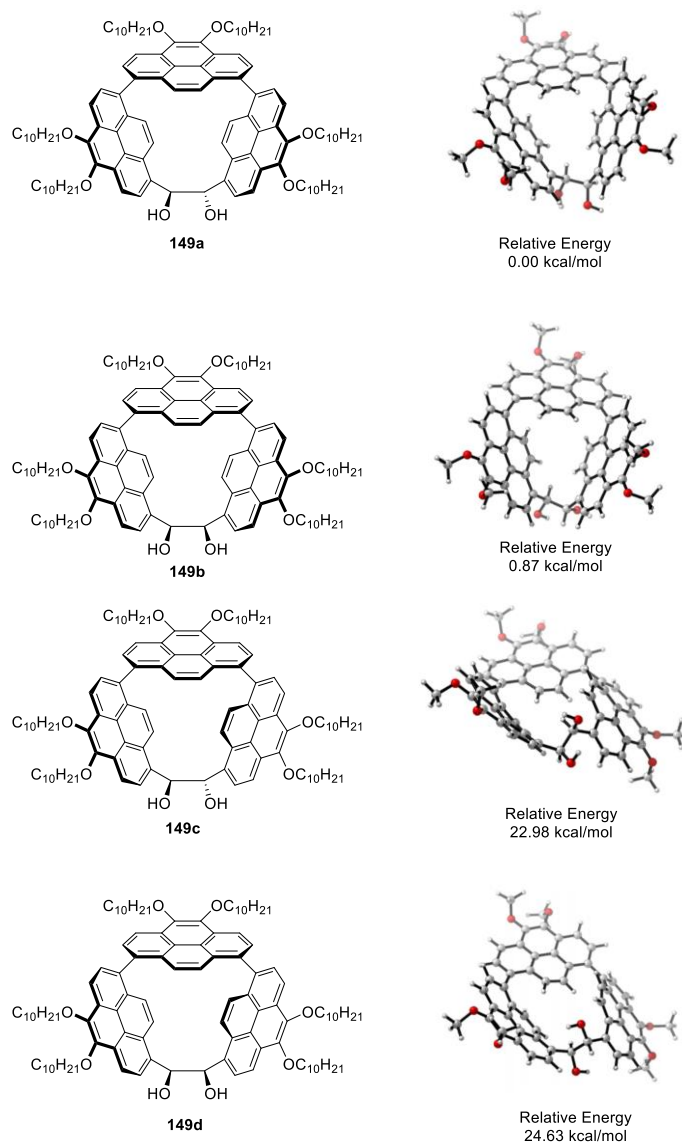


Figure 3.14 Relative energies of diols **149a** – **149d**.

Another possibility was that the minor component of **145** was macrocycle **150**, which consists of two trimer units that are connected by two alkene units (Figure 3.15). This compound would arise from an initial intermolecular McMurry reaction between two molecules of dialdehyde **146** followed by an intramolecular McMurry reaction. Three alkene isomers are possible (*E/E*, *E/Z* and *Z/Z*) as well as three conformational pairings of the two-

pyrene trimer (*syn/syn*, *syn/anti* and *anti/anti*). As such, it would be expected to have a complicated NMR spectrum with signals located close to those of (*Z*)-*syn*-**145**. LCMS analysis did not show a peak at $m/z = 3128$, but this might be due to an inability of the technique to produce ions of this mass in the gas phase.

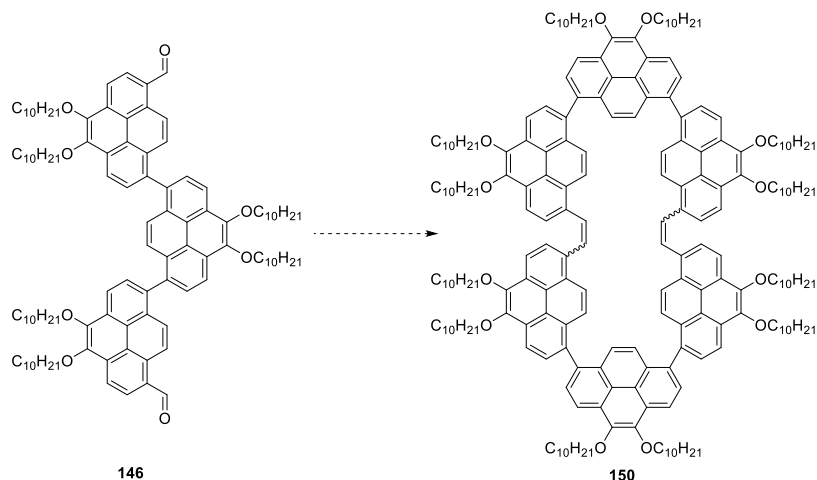
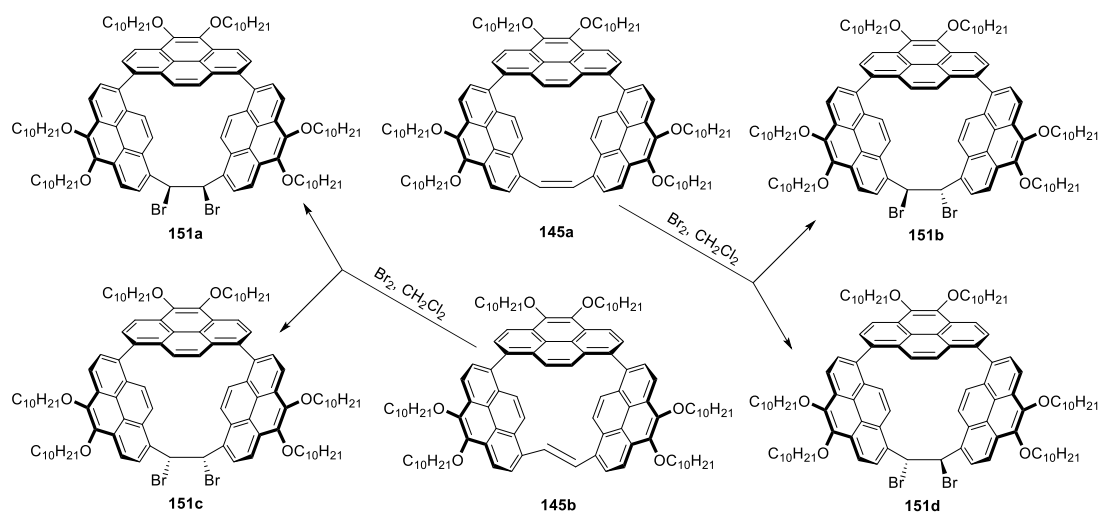


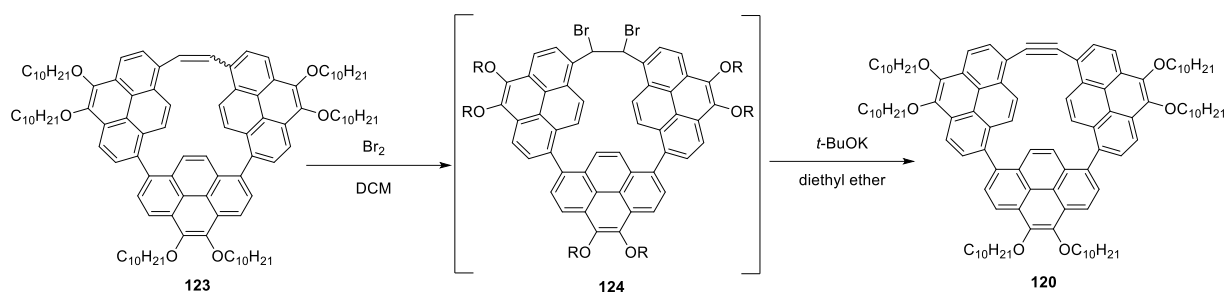
Figure 3.15 Possible dimerization of trimer dialdehyde (**146**) under McMurry conditions.

If *syn*-**145** is indeed a mixture of geometric isomers, then it would be reasonable to expect that application of Sondheimer's bromination / double dehydrobromination protocol should convert both isomers into the same cyclic alkyne **142**. A stock solution of bromine in dichloromethane was added to a solution of **145** and a rapid discoloration of the bromine was observed. TLC analysis showed the disappearance of the yellow, highly fluorescent spot for alkene **145** ($R_f = 0.45$, 30% CH_2Cl_2 / hexanes) and the formation of a single new blue-fluorescent streaking spot (R_f (leading edge) = 0.40, 30% CH_2Cl_2 / hexanes), which is presumably due to dibromides **151a** to **151d**. The complete disappearance of the yellow spot

for **145** is consistent with the minor product being alkene (*E*)-*syn*-**145**. The dichloromethane solvent was removed under reduced pressure and replaced with diethyl ether. A large excess of *t*-BuOK (ca. 6 equiv.) was then added and the mixture was stirred at room temperature. The reaction was monitored by TLC analysis and this showed that the blue-fluorescent streak attributed to dibromides **151a** to **151d** disappeared over a period of 12 h as a new green-fluorescent spot emerged ($R_f = 0.55$, 30% CH₂Cl₂ / hexanes).



Scheme 3.35 Possible bromides from the *syn*-conformers of *Z* and *E* geometric isomers of **145**.

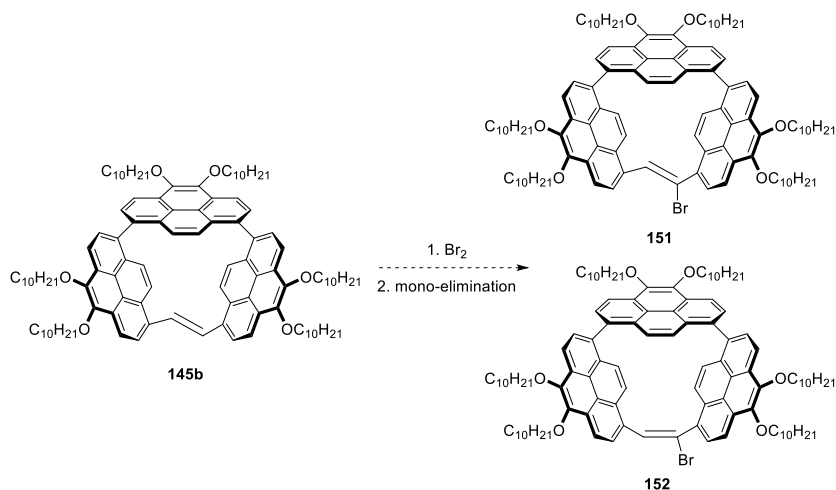


Scheme 3.38 Application of Sondheimer's methodology on alkene **142**.

Column chromatography was used to isolate the material giving rise to the green-fluorescent spot. As in the case of **145**, the ^1H NMR was found to be more complicated than was expected for alkyne **142**. The absence of the singlet at δ 5.83 that was attributed to the alkene protons of (*Z*)-*syn*-**145** confirmed that at least that component of the starting had been consumed. Signals at δ 7.54 (s) and 8.99 (d, $J = 9.5$ Hz) indicated that a C_s -symmetric trimer-containing molecule had been formed. It again appeared as though the desired product had been formed, but as a mixture with a minor compound in a *ca.* 8:1 ratio. The minor compound was clearly not the same as the minor component of **145** by NMR. Therefore, in agreement with TLC observations, it was not the case that only one of the components of the starting material reacted with bromine.

If the minor component of **145** is (*E*)-*syn*-**145**, then the possibilities are the (*Z*)-bromoalkene or (*E*) bromoalkene, which could be explained by the dibromide derived from (*E*)-*syn*-**145** undergoing elimination only once (Scheme 3.37); however, no evidence was found

for the formation of either vinyl bromide, and mass spectrometric analysis did not reveal a peak corresponding to the expected m/z value for the vinyl bromides nor were the characteristic 1:1 isotopic ratio seen in the mixture. In addition to this, a singlet that could correspond to the vinyl bromides remaining hydrogen is not found in the alkyne spectrum. In the same vein as the alkenes previously discussed, the *anti*-conformer of the cyclic alkyne **142** could be ruled out from its high (28 kcal/mol) relative energy compared to the *syn*-conformer, computed at the B3LYP/6-31G(d) level of theory (Figure 3.17). If the minor component of **145** is the macrocycle with two trimer units and two alkenes, then the product would be a macrocycle with two trimer units and two alkynes (Scheme 3.35).



Scheme 3.37 Possible synthesis of vinyl bromides **151** and **152**.

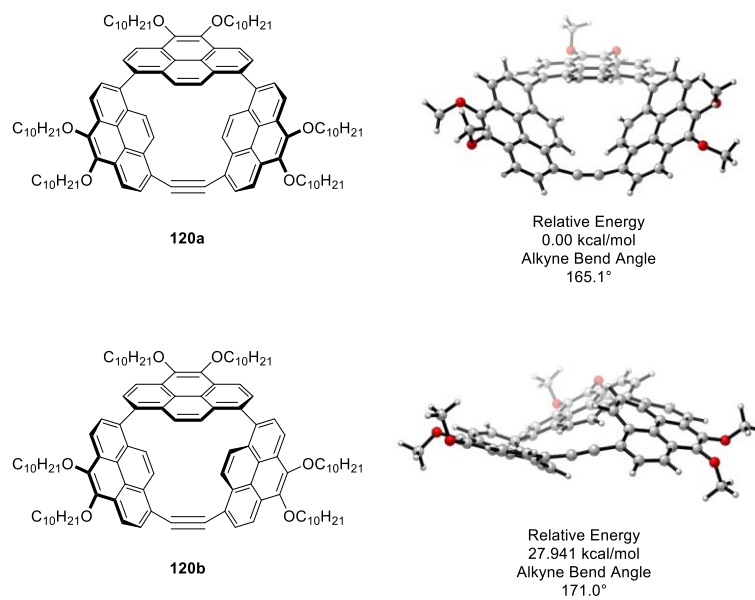
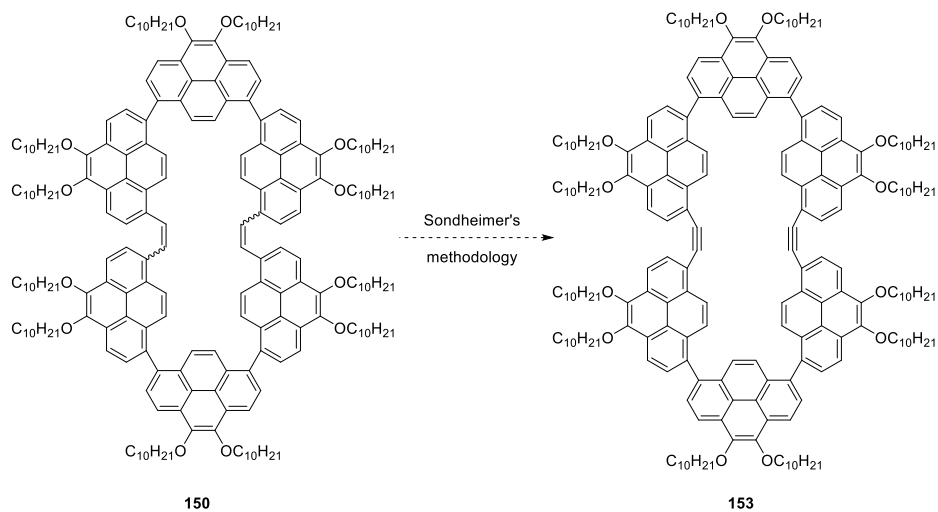


Figure 3.16 Calculated relative energies and bond angles of *syn*-120 (**120a**) and *anti*-120 (**120b**). (B3LYP/6-31G(d))



Scheme 3.36 Plausible synthesis of **153** if **150** is present in the **145** mixture.

Further evidence for the formation of alkyne **142** came from excellent agreement with calculated ^1H NMR shifts (Figure 3.13) and a characteristic resonance in the obtained ^{13}C NMR spectrum of the product. The sp -hybridized C atoms of alkyne signals typically appear at higher field than their sp^2 -hybridized counterparts. For example, the triply bonded carbon atoms in diphenyl acetylene **146** resonate at δ 89.43 ppm and those in Bodwell's unstrained trimer (**144**) appear at δ 95.45 ppm. By comparison, Jasti's strained hybrid (**137**) exhibits its alkyne resonance at somewhat lower field (δ 104.1 ppm). One would therefore expect the alkyne resonance in **142** to appear at lower field than that of [3]CPyA (**144**). Indeed, the spectrum of the crude product shows a weak, but clear signal at δ 103.45 ppm (Figure 3.14).

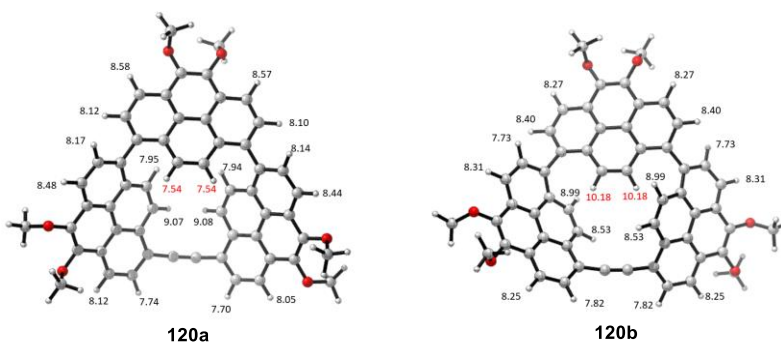


Figure 3.17 Calculated ^1H NMR shifts of *syn*-**120** (**120a**) and *anti*-**120** (**120b**).

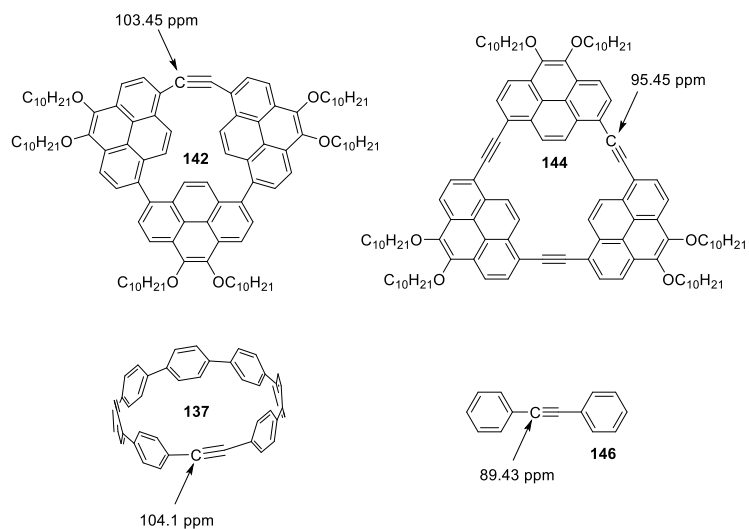
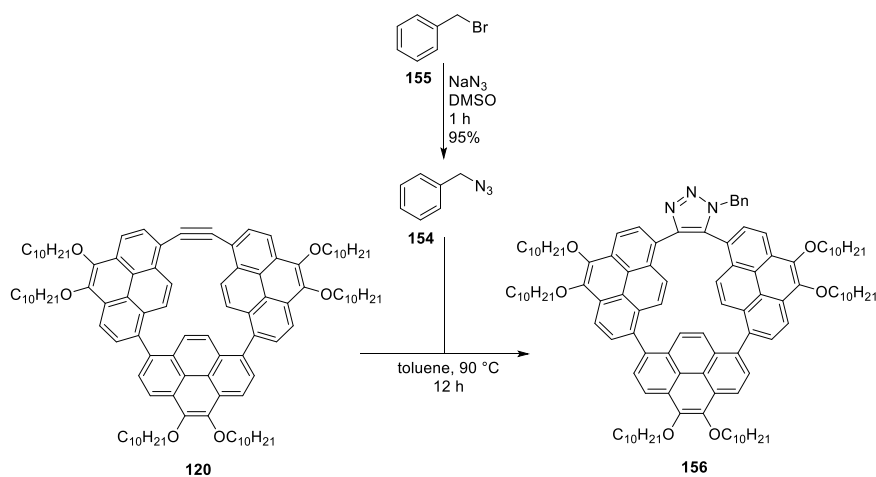


Figure 3.18 Comparison of ^{13}C NMR signals in strained alkynes **137** and **142** compared to unstrained models **146** and **144**.

The inability to obtain pure alkyne **142** was disappointing, but the possibility of performing a SPAAC reaction remained. Whether the minor component was a bromoalkene (**151** and/or **152**) neither of these compounds would be expected to undergo a SPAAC reaction. With this in mind, benzyl azide (**154**) was synthesized in high yield by the reaction of benzyl bromide (**155**) with sodium azide^[58] (Scheme 3.37). Reaction of this compound with the presumed alkyne **142** for 3 hours at 80 °C resulted in starting material being completely consumed by TLC. After flash column chromatography the compound was still heavily contaminated with excess benzyl azide, which can be conveniently removed under high vacuum with heating (Boiling point: 82°C to 85°C (16 mmHg)).^[59]



Scheme 3.37 Attempted SPAAC reaction with benzyl azide (**154**).

As expected, the NMR of the crude mixture was complicated. The substituted triazole in **156** destroys the symmetry of the skeleton. At the time of writing, characterization and conformation of SPAAC products was ongoing, as were attempts at using the alkyne in other reactions (*i.e.* oxidation, Diels-Alder, cobalt-catalyzed cyclotrimerization).

Conclusions

In conclusion, the pyrenylene trimer (Chapter 2) could be converted to dialdehyde **146** in 63% yield over two steps. Aldehyde **146** displays excellent propensity towards intramolecular cyclization under previously optimized McMurry coupling condition yielding cycloalkene **145**. In the same vein as Kawase and Oda's CPPA synthesis the alkene can be converted to an alkyne in a one-pot, two-step procedure. Currently work is underway to utilize the strained alkyne bearing the pyrenylene trimer skeleton.

References

1. C. J. Pedersen, *J. Am. Chem. Soc.* **1967**, *89*, 2495–2496.
2. C. J. Pedersen, *J. Am. Chem. Soc.* **1967**, *89*, 7017–7036.
3. C. J. Pederson, *Angew. Chem. Int. Ed.* **1988**, *27*, 1021–1027.
4. D. J. Cram, *Angew. Chem. Int. Ed.* **1988**, *27*, 1009–1112.
5. J.-M. Lehn, *Angew. Chem. Int. Ed.* **1988**, *27*, 89–112.
6. A. Y. Grosberg, A. R. Khoklov, *Giant Molecules*; Academic Press: San Diego, **1997**, p. 73.
7. Y. Fujioka, *Bull. Chem. Soc. Jpn.* **1984**, *57*, 3494–3506.
8. W. S. Rapson, R. G. Shuttleworth, J. N. van Niekerk, *J. Chem. Soc.* **1943**, 326–327.
9. G. Wittig, G. Lehmann, *Chem. Ber.* **1957**, *90*, 875–892.
10. H. A. Staab, F. Binnig, *Tetrahedron Lett.* **1964**, *5*, 319–321.
11. H. A. Staab, C. Winsche, *Chem. Ber.* **1968**, *101*, 887–890.
12. S. Scholz, D. Kondakov, B. Kondakov, K. Leo, *Chem. Rev.* **2015**, *115*, 8449–8503.
13. J. M. W. Chan, T. M. Swager, *Tetrahedron Lett.* **2008**, *49*, 4912–4914.
14. H. Taka, H. Kita, S. Sato, H. Isobe, *J. Org. Chem.* **2014**, *79*, 9735–9737.
15. J. Y. Xue, T. Izumi, A. Yoshi, K. Ikemoto, T. Koretsune, R. Akashi, R. Arita, H. Taka, H. Kita, S. Sato, H. Isobe, *Chem. Sci.* **2016**, *7*, 896–904.
16. K. Ikemoto, R. Kobayashi, S. Sato, H. Isobe, *Angew. Chem. Int. Ed.* **2017**, *56*, 6511–6514.
17. K. Ikemoto, J. Lin, R. Kobayashi, S. Sato, H. Isobe, *Angew. Chem. Int. Ed.* **2018**, *57*, 8555–8559.

18. Z. Sun, K. Ikemoto, T. M. Fukunaga, T. Koretsune, R. Arita, S. Sato, H. Isobe, *Science* **2019**, *363*, 151–155.
19. K. Ikemoto, S. Yang, H. Naito, M. Kotani, S. Sato, H. Isobe, *Nat. Commun.* **2020**, *11*, 1807–1813.
20. J. C. Walsh, G. J. Bodwell, *Commun. Chem.* **2020**, *93*, 1–4.
21. V. C. Parekh, P. C. Guha, *J. Ind. Chem. Soc.* **1934**, *11*, 95–100.
22. D. T. M. Wong, C. S. Marvel, *J. Polym. Sci., Polym. Chem. Ed.*, **1976**, *14*, 1637–1644.
23. O. M. Yaghi, H. Li, T. L. Groy, *Z. Kristallogr. - New Cryst. Struct.*, **1997**, *212*, 453–455.
24. F. G. Klarner, *Angew. Chem. Int. Ed.* **2017**, *14*, 3751–3752.
25. R. Friederich, M. Nieger, F. Vögtle, *Chem Ber.* **1993**, *7*, 1723–1732.
26. J. E. McMurry, G. J. Haley, J. R. Matz, J. C. Clardy, J. Mitchell, *J. Am. Chem. Soc.*, **1986**, *108*, 515–520.
27. R. Jasti, J. Bhattacharjee, J. B. Neaton, C. R. Bertozzi, *J. Am. Chem. Soc.* **2008**, *52*, 17646–17647.
28. P. J. Evans, E. R. Darzi, R. Jasti, *Nat. Chem.* **2014**, *6*, 404–408.
29. H. Takaba, H. Omachi, Y. Yamamoto, J. Bouffard, K. Itami, *Angew. Chem. Int. Ed.* **2009**, *33*, 6112–6116.
30. S. Yamago, Y. Wantanabe, T. Iwamoto, *Angew. Chem. Int. Ed.* **2010**, *49*, 757–759.
31. N. Hayase, Y. Miyauchi, Y. Aida, H. Sugiyama, H. Uekusa, Y. Shibata, K. Tanaka, *Org. Lett.* **2017**, *11*, 2993–2996.
32. Y. Tsuchido, R. Abe, T. Ide, K. Osakada, *Angew. Chem. Int. Ed.* **2020**, *59*, 1–6.
33. T. Iwamoto, E. Kayahara, N. Yasuda, T. Suzuki, S. Yamago, *Angew. Chem. Int. Ed.* **2014**, *25*, 6430–6434.

34. D. Lorbach, A. Keerthi, T. M. Figueira-Duarte, M. Baumgarten, M. Wagner, K. Müllen, *Angew. Chem. Int. Ed.* **2016**, *55*, 418–421.
35. R. Kurosaki, H. Hayashi, M. Suzuki, J. Jiang, M. Hatanaka, N. Aratani, H. Yamada, *Chem. Sci.* **2019**, *28*, 6785–6790.
36. R. Kurosaki, K. Matsuo, H. Hayashi, H. Yamada, N. Aratani, *Chem. Lett.* **2020**, *49*, 892–895.
37. A. N. Cook, *J. Am. Chem. Soc.* **1901**, *23*, 806–813.
38. H. N. C. Wong, P. J. Garratt, F. Sondheimer, *J. Am. Chem. Soc.* **1974**, *64*, 5604–5605.
39. T. Kawase, H. R. Darabi, M. Oda, *Angew. Chem. Int. Ed.* **1996**, *35*, 2664–2666.
40. H. N. C. Wong, P. J. Garratt, F. Sondheimer, *J. Am. Chem. Soc.* **1974**, *64*, 5604–5605.
41. T. Kawase, H. R. Darabi, K. Tanaka, M. Oda, *Angew. Chem. Int. Ed.* **2003**, *42*, 1624–1628.
42. M. A. Ali, M. S. Krishnan, *Mol. Phys.* **2009**, *107*, 2149–2158.
43. G. Venkataramana, P. Dongare, L. N. Dawe, D. W. Thompson, Y. Zhao, G. J. Bodwell, *Org. Lett.* **2011**, *13*, 2240–2243.
44. J. Wu, M. A. Dobrowolski, M. K. Cyrański, B. L. Merner, G. J. Bodwell, Y. Mo, P. v. R. Schleyer, *Mol. Phys.* **2009**, *107*, 1177–1186.
45. This is generally agreed upon, however a rigorous explanation is elusive.
46. S. Lee, E. Chenard, D. L. Gray, J. S. Moore, *J. Am. Chem. Soc.* **2016**, *42*, 13814–13817.
47. X. Zhou, R. R. Thompson, F. R. Fronczek, S. Lee, *Org. Lett.* **2019**, *21*, 4680–4685.
48. T. A. Schaub, J. T. Margraf, L. Zakharov, K. Reuter, R. Jasti, *Angew. Chem. Int. Ed.* **2018**, *57*, 16348–16355.

49. W. Zhao, H. Wu, Z. Liu, P. Zhong, L. Zhang, X. Huang, J. Cheng, *Chem. Commun.* **2006**, *46*, 4826–4828.
50. L.-H. Wang, N. Hayase, H. Sugiyama, J. Nogami, H. Uekusa, K. Tanaka, *Angew. Chem. Int. Ed.* **2020**, *59*, 17951–17957.
51. H. Tanaka, M. Ikenosako, Y. Kato, M. Fujiki, Y. Inoue, T. Mori, *Commun. Chem.* **2018**, *38*, 1–8.
52. J. C. Walsh, D. T. Hogan, K.-L. M. Williams, S. D. Brake, G. Venkataramana, T. A. Misener, B. J. Wallace, R. P. Johnson, D. W. Thompson, Y. Zhao, B. D. Wagner, G. J. Bodwell, *ChemPlusChem*, **2019**, *84*, 754–768.
53. M. Khadem, J. C. Walsh, G. J. Bodwell, Y. Zhao, *Org. Lett.*, **2016**, *18*, 2403–2406.
54. T. Itoh, H. Saitoh and S. Iwatsuki, *J. Polym. Sci., Part A: Polym. Chem.*, **1995**, *33*, 1589–1599.
55. K. S. Unikela, P. G. Ghasemabadi, V. Houska, L. N. Dawe, Y. Zhao, G. J. Bodwell, *Chem. Eur. J.*, **2020**, Early View.
56. K. C. Nicolaou; J.-J. Liu; Z. Yang; H. Ueno; E. J. Sorensen; C. F. Claiborne; R. K. Guy; C.-K. Hwang; M. Nakada & P. G. Nantermet, *J. Am. Chem. Soc.*, **1995**, *117*, 634–644.
57. Calculated by Prof. Yuming Zhao (Memorial University, chemistry department)
58. I. Wilkening, G. del Signore, C. P. R. Hackenberger, *Chem. Commun.*, **2011**, *47*, 349–351.
59. Alfa-Aesar specifications sheet.

Experimental Section

1,8-Bis(8-carboxaldehyde-4,5-didecoxyppyren-1-yl)-4,5-didecoxyppyrene (146): To a $-78\text{ }^{\circ}\text{C}$ (cooled by a dry ice/acetone bath) nitrogen-purged solution of trimer dibromide (**148**) (0.200 g, 0.118 mmol) in anhydrous THF (30 mL), *n*-BuLi (1.30 M, 0.725 mL, 0.942 mmol) was added dropwise. The reaction was allowed to stir at $-78\text{ }^{\circ}\text{C}$ for 5 min. *N*-formylpiperidine (0.212 g, 1.88 mmol) was added and the dry ice/acetone bath was removed. The reaction mixture was allowed to warm to rt and stirred for a further 1.5 h. The reaction was quenched with 10% HCl(aq) (10 mL) and the organic solvents were removed under reduced pressure. The reaction mixture was extracted with CH_2Cl_2 ($3 \times 30\text{ mL}$). The combined organic layers were washed with 10% HCl(aq) ($5 \times 60\text{ mL}$) and subsequently dried over anhydrous Na_2SO_4 . The solvent was removed under reduced pressure to yield crude (**146**) as an orange oil. The crude product was subjected to silica gel column chromatography (CH_2Cl_2 /hexanes, 1:2) to yield compound (**146**) as a viscous orange oil (0.135 g, 0.085 mmol, 72%). R_f (50% CH_2Cl_2 /hexanes) = 0.55 and 0.15; $^1\text{H NMR}$ (CDCl_3 , 300 MHz): δ = 10.74 (s, 2H), 9.20 (d, J = 9.6 Hz, 2H), 8.81 (d, J = 8.0 Hz, 2H), 8.67 (d, J = 7.8 Hz, 2H), 8.65 (d, J = 7.8 Hz, H), 8.60–8.45(m, 4H), 8.25 (d, J = 8.0 Hz, 2H), 8.15 (d, J = 8.0 Hz, 2H), 8.12–8.02 (m, 2H), 7.94 (d, J = 9.6 Hz, 2H), 7.87 (d, J = 9.3 Hz, 2H), 7.62 (d, J = 9.2 Hz, 2H), 4.58–3.96 (m, 12H), 2.11–1.86 (m, 8H), 1.76–1.57 (m, 16H), 1.55–1.16 (m, 72H), 0.97–0.81 (m, 18H); $^{13}\text{C NMR}$ (CDCl_3 , 75 MHz): δ = 192.75, 147.06, 144.35, 144.12, 143.55, 137.79, 134.76, 134.04, 131.50, 130.07, 129.66, 129.48, 129.29, 128.94, 128.42, 126.77, 126.25, 125.99, 125.44, 124.52, 122.99, 122.98, 121.09, 119.02, 118.99, 74.04, 73.98, 73.94, 31.97, 31.95, 30.68, 29.75, 29.73, 29.40, 26.40, 26.34, 22.74,

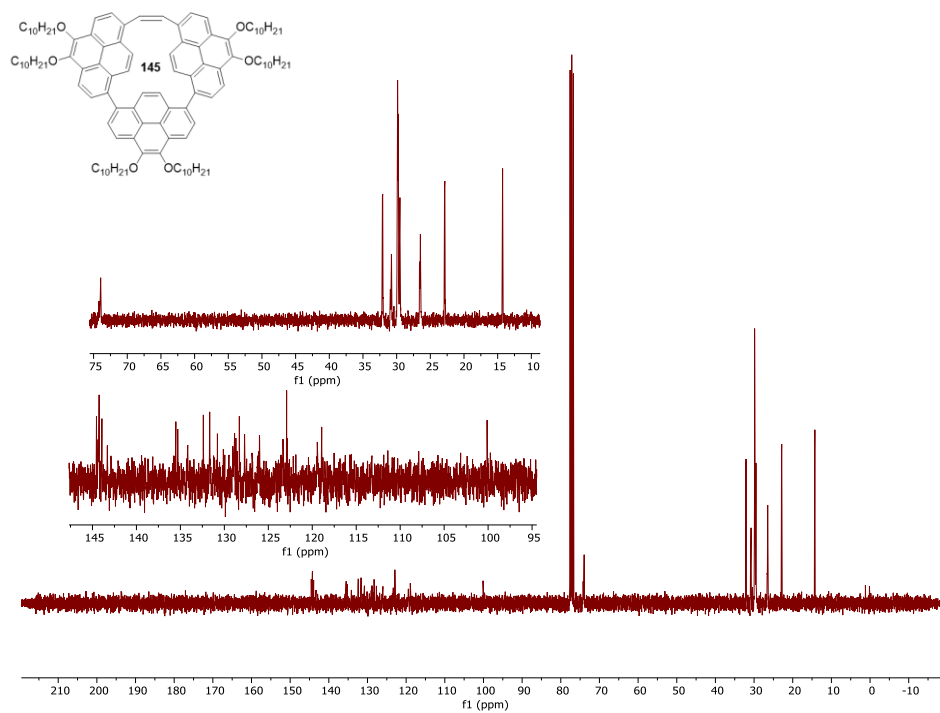
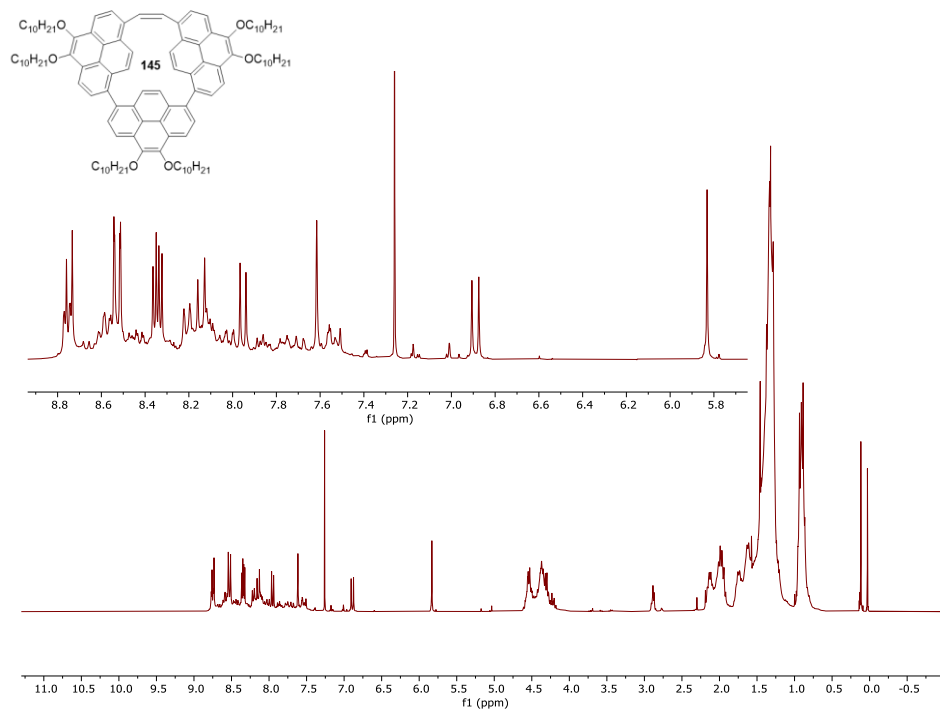
22.72, 14.16, 14.14; HRMS (APPI, positive mode) m/z for $C_{110}H_{146}O_8$ calcd. 1595.1065, found 1595.1018 $[M]^+$.

C₁₀ Cyclopyrenetrimerene (145): To an oven-dried 500 mL 2-neck round-bottomed flask equipped with two rubber septa was added anhydrous THF (SPS) (100 mL) and zinc dust (10 micron) (2.70 g, 41.3 mmol). Titanium(IV) chloride (2.30 mL, 21.0 mmol) was then added slowly (note: the $TiCl_4$ reacts violently to produce a yellow solid that spatters the walls. Once addition is complete the flask can be removed from its clamp and tilted to contact the solid with solvent and it will slowly dissolve) to the stirred slurry at room temperature under nitrogen atmosphere (balloon) resulting in a color change from colorless to pale blue. The slurry was heated at reflux for 1 h, during which time a dark brown colour persisted (the solution appears black, but at the meniscus, or by swirling the flask its brown color is evident, the loss of this colour is detrimental and should be considered a clear indication of a failed reaction). Pyridine (2.50 mL, 31.0 mmol)(distilled over CaH_2 on to activated 4 Å MS) was added by syringe and stirring was continued at reflux for a further 10 min. Dialdehyde **146** (250 mg, 0.156 mmol) in THF (10 mL) was then added slowly over 10 min and the reaction mixture was heated at reflux for a further 3 h. The hot reaction mixture was poured into dichloromethane (100 mL) and enough silica gel was added (~20 g) for the mixture to become a free-flowing powder after the solvents were removed under reduced pressure. The residue was subjected to column chromatography (5% dichloromethane/hexanes, then 15% dichloromethane/hexanes) to afford **145** as a yellow oil (184 mg, 75%). R_f (15% CH_2Cl_2 /hexanes) = 0.30; 1H NMR (300 MHz, $CDCl_3$) major component: δ = 8.75 (d, J = 8.0

Hz, 2H), 8.53 (d, $J = 8.0$ Hz, 2H), 8.52 (d, $J = 8.0$ Hz, 2H), 8.35 (d, $J = 8.1$ Hz, 2H), 8.34 (d, $J = 8.1$ Hz, 2H), 8.21 (d, $J = 8.1$ Hz, 2H), 8.15 (d, $J = 9.3$ Hz, 2H), 7.96 (d, $J = 8.1$ Hz, 2H), 7.62 (s, 2H), 6.89 (d, $J = 9.4$ Hz, 2H), 9.20 (d, $J = 9.6$ Hz, 2H), 5.83 (s, 2H), 4.63–4.17 (m, 12H), 2.23–1.88 (m, 8H), 1.83–1.14 (m, 88H), 1.01–0.78 (m, 18H); ^{13}C NMR (75 MHz, CDCl_3) $\delta =$ 144.54, 144.25, 143.93, 135.52, 135.30, 132.39, 131.67, 130.79, 129.05, 128.84, 128.64, 128.30, 127.70, 126.00, 122.92, 119.43, 118.93, 100.11, 73.95, 32.14, 32.11, 30.93, 30.77, 29.86, 29.81, 29.76, 29.55, 29.51, 26.61, 26.48, 22.89, 22.84, 14.32, 14.27; HRMS (APPI, positive mode) m/z for $\text{C}_{110}\text{H}_{146}\text{O}_6$ calcd. 1563.1119, found 1563.1066 $[\text{M}]^+$.

C₁₀Cyclopyrenetrimeryne (142). To an oven-dried 100 mL round-bottomed flask was added alkene (145) (100 mg, 0.064 mmol) and CHCl_3 (10 mL). The solution was stirred at room temperature and a solution of Br_2 (0.011 g, 0.003 mL, 0.067 mmol) in CHCl_3 (3 mL) was added dropwise. After addition was complete, the solvent was removed under reduced pressure and replaced with diethyl ether (10 mL). Potassium *tert*-butoxide (0.072 g, 0.639 mmol) was added in one portion and the flask was sealed with a rubber septum and fitted with a nitrogen balloon. The solution was stirred for 12 h at room temperature and quenched with water (5 mL). The reaction mixture was extracted with hexanes (3×20 mL) and the combined organic extracts were dried over anhydrous MgSO_4 . Removal of the solvent by rotary evaporation afforded an orange oil): R_f (30% CH_2Cl_2 /hexanes) = 0.55; ^1H NMR (300 MHz, CDCl_3) major component: $\delta =$ 8.98 (d, $J=9.5$ Hz, 2H), 8.75 (d, $J=8.0$ Hz, 2H), 8.67 (d, $J=8.2$ Hz, 2H), 8.47 (d, $J=8.2$ Hz, 2H), 8.40 (d, $J=8.2$ Hz, 2H), 8.36 (d, $J=8.0$ Hz, 2H), 8.09 (d, $J=8.2$ Hz, 2H), 7.98 (d, $J=9.5$ Hz, 2H), 7.54 (s, 2H), 4.61–4.12 (m, 12H), 2.18–1.88 (m, 12H), 1.81–1.14 (m, 84H), 0.99–0.78 (m, 18H); ^{13}C NMR (75 MHz, CDCl_3) $\delta =$ 144.99, 144.90, 144.27,

136.44, 135.39, 131.90, 130.18, 129.91, 129.34, 128.89, 128.84, 127.68, 127.05, 126.01, 123.38, 123.31, 122.81, 119.36, 119.26, 103.45, 74.18, 74.06, 32.11, 32.08, 30.87, 30.77, 30.71, 29.91, 29.86, 29.83, 29.78, 29.75, 29.56, 29.52. 26.58, 26.48, 26.46, 22.88, 22.85, 22.83, 14.30, 14.28, 14.25. HRMS could not be obtained for this compound .

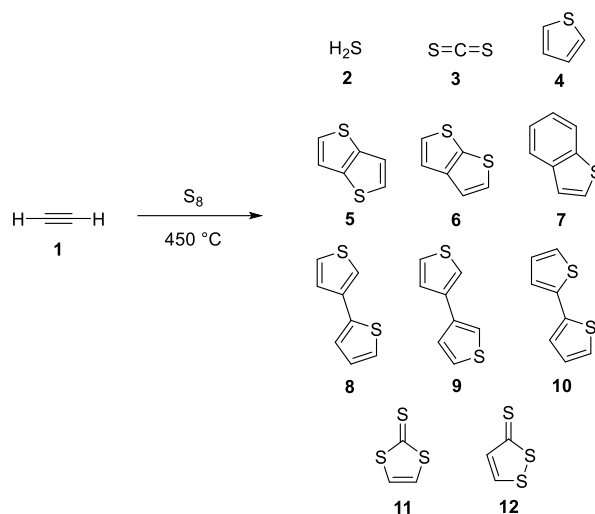


Chapter 4

Oligopyrenylene Extended TTFVs

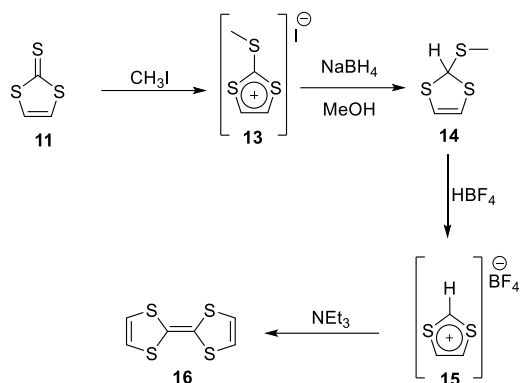
Introduction

The structural units that are of particular interest in this Chapter have a history that goes back more than 85 years. It was known in the early 20th century that the high temperature reaction of elemental sulfur and acetylene (**1**) yields a complicated mixture of products, the major components of which are hydrogen sulfide (**2**), carbon disulfide (**3**) and thiophene (**4**) (Scheme 4.1). Also produced is a red oil that can be separated by distillation with superheated steam. In 1935, Challenger and Harrison^[1] reported the fractionation of this red oil at 15 mmHg and elucidated the nature of its chemical components, which they reported in a series of papers between 1945^{[2][3][4]} and 1953.^[5] The colorless fraction obtained from 90 to 120 °C was comprised of thiophenes **4-7** and a second fraction obtained from 120 to 140 °C consisted mostly of the isomeric series of bithienyls **8, 9** and **10**. Finally, a third fraction obtained from 140 to 165 °C was obtained as a dark red oil. Upon cooling, a bright orange solid formed and it was found to contain mainly two isomers of C₃H₂S₃, **11** and **12**. It was then discovered that **12**, which possesses a sulfur–sulfur bond, is easily destroyed in a boiling aqueous sodium hydroxide solution, leaving pure **11**.



Scheme 4.1 The high temperature reaction of acetylene with elemental sulfur and the various products.

Two decades later, Fred Wudl used thione **11** to great effect.^[6] Treatment of **11** with methyl iodide resulted in the facile methylation of the thioketone unit to afford salt **13**. The ease with which this process occurs is attributable to the 6 π -electron aromatic character of the dithiolium cation. The aromatic cation could then be reduced with sodium borohydride to afford **14** and subsequent dethioalkylation by fluoroboric acid yielded the parent dithiolium cation **15**. This aromatic cation underwent dimerization in the presence of triethylamine, yielding tetrathiafulvalene **16**.



Scheme 4.2 Wudl's synthesis of the parent TTF **16**.

With the parent TTF in hand, Wudl set out to explore the compound's redox behavior. Astonishingly, upon reaction with a single molar equivalent of chlorine gas, an extraordinarily stable radical cation was obtained. Radical cation of **16a** could be isolated as a brilliant purple solid, which was easily crystallized and handled in air. The compound was even soluble and stable in aqueous solution.^[7] Further oxidation afforded dication **16b**, which was relatively unstable, having a half-life of 6 hours at room temperature. Investigation of the electrochemical properties of the parent TTF and the radical cation yielded unexpected results. Measuring the electronic conductivity of the parent compound **16** showed that the molecule was two orders of magnitude more conducting than ferrocene. This was a step in the right direction (ferrocene $10^{14} \Omega \text{ cm}$ and **16**, $10^{12} \Omega \text{ cm}$), but when the radical cation was measured, there was a precipitous drop in resistivity, falling 12 orders of magnitude to $3.7 \pm 1 \Omega \text{ cm}$. In 1973, shortly after Wudl's discovery, Ferraris *et al.*^[8] found that forming a 1:1 charge transfer complex of TTF and TCNQ, the resistance plummeted even further. This was the discovery of the first organic metal, with a resistivity measured at $1.47 \times 10^{-4} \Omega \text{ cm}$ (*cf.* copper metal $6 \times 10^{-5} \Omega \text{ cm}$). The exciting electrical properties of this material were attributed to high symmetry

(D_{2h}), which diminishes random potentials caused by disorder, four sulfur atoms, which imbue the molecule with high polarizability and minimization of the Columbic repulsion between adjacent TCNQ radical anions.^[8]

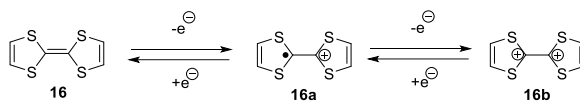


Figure 4.1 Stepwise oxidation of parent TTF **16**.

A number of π -extended TTF derivatives have been reported, which feature the presence of a pi system (either a PAH or multiple double bonds) between the two dithiafulvene (DTF) moieties, but none of the many derivatives of this type have been exploited as much as the TTF vinylogues, namely TTFVs.^{[9][10]} The TTFV moiety preserves the redox activity of the parent TTF, but the extra carbon-carbon double bond brings with it an interesting property. Neutral TTFV prefers a *syn* conformation, taking advantage of sulfur-sulfur van der Waals type interactions (Figure 4.2). However, upon oxidation to the corresponding dication **18**, a drastic change in conformation occurs. To minimize the Coulombic repulsion of the two aromatic cations, the oxidized TTFV now prefers an *anti* conformation. This is quite a useful property when viewed through the lens of molecular switches. There are many molecular motifs that undergo switching behavior, but very few have the attractive property of undergoing a large change in shape upon switching. This massive change in shape could be useful in the design of catch and release molecular devices.

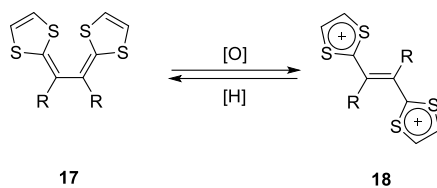
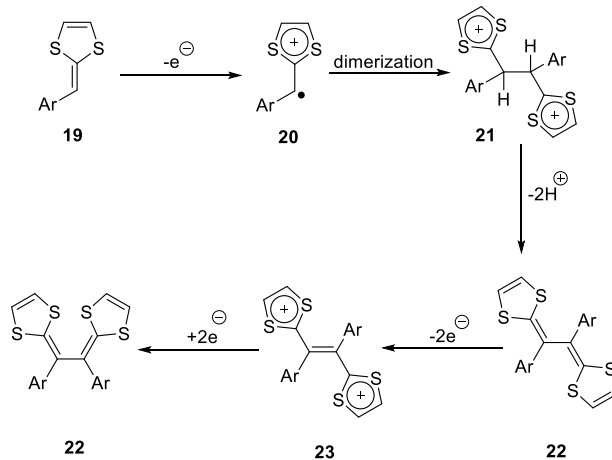


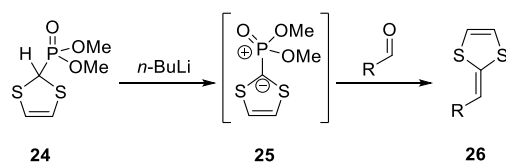
Figure 4.2 Redox switching of TTFV.

TTFVs are easily prepared under mild conditions from the corresponding dithiafulvenes (DTFs). DTFs are in turn easily oxidized to the corresponding radical cation by virtue of the aromatic stabilization energy gained in producing dithiolium ions and, especially in the R=aryl derivatives, due to the resonance stabilization of the radical at the benzylic position. The radical, adjacent to both a ring bearing a full positive charge and an electron donating aryl group may also benefit from the captodative effect.



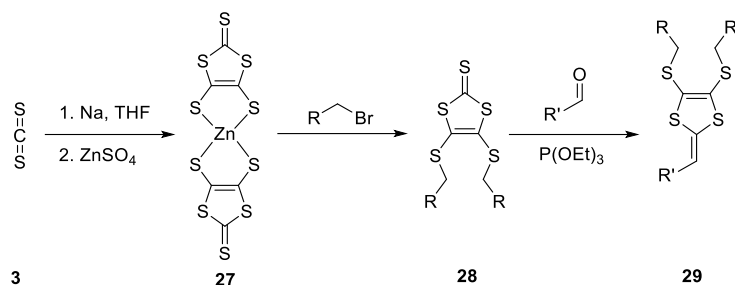
Scheme 4.3 Radical dimerization of a DTF to form a TTFV.

Experimentally, this multistep conversion from DTF to TTFV is accomplished easily. Molecular iodine is a suitable oxidant to readily generate the radical cation **20** from its neutral form. The radical cation undergoes dimerization and then loss of two protons to afford TTFV **22**, which is then quickly oxidized into TTFV dication under the oxidative reaction conditions. Reductive workup of the reaction mixture leads to neutral TTFV **22** as the final product, which can be achieved by many reducing reagents; however, sodium thiosulfate is a convenient reductant and the one utilized most often. Previously, the DTF units were installed using a reaction similar to the Horner-Wadsworth-Emmons reaction. For instance, the ylide **25** generated from **24** can be coupled with an aldehyde or ketone to yield DTF **26** (Scheme 4.4). In this method, the synthesis of the phosphonate precursor is usually long and low yielding, hampering the broader application of this chemistry.^[11]



Scheme 4.4 Obsolete synthesis of DTFV moieties using the Horner-Wadsworth-Emmons reaction.

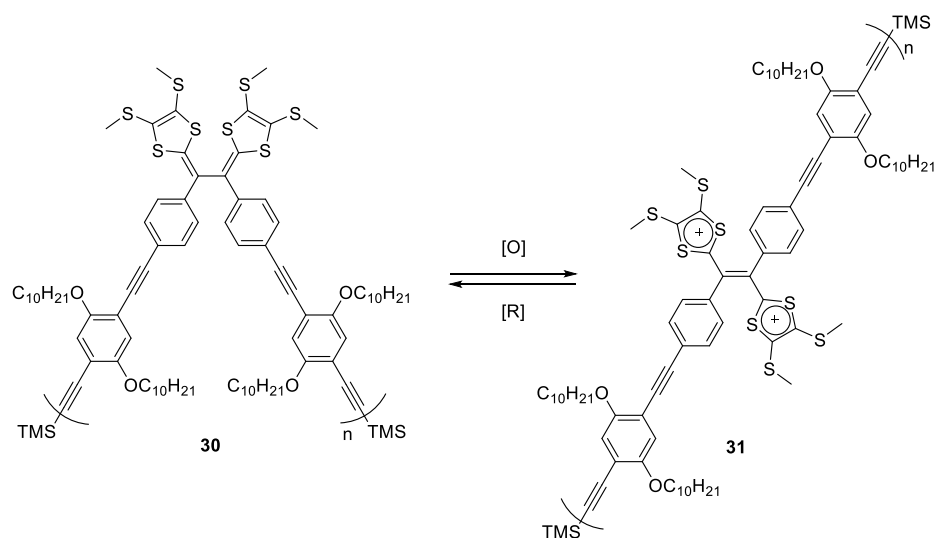
A major advance in DTF chemistry came with the advent of a simple synthesis of the dithiaalkylthioxanthone **28**. Easily prepared on a mole scale through the trimerization of carbon disulfide (**3**), Bryce and co-workers demonstrated that thioxanthone **28**, like **24**, can be coupled with aldehydes in the presence of a trialkyl phosphite at reflux to yield DTFs in high yield (Scheme 4.5).^[12]



Scheme 4.5 Large scale synthesis of dithiaalkyl-DTF precursor.

An excellent example of the utility of the TTFV moiety's switching behavior comes from the Zhao group.^[13] Utilizing the preferred *syn* relationship between the dithiolane rings in the neutral state, Zhao *et al.* produced a polymer incorporating both aromatic units and many solubilizing groups. The polymer was easily produced using Sonogashira conditions to yield mainly the hexamer. Molecular modeling revealed the hexamer would likely be highly folded in the neutral state with a lumen approximately 3 nm in diameter. Zhao reasoned that with a lumen of this size it could be possible for the molecule, aided by π - π interactions, to wrap itself around certain types of single-walled carbon nanotubes. With the numerous decoxy groups on the polymer backbone, the resulting foldamer/nanotube assemblies become soluble, allowing for selective dissolution of single-walled carbon nanotubes according to their diameters and/or electronic nature. Then, upon oxidation and switching the polymer from highly twisted to nearly linear, the solubilized nanotube/polymer assemblies could be dissociated to release relatively pure single-walled carbon nanotubes as precipitate. This method can be used to sort single-walled carbon nanotubes out of as-prepared carbon

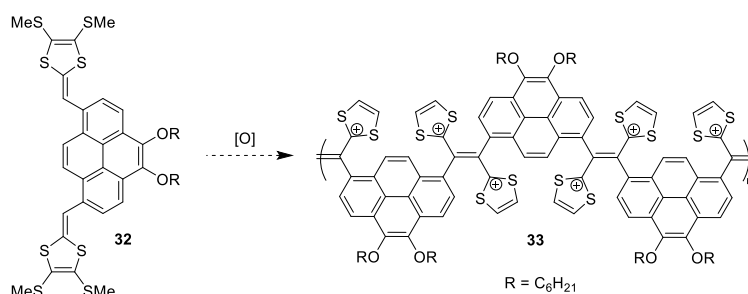
nanotubes. Importantly, the oxidized polymer could be reversibly reduced back to its starting form and reused.



Scheme 4.6 Zhao's TTFV containing polymers.

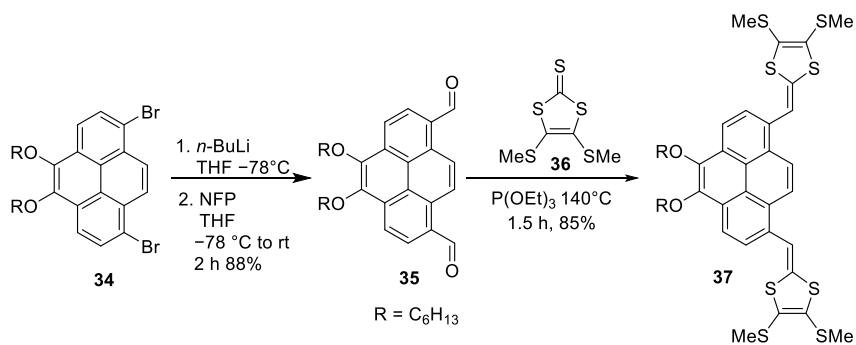
Results

An attractive molecular target in the context of this backdrop is the bis(DTF) **32**, which could conceivably come from 4,5-didecoxy-pyrene-1,8-dicaboxaldehyde (**35**) (Scheme 4.7). Pyrene is known to irreversibly bind to carbon nanotubes^[14] and with long alkyl groups to aid in solubility, it is reasonable to think that the polymer derived from the radical polymerization of the DTF groups to generate a pyrene-TTFV hybrid polymer could be an interesting candidate for solubilizing carbon nanotubes like Zhao's polymer **30**.



Scheme 4.7 Proposed structure for the product of radical polymerization. SMe groups omitted for clarity.

To accomplish the synthesis of monomer **36**, dibromide **33** (Chapter 2) was subjected to a two-step procedure consisting of halogen-metal exchange with *n*-BuLi followed by quenching of the aryl lithium with NFP. This furnished dialdehyde **35** in 88% yield. This initially was problematic with low yields and difficult separations, but after taking inspiration from Hopf and replacing DMF with *N*-formylpiperidine,^[15] the yields increased and only small amounts of monoaldehydes were generated, thereby making the separation much easier. With dialdehyde **35** in hand, it was treated with three equivalents of dithiamethylthioxanthone **36** in triethyl phosphite at reflux. After removal of the high boiling solvent by distillation and column chromatography, the bis(DTF)pyrene **36** was isolated in 85% yield as a lustrous orange solid.



Scheme 4.8 Synthesis of pyrene-TTFV hybrid **37**.

Attention was then turned to the polymerization reaction of **36**. Several attempts were made to achieve this transformation using varying amounts (3.0-30.0 equiv.) of I_2 , NaIO_3 , $\text{PhI}(\text{OAc})_2$ at different temperatures (0, 25 and 40°C), but only the starting material was recovered after reductive workup. In an attempt to elucidate the cause of this puzzling lack of reactivity, a cyclic voltammogram of **37** was acquired.

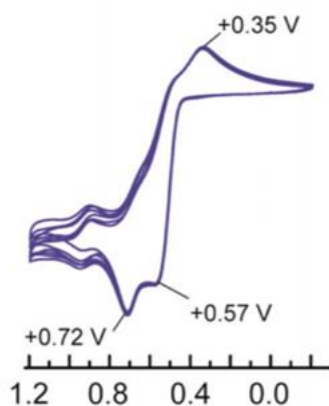


Figure 4.3 Cyclic voltammogram of **37**, Bu_4NBF_4 (0.1 M). Working electrode: glassy carbon. Reference electrode: Ag/AgCl (3 M NaCl). Counter electrode: Pt. Scan rate: 0.3 V/s.

The voltammogram revealed that, while the compound was indeed oxidized easily, to the diradical dication in a stepwise fashion, the process was apparently reversible. Over multiple scans, no changes were observed that would correspond to the formation of TTFV units, indicating no radical coupling reactions were taking place. Although the electrochemistry was consistent with the failed polymerization reactions, the results begged another question: why are the easily oxidized, spatially distant DTF groups not reactive toward polymerization? To address this question, **37** was titrated with an oxidant while monitoring the UV-vis spectra. $\text{PhI}(\text{OAc})_2$ was utilized instead of iodine as the oxidant since iodine absorbs light strongly and $\text{PhI}(\text{OAc})_2$ does not. The titration revealed the gradual disappearance of the pyrene-based absorption and the emergence of a naphthalene like absorbance. Additionally, the structure of the expected diradical dication **37a** was calculated at the B3LYP/6-31G(d) level of theory and it was found to have very low radical density on

the benzylic positions. Taken together, this allowed the conclusion to be drawn that the diradical was internally recombining.^[16] Such a recombination had initially thought to have been unlikely because it would entail the loss of the 74.6 kcal/mol of aromatic stabilization energy (ASE) of the pyrene system^[17] and its replacement by only 40.1 kcal/mol of ASE due to the naphthalene system.^[18] Clearly, the radical recombination outweighs the loss of ASE.

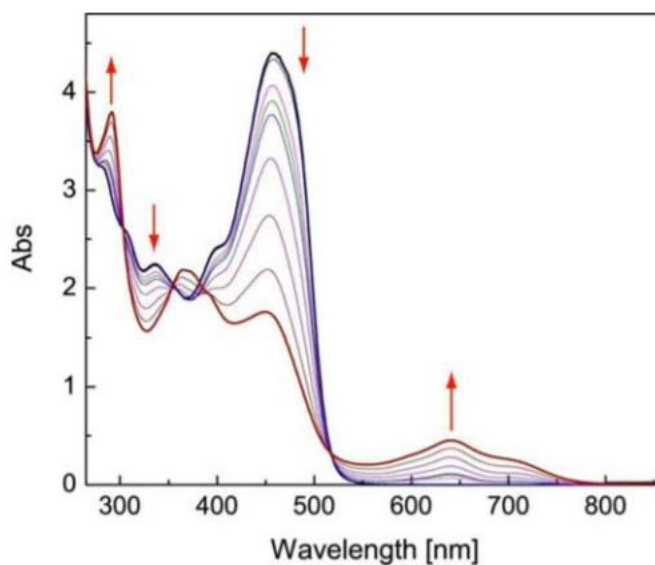


Figure 4.4 Oxidative UV-Vis titration of compound **37** (1.22×10^{-4} M in CHCl_3) with $\text{PhI}(\text{OAc})_2/\text{CF}_3\text{SO}_3\text{H}$ (1 : 4 molar ratio) at room temperature.

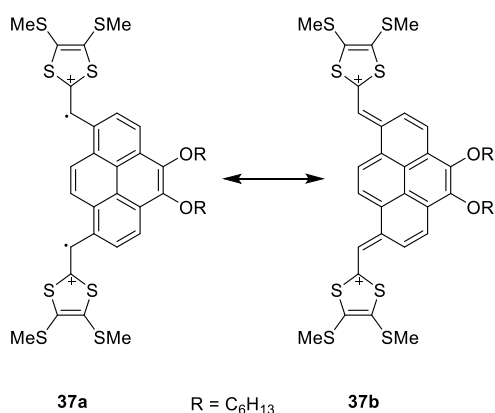
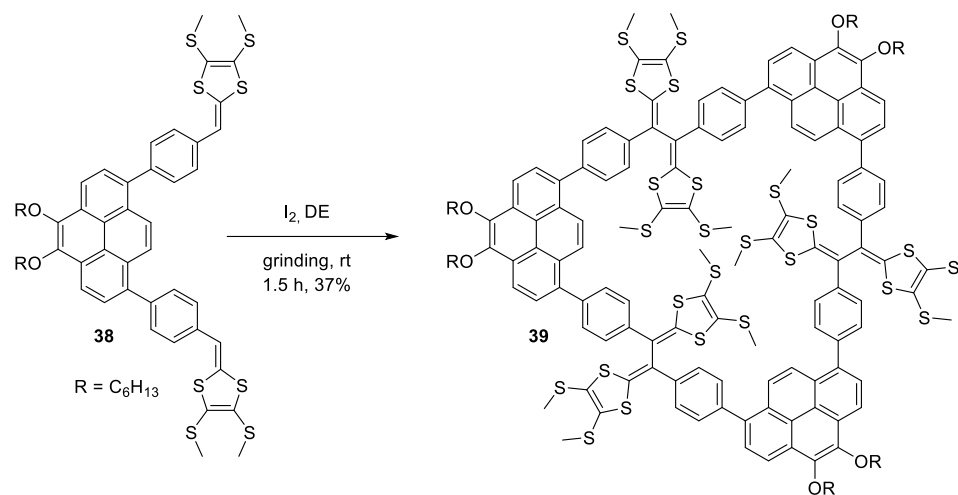


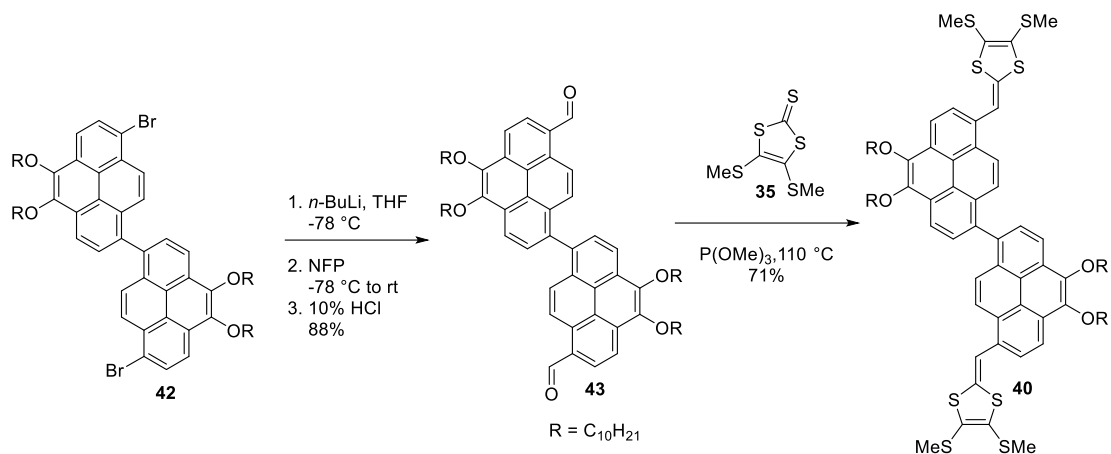
Figure 4.5 Proposed resonance structures accounting for the lack of reactivity.

Since the internal recombination of the diradical precluded **32** from undergoing any polymer or macrocycle formation, the notion of reducing the electronic communication between the two radicals was investigated. One potential way of accomplishing this was the introduction of phenylene spacers between the pyrene and DTF units. This would establish two biaryl bonds in the pathway between the two radicals, which would naturally reduce the electronic interaction between them when the dihedral angles about the biaryl bonds are anything other than 0° or 180°. In this vein, in collaboration with the Zhao group again, 1,4-phenylene spacers were installed by Suzuki coupling from 1,8-bromo-4,5-didecoxy pyrene (**34**). With this added electronic spacing between the two radicals, the intermolecular radical coupling behavior was turned on and the Zhao lab could produce an interesting macrocyclic trimer **39** in 37% yield by combining iodine with the π -extended monomer in the solid state. This same solid-state oxidation condition was tried for monomer **37**, but this only yielded starting material after reductive workup.



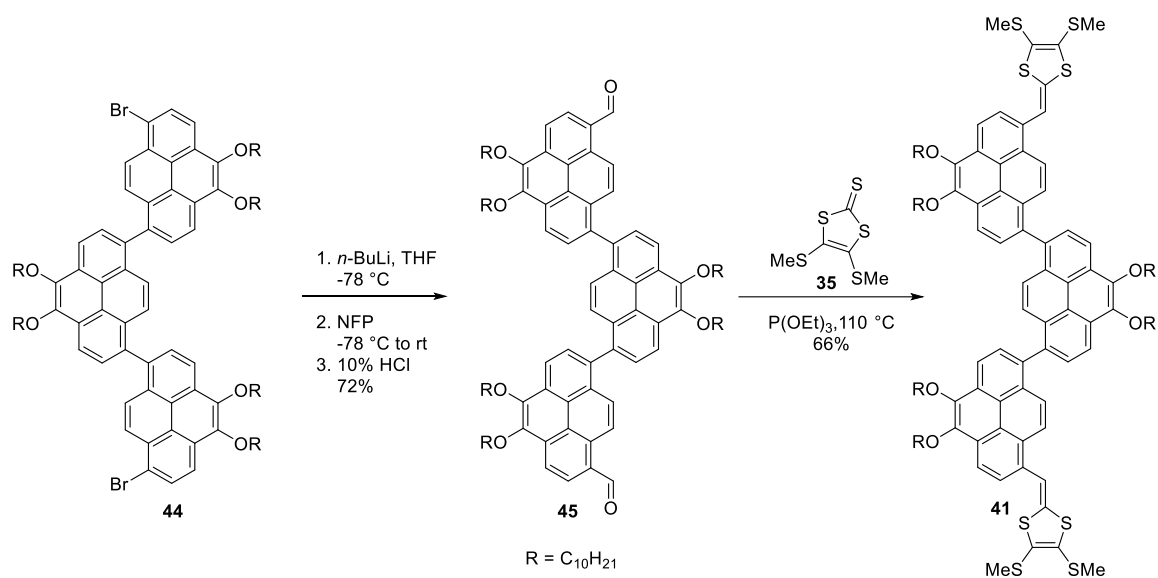
Scheme 4.9 Macrocyclization of **38** in the solid state. (R = Decyl)

In light of these results, the DTF compounds **40** and **41**, based on the pyrene dimer and trimer described in Chapter 2 become attractive targets. Instead of a phenylene linker, the DTFV units could be decoupled through pyrene-pyrene biaryl bonds, which have dihedral angles of 68-76°.^[19]



Scheme 4.10 Synthesis of pyrene dimer bis(DTF) **40**.

Trimer dibromide **44** underwent the lithiation/formylation procedure in 72% yield to produce dialdehyde **45** as a mixture of separable diastereomers (Chapter 3). Subsequent Bryce olefination of **45** (a mixture of isomers) proceeded in 66% yield to deliver the trimer bis(DTF) **41**. The mixture of isomers like all the compounds reported in Chapter 2 are inseparable and come as a single tight spot on TLC. The power of the DTF group to quench fluorescence is noteworthy. The pyrene trimer skeleton, which has a fluorescence quantum yield of 0.83 in solution and in the neat liquid state, was rendered essentially non-emissive (TLC-UV lamp). In the context of Chapter 2, it is worth noting that these redox active molecules bearing the pyrene dimer and trimer skeletons were isolated as viscous liquids.



Scheme 4.11 Synthesis of pyrene trimer bis(DTF) **41**.

The electrochemical properties, applications and possibility of cyclization of the series of pyrene-DTFV hybrids are currently underway in collaboration with the Stockmann and Zhao groups at Memorial University.

Conclusions

In conclusion, a series of pyrene-DTFV hybrids were synthesized with 1, 2 and 3 pyrenyl units separating the DTFV units. Building on previous work of the mono-pyrene system which showed internal radical coupling and a complete lack of reactivity of **37**, which was mediated by adding biaryl spacers in **38**. Utilizing the oligomers produced in chapter 2,

homologues, **40** and **41** were synthesized bearing only pyrenes. **41** can be thought to be analogous with **38**, now with a purely pyrenyl core.

References

1. F. Challenger, K. Harrison, *J. Inst. Pet. Tech.*, **1935**, *21*, 135–151.
2. F. Challenger, P. H. Clapham, R. Emmott, *J. Inst. Pet.*, **1948**, *34*, 922–934.
3. F. Challenger, R. Emmott, *J. Inst. Pet.*, **1951**, *37*, 395–399.
4. J. Bruce, F. Challenger, H. B. Gibson, W. E. Allenby, *J. Inst. Pet.*, **1948**, *34*, 226–331.
5. F. Challenger, E. A. Mason, E. C. Holdsworth, R. Emmott, *J. Chem. Soc.*, **1953**, 292–304.
6. F. Wudl, G. M. Smith, E. J. Hufnagel, *J. Chem. Soc., Chem. Commun.*, **1970**, 1453–1454.
7. F. Wudl, D. Wobschall, E. J. Hufnagel, *J. Am. Chem. Soc.*, **1972**, *94*, 670–672.
8. J. Ferraris, D. O. Cowan, V. V. Walatka, J. H. Perlstein, *J. Am. Chem. Soc.*, **1973**, *95*, 948–955.
9. Y. Zhao, G. Chen, K. Mulla, I. Mahmud, S. Liang, P. Dongare, D. W. Thompson, L. N. Dawe, S. Bouzan, *Pure. Appl. Chem.*, **2012**, *84*, 1005–1025.
10. M. F. Abdollahi, Y. Zhao, *New J. Chem.*, **2020**, *44*, 4681–4693.
11. G. Steimecke, H. J. Sieler, R. Kirmse, E. Hoyer, *Phosphor. Sulf.*, **1979**, *7*, 49–55.
12. C. A. Christensen, A. S. Batsanov, M. R. Bryce, *J. Org. Chem.*, **2007**, *72*, 1301–1308.
13. S. Liang, G. Chen, J. Peddle, Y. Zhao, *Chem. Commun.*, **2012**, *48*, 3100–3102.

14. M. Meran, P. D. Akkus, O. Kurkcuoglu, E. Baysak, G. Hizal, E. Haciosmanoglu, A. Unlu, N. Karatepe, F. S. Guner, *Langmuir*, **2018**, *34*, 12071–12082.
15. L. Bondarenko, I. Dix, H. Hinrichs, H. Hopf, *Synthesis*, **2004**, *16*, 2751–2759.
16. M. Khadem, J. C. Walsh, G. J. Bodwell, Y. Zhao, *Org. Lett.*, **2016**, *18*, 2403–240.
17. J. Wu, M. A. Dobrowolski, M. K. Cyrański, B. L. Merner, G. J. Bodwell, Y. Mo, P. v. R. Schleyer, *Mol. Phys.* **2009**, *107*, 1177–1186.
18. D. Setiawan, E. Kraka, D. Cremer, *J. Org. Chem.* **2016**, *81*, 9669–9686.
19. M. A. Zwijnenburg, *J. Phys. Chem. C* **2012**, *116*, 20191–20198.

Experimental

4,5-Dihexoxypyrene-1,8-dicarboxaldehyde (35) To a $-78\text{ }^{\circ}\text{C}$ (cooled by a dry ice/acetone bath) nitrogen-purged solution of 1,8-dibromo-4,5-dihexoxypyrene (**34**) (0.444 g, 0.792 mmol) in anhydrous THF (150 mL) was added *n*-BuLi (1.30 M, 4.87 mL, 6.33 mmol) dropwise. The reaction mixture was allowed to stir at $-78\text{ }^{\circ}\text{C}$ for 5 min. *N*-formylpiperidine (1.44 g, 12.7 mmol) was added and the dry ice/acetone bath was removed. The reaction mixture was allowed to warm to rt and stirred for a further 1.5 h. The reaction was quenched by the addition of a 10% HCl(aq) solution (25 mL) and the organic solvents were removed under reduced pressure. The resulting mixture was extracted with CH_2Cl_2 ($2 \times 50\text{ mL}$). The combined organic layers were washed with a 10% HCl(aq) solution ($2 \times 200\text{ mL}$), dried over anhydrous Na_2SO_4 and gravity filtered. The solvent was removed under reduced pressure to yield a dark orange oil, which was subjected to silica gel column chromatography

(CH₂Cl₂/hexanes, 3:1) to yield compound **35** as a canary yellow solid (0.320 g, 0.697 mmol, 88%). *R_f* (70% CH₂Cl₂/hexanes) = 0.30; ¹H NMR (CDCl₃, 300 MHz): δ = 10.82 (s, 2H), 9.56 (s, 2H), 8.72 (d, *J* = 8.2 Hz, 2H), 8.54 (d, *J* = 8.2 Hz, 2H), 4.38 (t, *J* = 6.7 Hz, 4H) 2.05-1.94 (m, 4H), 1.68–1.55 (m, 4H), 1.46–1.35 (m, 8H), 1.01–0.88 (m, 6H); ¹³C NMR (CDCl₃, 75 MHz): δ = 192.7, 146.0, 133.5, 131.8, 130.0, 127.9, 126.1, 122.4, 120.8, 74.2, 31.9, 30.5, 26.4, 22.7, 14.1; HRMS (APCI, positive mode) calcd for C₃₀H₃₄O₄ 458.2457, found 458.2411 [M]⁺.

4,5-Dihexoxy-1,8-bis(4,5-bis(methylthio)-2,3-dithia-6-fulvenyl)pyrene (37): A solution of 4,5-dihexoxy-pyrene-1,8-dicarbaldehyde (**35**) (2.00 g, 4.36 mmol) and 4,5-bis(methylthio)-1,3-dithiole-2-thione (**36**) (0.835 g, 25.9 mmol) in P(OEt)₃ (100 mL) was heated at 140 °C for 3 h. After cooling, the bulk of the unreacted P(OEt)₃ was removed by vacuum distillation and the resulting red-colored residue was passed through a short plug of silica gel (CH₂Cl₂) to remove the last traces of P(OEt)₃. The solvent was removed under reduced pressure and the residue was subjected to silica gel flash column chromatography (CH₂Cl₂/hexanes, 1:5) to yield pure compound **37** (3.02 g, 3.70 mmol, 85%) as a bright orange solid. m.p. > 150 °C (decomp.); IR (neat): ν = 2948, 2914, 2865, 1599, 1556, 1466, 1376, 1272, 1073, 831 cm⁻¹; *R_f* (10% CH₂Cl₂/hexanes) = 0.40; ¹H NMR (CDCl₃, 300 MHz): δ = 8.44 (d, *J* = 8.2 Hz, 2H), 8.21 (s, 2H), 8.01 (d, *J* = 8.3 Hz, 2H), 7.32 (s, 2H), 4.31 (t, *J* = 6.7 Hz, 4H), 2.49 (s, 2H), 2.37 (s, 6H), 1.97–1.82 (m, 4H), 1.62–1.55 (m, 4H), 1.43–1.37 (m, 8H), 0.94–0.88 (m, 6H); ¹³C NMR (CDCl₃, 75 MHz): δ = 144.1, 134.8, 130.6, 128.2, 127.6, 126.7, 124.6, 124.6, 123.6, 123.4, 119.6, 112.8, 74.00, 31.90, 30.70, 26.10, 22.8, 19.14, 19.09, 14.20; HRMS (APCI, positive mode) *m/z* calcd for C₄₀H₄₆O₂S₈ 814.1263, found 814.1244 [M]⁺.

1,1'-Bi-4,5-didecoxy-8-formylpyrene (43): To a $-78\text{ }^{\circ}\text{C}$ (cooled by a dry ice/acetone bath) nitrogen-purged solution of dibromide **42** (0.300 g, 0.253 mmol) in anhydrous THF (50 mL), was added *n*-BuLi (1.30 M, 1.56 mL, 2.02 mmol) dropwise. The reaction was allowed to stir at $-78\text{ }^{\circ}\text{C}$ for 5 min. *N*-formylpiperidine (0.457 g, 4.04 mmol) was added and the dry ice/acetone bath was removed. The reaction mixture was allowed to warm to rt and stirred for a further 1.5 h. The reaction was quenched with 10% HCl(aq) (20 mL) and the organic solvents were removed under reduced pressure. The reaction mixture was extracted with CH_2Cl_2 ($3 \times 50\text{ mL}$). The combined organic layers were washed with 10% HCl(aq) ($5 \times 100\text{ mL}$) and subsequently dried over anhydrous Na_2SO_4 . The solvent was removed under reduced pressure to yield crude **43** as an orange oil. The crude product was subjected to silica gel column chromatography (CH_2Cl_2 /hexanes, 1:2) to yield compound **43** as a yellow solid (0.241 g, 0.923 mmol, 88%). R_f (50% CH_2Cl_2 /hexanes) = 0.30; $^1\text{H NMR}$ (CDCl_3 , 300 MHz): δ = 10.73 (s, 2H), 9.22 (d, J = 9.6 Hz, 2H), 8.81 (d, J = 8.1 Hz, 2H), 8.67 (d, J = 8.2 Hz, 2H), 8.50 (d, J = 8.2 Hz, 2H), 8.23 (d, J = 8.1 Hz, 2H), 7.90 (d, J = 9.6 Hz, 2H), 4.51 (t, J = 6.7 Hz, 4H), 4.40 (t, J = 6.7 Hz, 4H), 2.10–2.01 (m, 8H), 1.71–1.60 (m, 16H), 1.39–1.26 (m, 40H), 0.99–0.81 (m, 12H); $^{13}\text{C NMR}$ (CDCl_3 , 75 MHz): δ = 192.82, 179.01, 156.86, 149.82, 147.00, 143.69, 136.87, 134.05, 131.74, 130.88, 129.62, 129.49, 126.85, 123.31, 122.58, 121.04, 118.59, 74.29, 74.08, 31.95, 31.93, 30.68, 30.59, 29.72, 29.66, 29.65, 29.64, 29.62, 29.60, 29.39, 29.38, 26.36, 26.33, 22.73, 22.71, 14.15, 14.13; HRMS (APCI, positive mode) m/z calcd. for $\text{C}_{74}\text{H}_{98}\text{O}_6$ 1082.7363, found 1082.7375 $[\text{M}]^+$.

1,1'-Bi-4,5-didecoxy-8-(4,5-bis(methylthio)-2,3-dithia-6-fulvenyl)pyrene (40): A solution of dimer dialdehyde (**41**) (0.200 g, 0.185 mmol) and thione (**35**) (0.125 g, 0.556 mmol) in P(OMe)₃ (5 mL) was heated to 108 °C for 3 h. After cooling, the unreacted P(OMe)₃ was removed by vacuum distillation and resulting red-colored residue was passed through a short plug of silica gel (CH₂Cl₂) to remove the last traces of P(OEt)₃. The solvent was removed under reduced pressure and the residue was subjected to silica gel flash column chromatography (CH₂Cl₂/hexanes, 1:5) to yield compound **40** (0.189 g, 0.131 mmol, 71%) as a deep orange oil. R_f (20% CH₂Cl₂/hexanes) = 0.35; ¹H NMR (CDCl₃, 300 MHz): δ = 8.66 (d, *J* = 8.1 Hz, 2H), 8.55 (d, *J* = 8.3 Hz, 2H), 8.15 (d, *J* = 8.1 Hz, 2H), 8.08 (d, *J* = 8.3 Hz, 2H), 8.00 (d, *J* = 9.5 Hz, 2H), 7.68 (d, *J* = 9.5 Hz, 2H), 7.23 (s, 2H), 4.43 (t, *J* = 6.8 Hz, 4H), 4.41 (t, *J* = 6.8 Hz, 4H), 2.43 (s, 6H), 2.36 (s, 6H), 2.05–1.89 (m, 8H), 1.70–1.61 (m, 16H), 1.41–1.24 (m, 40H), 0.98–0.87 (m, 12H); ¹³C NMR (CDCl₃, 75 MHz): δ = 143.11, 143.02, 134.57, 133.60, 129.46, 128.87, 128.20, 127.87, 127.11, 126.43, 125.56, 124.86, 123.47, 123.25, 122.32, 122.18, 118.46, 118.28, 111.61, 72.91, 30.93, 30.90, 29.65, 28.71, 28.65, 28.63, 28.37, 28.35, 25.35, 21.70, 21.68, 17.91, 13.13, 13.10; HRMS (APCI, positive mode) *m/z* calcd for C₈₄H₁₁₀O₄S₈ 1438.61698, found 1438.61857 [M]⁺.

4,5-Didecoxy-1,8-diformylpyren-1-yl)pyrene (41): See Chapter 3.

4,5-Didecoxy-1,8-bis(4,5-didecoxy-8-(4,5-bis(methylthio)-2,3-dithia-6-fulvenyl)pyren-1-yl)pyrene (41): A solution of trimer dialdehyde (**45**) (0.200 g, 0.125 mmol) and thione (**35**) (0.85 g, 0.38 mmol in P(OMe)₃ (5 mL) was heated to 108 °C for 3 h. After cooling, the unreacted P(OMe)₃ was removed by vacuum distillation and resulting red-colored residue was passed through a short silica plug (CH₂Cl₂) to remove the last traces of P(OMe)₃. The solvent was removed under reduced pressure and the residue was subjected to silica gel flash column chromatography (CH₂Cl₂/hexanes, 1:5) to yield compound **41** (0.161 g, 0.083 mmol, 66%) as a deep orange oil. *R*_f(20% CH₂Cl₂/hexanes) = 0.30; ¹H NMR (CDCl₃, 300 MHz): δ = 8.7545 and 8.7495 (2 × d, *J* = 8.1 Hz, 2H), 8.56 (d, *J* = 8.1 Hz, 2H), 8.50 and 8.49 (2 × d, *J* = 8.2 Hz, 2H), 8.20 (d, *J* = 8.2 Hz, 2H), 8.15–7.94 (m, 8H), 7.76 and 7.69 (2 × d, *J* = 9.5 Hz, 2H), 7.55 and 7.49 (2 × s, 2H), 7.22 and 7.20 (2 × s, 2H), 4.54 (t, *J* = 6.7 Hz, 4H), 4.45–4.28 (m, 8H), 2.44 (s, 1H), 2.41 (s, 1H), 2.33 (s, 1H), 2.29 (s, 1H), 2.17–1.93 (m, 12H), 1.84–1.16 (m, 84H), 1.00–0.80 (m, 18H); ¹³C NMR (CDCl₃, 75 MHz): δ = 143.20, 143.04, 143.02, 142.93, 134.54, 134.53, 133.50, 129.37, 128.89, 128.85, 128.83, 128.79, 128.18, 127.88, 127.76, 127.74, 127.03, 127.01, 126.37, 124.85, 124.76, 123.38, 122.29, 122.25, 122.21, 122.17, 122.11, 118.35, 118.15, 118.13, 111.61, 73.01, 72.83, 30.92, 30.90, 30.86, 29.71, 29.59, 28.73, 28.67, 28.65, 28.60, 28.57, 28.37, 28.34, 28.31, 25.40, 25.30, 21.69, 21.67, 21.64, 17.89, 17.88, 17.84, 13.11, 13.08; HRMS (APCI, positive mode) *m/z* calcd. for C₁₂₀H₁₅₈S₈O₆ 1950.9824, found 1950.9819 [M]⁺.

